2016

AN EXPERIMENTAL INVESTIGATION OF THE EFFECT OF TEMPERATURE AND SPACE VELOCITY ON THE PERFORMANCE OF A CU-ZEOLITE FLOW-THROUGH SCR AND A SCR CATALYST ON A DPF WITH AND WITHOUT PM LOADING

Vaibhav Kadam
Michigan Technological University, vkadam@mtu.edu

AN EXPERIMENTAL INVESTIGATION OF THE EFFECT OF TEMPERATURE AND SPACE VELOCITY ON THE PERFORMANCE OF A CU-ZEOLITE FLOW-THROUGH SCR AND A SCR CATALYST ON A DPF WITH AND WITHOUT PM LOADING

By

Vaibhav Kadam

A THESIS

Submitted in partial fulfillment of the requirements for the degree of

MASTER OF SCIENCE

In Mechanical Engineering

MICHIGAN TECHNOLOGICAL UNIVERSITY

2016

This thesis has been approved in partial fulfillment of the requirements for the Degree of MASTER OF SCIENCE in Mechanical Engineering.

Department of Mechanical Engineering – Engineering Mechanics

Thesis Co-Advisor:	*Dr. Jeffrey Naber*
Thesis Co-Advisor:	*Dr. John Johnson*
Committee Member:	*Dr. David Shonnard*
Department Chair:	*Dr. William Predebon*

Table of Contents

List of Figures

List of Tables

Acknowledgements

I would like to thank every individual and institution that supported and assisted me in any way during this research and helped me complete this thesis.

Foremost, I would like to express my sincere gratitude to my advisors, Dr. Jeffrey Naber and Dr. John Johnson for providing the opportunity and continuous guidance, without which this thesis would not have been possible. Dr. Jeffrey Naber helped me understand and analyze the experimental data, as well as troubleshoot the problems in the test cell. Dr. John Johnson was supportive in understanding the experimental data critically to ensure data integrity and provided continuous guidance during my efforts to write this thesis. I would like to thank Dr. David Shonnard for being on my research committee.

I would like to thank my past and present colleagues at Michigan Tech, Erik Gustafson, Krishnan Raghavan, Saksham Gupta and Sagar Sharma for their assistance during the engine testing and Rajesh Chundru for providing me necessary information to perform the modeling work. I would like to thank Paul Dice, Steve Lehmann and Christopher Pinnow who helped me in various ways during the course of this research. I would also like to thank Krishna Chilumukuru from Cummins for providing information and support for the experimental work of the research.

I would like to thank the MTU Diesel Engine Aftertreatment Research Consortium for providing me the financial support during this research. Cummins has also provided the ISB 2013 engine, the production aftertreatment system and the supporting hardware and the software used in this research. Johnson Matthey and Corning provided the SCRF®, which was studied in this research.

Last but not the least, I would like to thank my family and friends for their constant encouragement and support during the course of this research.

Abbreviations, Notations and Symbols

EPA	Environmental Protection Agency
DOC	Diesel Oxidation Catalyst
DPF	Diesel Particulate Filter
SCR	Selective Catalytic Reduction
SCR-on-filter	Diesel Particulate Filter coated with SCR Catalyst
SCRF®	SCR-on-filter developed by Johnson Matthey
NO_x	Oxides of Nitrogen (Usually NO and NO_2)
PM	Particulate Matter
CO	Carbon Monoxide
NO	Nitrogen Oxide
CO_2	Carbon Dioxide
NO_2	Nitrogen Dioxide
NH_3	Ammonia
HC	Hydrocarbons
CPF	Catalyzed Particulate Filter
AR	Active Regeneration
PO	Passive Oxidation
DEF	Diesel Exhaust Fluid
H_2O	Dihydrogen Monoxide (Water)
MTU	Michigan Technological University

SCR-F	SCR on a DPF model
A	Pre Exponential Factor
E_a	Activation Energy
R	Universal Gas Constant
T	Temperature
RR	Reaction Rate
HD	Heavy Duty
ANR	Ammonia to NO_x Ratio
UDOC	Upstream of the DOC
DDOC	Downstream of the DOC
DCPF	Downstream of the CPF
USCRF®	Upstream of the SCRF®
DSCRF®	Downstream of the SCRF®
ECM	Engine Control Module
H/C	Hydrogen to Carbon Ratio

Abstract

The heavy-duty diesel (HDD) engines use the diesel oxidation catalyst (DOC), catalyzed particulate filter (CPF) and urea injection based selective catalytic reduction (SCR) systems in sequential combination, to meet the US EPA 2010 PM and NO_x emission standards. The SCR along with a NH_3 slip control catalyst (AMOX) offer NO_x reduction >90 % with NH_3 slip <20 ppm. However, there is a strong desire to further improve the NO_x reduction performance of such systems, to meet the 2015 California Optional Low NO_x Standard. Integrating SCR functionality into a diesel particulate filter (DPF), by coating the SCR catalyst on the DPF, offers potential to reduce the system cost and packaging weight/ volume. It also provides opportunity to increases the SCR volume without affecting the overall packaging, to achieve NO_x reduction efficiencies >95 %.

In this research, the NO_x reduction and NH_3 storage performance of a Cu-zeolite SCR and Cu-zeolite SCR catalyst on a DPF (SCRF®) were experimentally investigated based on the engine experimental data at steady state conditions. The experimental setup and test procedures for evaluation of NO_x gaseous emissions and PM oxidation performance of the SCRF®, including pressure drop and the temperature distribution with and without PM loading in the SCRF® are described. The experimental data for the production-2013-SCR and the SCRF® were collected (with and without PM loading in the SCRF®) on a Cummins ISB 2013 engine, at varying inlet temperatures, space velocities, inlet NO_x concentrations and NO_2/NO_x ratios, to evaluate the NO_x reduction, NH_3 storage and NH_3 slip characteristics of the SCR catalyst. The SCRF® was loaded with 2 and 4 g/L of PM prior to the NO_x reduction tests to study the effect of PM loading on the NO_x reduction and NH_3 storage performance of the SCRF®.

The 1-D SCR model developed at MTU was calibrated to the engine experimental data obtained from the seven NO_x reduction tests conducted with the production-2013-SCR. The performance of the 1-D SCR model was validated by comparing the simulation and experimental data for NO, NO_2 and NH_3 concentrations at the outlet of the SCR. The NO and NO_2 concentrations were calibrated to ±20 ppm and NH_3 was calibrated to ±20 ppm.

The experimental results for the production-2013-SCR indicate that the NO_x reduction of 80 – 85% can be achieved for the inlet temperatures below 250°C and above 450°C and NO_x reduction of 90 – 95% can be achieved for the inlet temperatures between 300 – 350°C, at ammonia to NO_x ratio (ANR) 1.0, while the NH_3 slip out of the SCR was <75 ppm. Conversely, the SCRF® showed 90 – 95 % NO_x reduction at ANR of 1.0, while the NH_3 slip out of the SCRF® was >50 ppm, with and without PM loading in the SCRFc, for the inlet temperature range of 200 – 450 °C, space velocity in the range of 13 to 48 k/hr and inlet NO_2/NO_x in the range of 0.2 to 0.5. The NO_x reduction in the SCRF® increases to >98 % at ANR 1.2. However, the NH_3 slip out of the SCRF® increases significantly at ANR 1.2.

The effect of PM loading at 2 and 4 g/L on the NO_x reduction performance of the SCRF® was negligible below 300 °C. However, with PM loading in the SCRF®, the NO_x reduction decreased by 3 – 5% when compared to the clean SCRF®, for inlet temperature >350 °C. Experimental data were also collected by reference [1] to investigate the NO_2 assisted PM oxidation in the SCRF® for the inlet temperature range of 260 – 370 °C, with and without urea injection and thermal oxidation of PM in the SCRF® during active regeneration for the inlet temperature range of 500 – 600 °C, without urea injection. The experimental data obtained from this study and [1] will be used to develop and calibrate the SCR-F model at Michigan Tech. The NH_3 storage for the production-2013-SCR and the SCRF® (with and without PM loading) were determined from the steady state engine experimental data. The NH_3 storage for the production-2013-SCR and the SCRF® (without PM loading) were within ±5 gmol/m^3 of the substrate, with maximum NH_3 storage of 75 – 80 gmol/m3 of the substrate, at the SCR/SCRF® inlet temperature of 200°C. The NH_3 storage in the SCRF®, with 2 g/L PM loading, decreased by 30%, when compared to the NH_3 storage in the SCRF®, without PM loading. The further increase in the PM loading in the SCRF®, from 2 to 4 g/L, had negligible effect on NH_3 storage.

Chapter 1. Introduction

Heavy duty diesel engines are used as the power plants in stationery applications, on-road and off-road vehicles. They can significantly reduce CO_2 emissions, but they produce mainly emissions of nitrogen oxides (NO_x) and particulate matter (PM) that need to be controlled to meet the emission standards. Various agencies around the world have been working to regulate the emissions. The tail pipe emission standards for heavy duty diesel engines have been regulated since 1974 by the Environmental Protection Agency (EPA) in the U.S. The evolution of emission standards in the U.S. from year 2004 – 2015 is shown in Table 1.1.

Diesel engine emissions are controlled with technologies such as high pressure fuel injection system, turbocharging, cooled exhaust gas recirculation (EGR) and multiple fuel injections using piezo injectors. Diesel engine manufacturers of heavy-duty on-road vehicles implemented the usage of Diesel Particulate Filter (DPF) in 2007 to meet the standards for PM. Present aftertreatment systems typically consists of a Diesel Oxidation Catalyst (DOC), a Catalyzed Particulate Filter (CPF), Selective Reduction Catalyst (SCR) with the urea injection assembly and Ammonia Oxidation Catalyst (AMOX) to meet the gaseous and PM emissions, post 2010.

Table 1.1: US EPA & California Emission Standards for Heavy-Duty CI Engines, g/bhp·hr [2]

Emission Gases	**EPA Standard - Implementation Year**			
	2004	**2007-09**	**2010**	**2015**
NO_x	2.00*	1.2	0.2	0.02**
NMHC	0.5*	0.14	0.14	0.14
CO	15.5	15.5	15.5	15.5
PM	0.1	0.01	0.01	0.01

NOTE: "*" - Alternative standard: NMHC+NO_x = 2.5 g/bhp.hr
"**" - Manufactures may choose California Optional Low NO_x Standard

1.1 Diesel Aftertreatment Systems

A typical arrangement of components in the aftertreatment system for a heavy duty diesel engine is shown in the Figure 1.1.

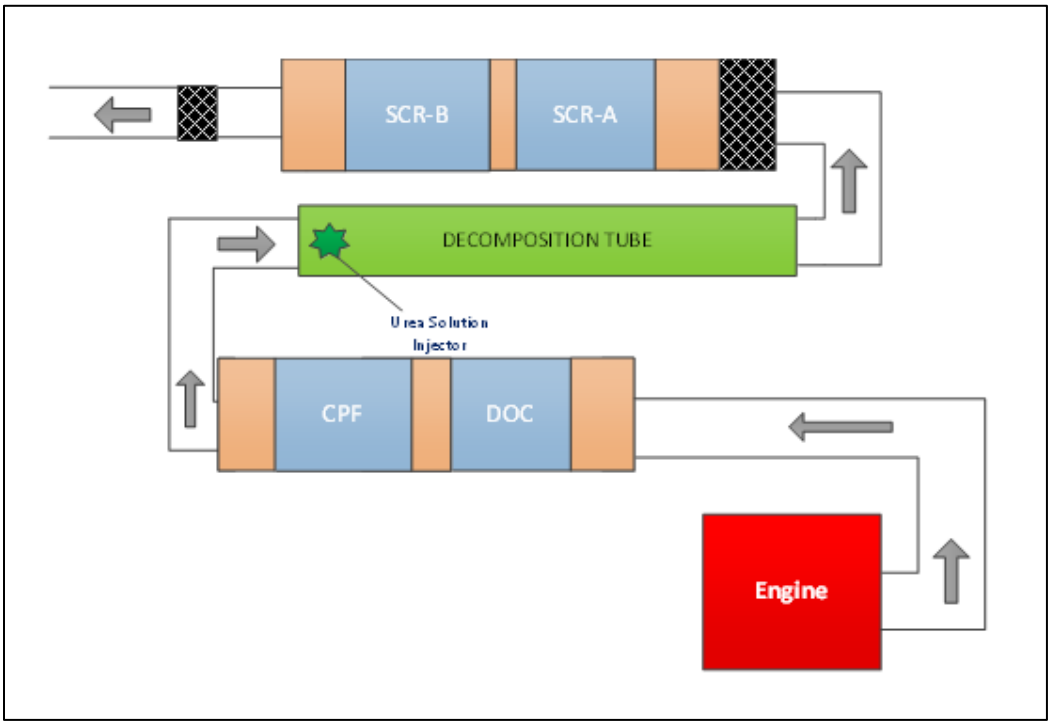

Figure 1.1: Overall schematic of the Cummins ISB 2013 production aftertreatment system [3]

The first component is a DOC, which is a flow through catalyst that oxidizes the HC, CO and NO in the exhaust stream into H_2O, CO_2 and NO_2. For diesel engines, the proportion of NO_2 in total engine-out NO_x is typically 5 - 15%. The oxidation of NO to NO_2 provides an increased rate of NO_2 assisted oxidation of PM in the CPF and helps in maintaining higher NO_2/NO_x ratio needed for better NO_x reduction in the SCR [4]. The HC conversion efficiency increases with an increase in exhaust temperature, whereas the NO to NO_2 conversion efficiency is maximum at 340 °C DOC inlet temperature, and decreases for temperatures less or more than 340 °C [5].

The CPF is a wall flow device, with every other channel open at the inlet but closed at the outlet end. The CPF filters the PM in the exhaust gas and oxidizes the PM accumulated in the filter either by passive oxidation or active regeneration. The NO_2 assisted oxidation occurs due to reaction between the PM accumulated in the CPF and the NO_2 present in the exhaust gases, at temperatures between 250 – 400 °C. The thermal oxidation occurs due to reaction between PM accumulated in the CPF and the O_2 present in the exhaust gases, at exhaust temperatures higher than 400°C. Both the mechanisms of PM oxidation occur simultaneously. These mechanisms are explained in detail in reference [3, 6, 7].

The SCR system is a flow through substrate which reduces the NO_x in the exhaust gas into N_2 and H_2O using the urea solution injected in the decomposition tube. The urea solution with 32.5 % urea concentration by weight, also known as diesel exhaust fluid (DEF) is used as the reducing agent. The DEF is dosed into the exhaust gases using an injector into the decomposition tube. The decomposition tube helps in mixing the DEF spray with the exhaust flow and also accelerates the urea hydrolysis and thermolysis process [8]. The urea decomposes into NH_3 and isocyanic acid. The isocyanic acid further decomposes into NH_3 and CO_2 on the SCR catalytic surface [8]. The NH_3 produced by decomposition of the urea is adsorbed and stored on the SCR catalytic surface. The NO_x in the exhaust gases is reduced by the NH_3 stored on the SCR catalyst.

The SCR substrate is a honeycomb structure with a typical channel density of 400 cells per square inch (CPSI). The substrate is made from the ceramic material such as cordierite and titanium oxide. The catalytic components such as oxides of vanadium and tungsten, iron (Fe) or copper (Cu) zeolites and precious metals are coated on the channels of the SCR. The performance of various catalysts, based on the published literature will be discussed in the next chapter.

The AMOX is placed after the SCR substrates or on the back of a substrate to oxidize the NH_3 that slips out of the SCR due to various reasons including over injection of DEF, low exhaust temperatures and the effect of an aged SCR catalyst. NH_3 is oxidized to N_2 and H_2O. Figure 1.1 shows a SCR-A substrate that just has a SCR catalyst and SCR-B

represents a substrate coated with the SCR catalyst in the front and the AMOX on the back of the substrate.

1.2 Motivation

The California optional emission regulations for 2015 require high NO_x reduction (>95%) and low NH_3 slip (<10 ppm). Hence, it is important to understand the NO_x reduction performance of the SCR catalyst and the effect of various inlet temperatures, space velocities, inlet NO_x concentrations and NO_2/NO_x ratios on the NO_x reduction performance of the SCR catalyst. In order to change the SCR design to achieve improved performance and reduced complexity of the SCR systems, extensive studies along with modeling efforts are required. An SCR model calibrated to experimental data provides possibilities to estimate the SCR states which cannot be directly measured [9].

The diesel engine aftertreatment catalysts can be arranged either in DOC + CPF + SCR or DOC + SCR + CPF, although each configuration has advantages and disadvantages; the selection of configuration will depend on issues such as the need for rapid light-off of the SCR, for maximizing passive regeneration, for adequate urea mixing, and for packaging space [10]. Furthermore, the California optional emission standards for year 2015 will require even lower tailpipe NO_x emissions when compared to year 2010. One potential approach would be increasing the catalyst volume, but it will increase the cost of the system due to the precious metals involved and could cause packaging problems.

The SCR catalyst on a DPF is also known as a SDPF and SCR-in-DPF is an upcoming technology in the field of diesel aftertreatment systems which provides a cost-effective solution to reduce NO_x and PM using a single aftertreatment device [11]. One way to make the SCR on a DPF is by coating the SCR catalyst on the DPF substrate. The reduced aftertreatment volume achieved by the integration of SCR and DPF provides opportunity for packaging flexibility and improved thermal management [12].

The SCR catalyst on a DPF used in this study is known as the SCRF®, and it was developed and supplied by Johnson Matthey and Corning. The SCRF® is a wall flow device (DPF) in which the substrate is coated with a Cu-zeolite based SCR catalyst. Thus,

the NO_x and PM can be controlled using a single device. The substrate of the SCRF® used in this study is made from cordierite and was supplied by Corning. The PM accumulated in the SCRF® is oxidized by NO_2 assisted oxidation and thermal oxidation. The NO_x in the exhaust gas is reduced by the SCR reactions occurring on the SCR catalyst.

The total volume of the production aftertreatment components and the SCRF® is given in Table 1.2. It can be observed that the volume of the production aftertreatment is almost 10 liters higher than the DOC + SCRF®. This indicates that an additional SCR brick could be used and still maintain the weight to volume ratio similar to the production aftertreatment system. The additional NO_x reduction catalyst would help to achieve the 2015 emission standards shown in Table 1.1.

Table 1.2: Volume comparison of the Production and DOC-SCRF® systems [3]

Component	**Volume (L)**		
	Production	**DOC + SCRF®**	**DOC + SCRF® + SCR-B**
	(Present)	(Option 1)	(Option 2)
DOC	4.2	4.2	4.2
CPF	10.4	-	-
SCRF®	-	17.0	17.0
SCR-A	8.52	-	-
SCR-B	11.4	-	11.4
AMOX	-	2.9	-
Total	**34.5**	**24.1**	**32.6**

1.3 Goals and Objectives

One of the goals of this research is to investigate with the experimental data the NO_x reduction performance of the production-2013-SCR, calibrate the high fidelity MTU 1-D SCR model developed by Dr. Song [9] to simulate the SCR outlet gaseous concentrations (NO, NO_2 and NH_3), investigate the NO_x reduction and NH_3 storage performance of the SCRF® and compare it with the performance of the production-2013-SCR.

The production-2013-SCR from the Cummins ISB 2013 diesel engine aftertreatment system and the SCRF® will be used to conduct experiments as a part of the Diesel Engine Aftertreatment Consortium efforts at MTU. The experimental data will be collected by varying the SCR and the SCRF® inlet temperature, space velocity, NO_x concentration and NO_2/NO_x ratio. Experimental data for the SCRF® will be collected from configuration 1, 2 and 3, which will be used to determine the PM oxidation, PM loading, PM filtration, pressure drop and temperature distribution characteristics of the SCRF® with and without urea injection and the NOx reduction and NH_3 storage in the SCRF®, with 0, 2 and 4 g/L PM loading in the SCRF®. Configuration 1 and 2 consist of a DOC and a SCRF®. However, in configuration 2, a CPF will be placed upstream of the SCRF® during the tests designed to collect experimental data without PM loading in the SCRF®. Configuration 3 consists of a DOC, a SCRF® and a SCR downstream of the SCRF®. A SCR-F model will be developed from the MPF model for the CPF [13], with the addition of the SCR equations from the MTU 1-D SCR model [9] and the experimental data from the SCRF® will be utilized to validate and calibrate the SCR-F model.

The following objectives were developed to meet the research goals:

1) Develop the procedures and identify the test conditions for steady state testing of the Cummins ISB 2013 engine and the aftertreatment system to characterize the NO_x gaseous emissions performance of the production-2013-SCR and the SCRF® including the pressure drop and temperature distribution data needed for calibrating the SCR-F model.
2) Conduct the NO_x experimental tests as a function of ANR to evaluate the NO_x emission performance of the ISB 2013 production-2013-SCR and the SCRF® and collect data for the 1-D SCR and the SCR-F models. The procedures developed in Objective 1 will be used to collect the experimental data. The data from the production-2013-SCR will be considered as the baseline SCR performance and will be used to compare to the SCRF® data and the SCRF® data will be used to develop and calibrate the SCR-F model.

3) Analyze the data for the production-2013-SCR and the SCRF® to determine the NO_x conversion efficiency, NH_3 slip and NH_3 storage. The effect of parameters such as space velocity, SCR and SCRF® inlet temperature, SCR and SCRF® inlet NO, NO_2 and NO_x concentrations, ANR and NO_2/NO_x ratios will be used to explain the outlet gaseous concentrations (NO, NO_2 and NH_3) and the NO_x conversion efficiency. The data consistency will be checked based on nitrogen balance across the SCR and SCRF®. These data will be used for determining the ANR for the experimental tests with a SCRF® plus SCR system.
4) Calibrate the 1-D SCR model using the engine experimental data by determining the storage parameters and the pre-exponential factors for the SCR reactions. Validate the model performance by comparing the simulation results and the experimental data.
5) The SCRF® performance will be determined with 2 and 4 g/L of PM and without PM in the SCRF® (0 g/L) and the SCR and the SCRF® performance, with and without PM in the SCRF® will be analyzed and compared to the published literature.

1.4 Thesis Outline

The thesis discusses the NO_x reduction performance of the SCR and the SCRF® based on the experimental study conducted on the Cummins ISB 2013 engine with the production-2013-SCR and the SCRF®. This chapter presented the brief introduction and the motivation for the research. The importance of the aftertreatment system was explained, followed by the goals and objectives of the research.

Chapter 2 provides a literature review of the published papers relating to the SCR and the SCR catalyst on the DPF systems. Information regarding the performance of the components, based on the experimental and modeling studies were collected from the previous technical papers from different organizations.

Chapter 3 discusses the test cell layout and the experimental procedures used for collecting the experimental data. The testing facilities and specific instruments are

introduced. The various test procedures and the test matrices are discussed. The important modifications in the test procedure are explained.

Chapter 4 presents the results of this study. The data analysis and implementation of nitrogen balance methodology to validate the data consistency are explained. The NO_x reduction and NH_3 storage characteristics of the production-2013-SCR and the SCRF®, with and without PM loading in the SCRF® are discussed. Performance of the calibrated 1-D SCR model are explained by comparing the simulated and experimental results.

Chapter 5 summarizes the analyzed results from the experimental and the modeling studies and the conclusions of the research. Recommendations for future work are proposed.

Chapter 2. Literature Review

The urea-SCR technology has been the most effective solution to control NO_x emissions from diesel exhaust gas. The SCR technology was first applied in thermal power plants in 1970s and was commercially adopted for diesel engines about a decade ago [2]. The current hardware commonly uses a DOC+CPF+SCR system configuration to meet the heavy-duty emission regulations. Recently developed diesel engines are calibrated to produce high engine-out NO_x (1500 – 2000 ppm) to facilitate passive oxidation of PM in the DPF/CPF. This change in engine calibration further increases the demand for high NO_x conversion efficiency from the SCR system. Combining the functions of the SCR and the DPF (SCR-on-filter) provides the opportunity for design and packaging flexibility, improved thermal management and reduced aftertreatment volume in heavy duty diesel engine applications. Due to closer placement of the SCR-on-filter than the SCR, SCR-on-filter can operate at higher temperatures and hence achieve higher NOx conversion [12]. A literature review of the aspects related to the SCR and the SCR-on-filter from the published research are presented in the following sections of this chapter.

2.1 SCR Catalyst Formulations and Experimental Studies

The major SCR catalysts that are used and studied include Cu-zeolite, Fe-zeolite, vanadia and cerium based composite oxides. The vanadia SCR (V-SCR) catalysts consist of V_2O_5 as the active component impregnated on TiO_2. Barium (Ba), cerium (Ce), zirconium (Zr), terbium (Tb) and erbium (Er) are used to stabilize vanadium [14, 15]. SiO_2 and WO_3 are used to increase the thermal durability. The V-SCR has demonstrated maximum NO_x conversion between 300 to 450°C and superior resistance to sulfur poisoning [16]. Hence vanadia SCR is preferred in markets with high sulfur fuel.

The low melting of V_2O_5 leads to thermal deactivation of V-SCR and loss in NO_x conversion above 550°C [9, 17]. The maximum NO_x conversion efficiency for V-SCR after a 64 hours hydrothermal aging at 670°C was only about 20%, while for Fe and Cu-zeolite SCR, NO_x conversion efficiency was >90% after the same hydrothermal aging

procedure. A significant improvement in the durability of V-SCR after 100 hours of exposure at 650°C was reported by Spenglet et al. [16]. They found that the NO_x conversion efficiency, increased from 30% at 300°C catalyst temperature to 95%, by stabilizing the titania support and then immobilizing the vanadia catalyst on the titania. However, the V-SCR also releases toxic vanadium compounds such as V_2O_5, from the catalysts at temperatures beyond 600 °C. Hence, a formulation is needed which is efficient in NO_x conversion, thermally stable and more environmental friendly than the V-SCR.

The new generation SCR catalyst technologies also include Cu and Fe based zeolites. The characteristic of the Cu-zeolite and Fe-zeolite SCR from various references [4, 18, 19, 20, 21, 22, 23] are compared and summarized below.

- Cu-zeolite SCR demonstrates higher NO_x conversion efficiency than the Fe-zeolite SCR below SCR inlet temperatures of 350 °C, while Fe-zeolite SCR provides better NO_x conversion at temperatures >400 °C.
- Cu-zeolite SCR has higher NH_3 storage capacity than the Fe-zeolite SCR, which may be the main reason for higher NO_x reduction in Cu-zeolite SCR than the Fe-zeolite SCR at low temperatures. The NH_3 storage capacity and NO_x reduction performance is significantly affected by the catalyst aging.
- Both the catalysts exhibit a tendency to oxidize NH_3 above 300 °C with high selectivity to N_2 (>95%). However, higher surface oxidation was observed in Cu-zeolite SCR than the Fe-zeolite SCR, reducing the effective amount of NH_3 available for NO_x reduction reactions.
- The NO_x reduction performance of Cu-zeolite SCR is less dependent on the NO_2/NO_x ratio, compared to that of Fe-zeolite SCR. This is due to the ability of the Cu-zeolite SCR to oxidize the surface NO to NO_2 in situ. However, Fe-Zeolite provides better NO_x reduction than the Cu-zeolite SCR at an optimal NO_2/NO_x ratio of 0.5.
- Cu-zeolite shows lower NH_3 slip due to its higher NH_3 storage and NH_3 oxidation than the Fe-zeolite SCR.

- Cu and Fe-zeolite catalysts are thermally more stable than the vanadia based SCR at temperatures typical of diesel application with active regeneration. However, their performance can deteriorate irreversibly over time as a result of high temperature thermal deactivation.
- Cu-zeolite SCR exhibits less tolerance to sulfur poisoning than the Fe-zeolite SCR. The low temperature (<300 °C) performance of Cu-zeolite SCR decreased significantly upon exposure to SO_2. However, the sensitivity to SO_2 reduced at high temperatures, indicating occurrence of desulfation phenomenon.
- The Cu-zeolite produces higher concentration of N_2O than the Fe-zeolite SCR. N_2O formation could be regulated by optimizing the catalyst's oxidizing performance, the urea injection strategy and the NH_3 storage onto the catalyst to decrease the NH_3 slip.

Studies were performed to combine the Cu-zeolite and Fe-zeolite systems to obtain better performance when compared to individual catalysts. The simulation results of a combined system were presented in reference [24]. They concluded that the dual-brick configuration performs better than the dual-layer configuration in the temperature window of 100 to 600°C. The overall NO conversion reduces in the dual-layer catalyst due to the diffusional limitations at the intermediate temperature when compared to the dual-brick catalyst. The experimental results of combined Cu and Fe-zeolite SCR catalysts were presented in reference [22]. They observed that the combined-SCR catalysts achieved higher NO_x reduction during the WHTC and are capable of reducing NO_x over a wider range of operating temperature than achieved using either of the individual systems. The best NO_x reduction was achieved using a combined system with a Fe: Cu catalyst ratio of 1:2. To meet the challenge of high NO_x conversion at low temperature, a high porosity substrate which minimizes the pressure drop impact was studied in references [25, 26]. Hirose et al. [25] studied the effect of cell structure, Cu-zeolite amount, high porosity and high cell density on NO_x reduction and pressure drop. They concluded that increasing cell density, porosity and catalyst amount results in 10 –

15% increase in NO_x conversion at high and low temperatures. The improved NO_x conversion efficiency also helps in downsizing the SCR substrate volume by 40 – 50 %.

Recently, many types of doped cerium oxide based catalysts were also studied, such as Ce-Ta [27], Ce-Ti [28], Ce-Mo [29] and Ce-Cu-Ti [30], which demonstrated NO_x reduction similar to Cu-zeolite or Fe-zeolite catalysts as shown in Figure 2.1. These Ce-based composite oxide catalysts exhibit excellent oxygen storage-release capacity, redox properties in the NH_3-SCR reaction and increased area per gram of catalyst. Tao Zhang et al. [27] studied the novel $Ce_aTa_bO_x$ series catalysts prepared by co-precipitation method. The test results indicated that water vapor and SO_2 (150 ppm) inhibits the catalytic activity slightly at 300 °C which may be attributed to the competitive adsorption of H_2O and NH_3 molecules on the acid sites and deposition of ammonium sulfate on the surface of the catalyst which blocked the active sites [31, 32]. However, the NO_x conversion was still maintained at approximately 80%.

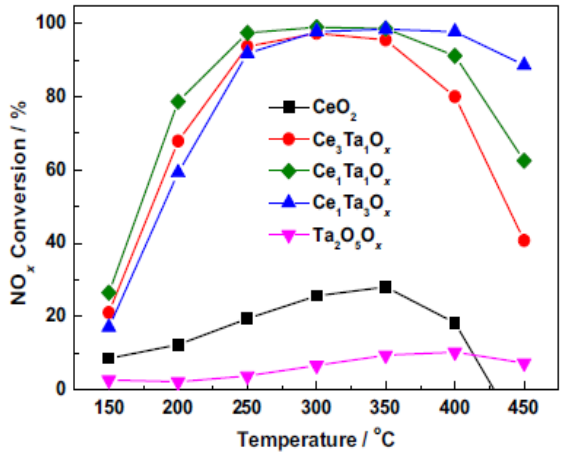

Figure 2.1: NO_x conversion of a cerium oxide based SCR as a function of temperature [27]

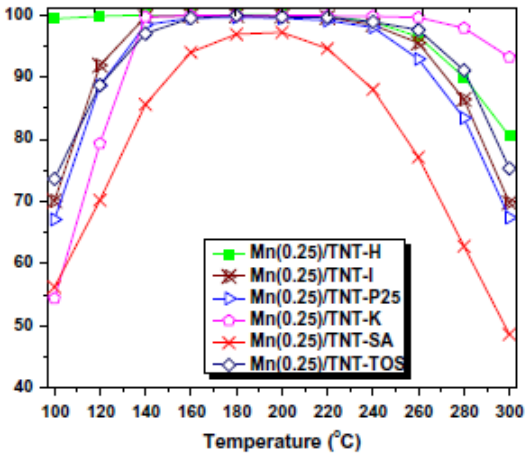

Figure 2.2: NO_x conversion of a Mn(0.25)/Ti based SCR as a function of temperature [33]

A series of manganese oxide based catalysts, supported on TiO_2 nanoparticles were also studied by references [33, 34, 35] since the manganese oxide based catalysts exhibit high NO_x reduction in the low temperature region. Pappas et al. [33] conducted reactor based experiments to study the optimal content of manganese oxide supported on titania

nanotubes and concluded that with the Mn/Ti atomic ratio of 0.25, maximum NO_x conversion efficiency can be achieved in the temperature range of 100 – 300°C. They also observed that the NO_x conversion efficiency greater than 95% can be achieved in the temperature range of 100 – 300°C by using the Hombikat type Mn/Ti SCR catalyst as shown in Figure 2.2. The catalyst exhibited high activity and resistance to steam deactivation.

2.2 Urea Dosing and Mixing Strategies

Due to the complexity of the urea-SCR system and stringent standards for NH_3 slipping out of the catalyst, the optimized urea dosing in the SCR becomes important. In today's applications, urea dosing is controlled using control algorithms that work on strategies including feed-forward control, closed-loop feedback and neutral network model to optimize the availability of NH_3 on the catalytic surface [36, 37, 38]. It is also important to understand how DEF sprays interact with changing exhaust conditions. Gaynor et al. [39] studied a range of dosing strategies in both, ambient air flow (25 – 30 °C) and hot-air flow (200 – 350 °C) to simulate the real world exhaust conditions. They observed that the strategy used to inject DEF has significant impact on spray deflection, spray atomization, droplet distribution and spray-wall impingement within the system. Dong et al. [40] observed that the low quality spray from an injector which used a single hole of 0.9 mm and 0.2 MPa assisted air pressure, leads to deposit formation within the pipe and the SCR catalyst inlet surface and decrease the NO_x conversion efficiency of the SCR. However, a high quality spray from an injector with four holes of diameter 0.25 mm and 0.8 MPa assisted air pressure can avoid the deposit formation.

2.3 SCR Deactivation Effects

The Cu-zeolite and Fe-zeolite based SCR catalysts have exhibited good NO_x reduction performance and durability. However, the catalysts may become deactivated after being exposed to sulfur or hydrocarbon (HC) compounds, prolonged high temperature thermal deactivation and Pt-Pd poisoning. The adverse effect of these factors on the SCR will be discussed in this section.

2.3.1 Sulfur Poisoning

Ultra-low sulfur diesel (ULSD with sulfur less than 15 ppm) has been used in the US since 2006. However, even with the use of ULSD, sulfur poisoning can negatively impact the overall SCR performance [41]. The impact of sulfur poisoning was more significant in Cu-zeolite than Fe-zeolite catalyst and the damaging effect was noted mainly below 300 °C [42, 43]. Theis et al. [43] found that for Cu-zeolite, the effect of continued exposure to SO_2 was significant and more sensitive at low temperatures than at the high temperatures, indicating that desulfation may occur at higher temperatures. For the Fe-zeolite catalysts, there was little impact of SO_2 on the NO_x conversion at low temperatures. It was concluded that the NO_x reduction performance of poisoned catalyst could be fully recovered after desulfation for 5-10 minutes of lean operation at 650 °C for Cu-zeolite and 750 °C for Fe-zeolite. It was also noticed that the NO_x reduction sensitivity to the presence of SO_2 at low temperature was reduced after multiple poisoning and desulfation cycles. Cavataio et al. [19] found similar results for desulfation of Cu-zeolite and Fe-zeolite catalyst. However, they concluded that the relatively high-temperature necessary for desulfation was related to the decomposition of sulfates, rather than a simple desorption of adsorbed SO_2.

2.3.2 SCR Thermal Aging

Aftertreatment systems exposed to high temperatures (>600°C), may cause irreversible damages to the catalysts and deteriorate the NO_x reduction performance of the SCR. Hence, it becomes important to understand the thermal aging and hydrothermal deactivation of the SCR catalyst. The hydrothermal aging effects were studied by references [44, 45, 46, 47]. In general, deactivation of zeolite catalysts by hydrothermal aging can occur by can occur through three mechanisms, i.e. dealumination, sintering and thermal collapse [48, 49]. When a zeolite is heated to elevated temperatures, its structure changes to denser crystalline phases, such as quartz [50]. The presence of water further accelerates this phase transition by attacking the aluminum site through a dealumination process causing loss of NH_3 storage capacity of the catalyst. The copper sintering

contributes to a loss of catalytic active sites, since the copper can be sequestered into large particles or removed from the catalyst [44]. Luo et al. [46] observed 10 – 15% loss in NO_x conversion efficiency at low and high SCR inlet temperatures, when hydrothermal temperatures were increased from 550 – 850°C. NH_3 storage at 200°C decreases from 2.4 to 1.8 g/L upon aging from 550°C to 850°C [51].

2.3.3 Hydrocarbon and Chemical Poisoning

It is well known that zeolites can absorb and store a considerable amount of hydrocarbons (HCs). HCs may reach the SCR catalyst, block the active sites and degrade the performance of the SCR causing a HC poisoning effect. Some HCs may get polymerized and form carbonaceous deposits on the catalyst. To regenerate the active sites, exposure to high temperatures will be required [52]. During the cold start conditions or when the upstream DOC is aged, significant amounts of HC can be stored on the SCR catalyst. The stored HC will be oxidized based on subsequent stages of operation and raising the temperature of the SCR causes thermal deactivation of the SCR [53]. It has been reported that the propylene has a negative effect on the zeolite and vanadia-based SCR, due to HC deposits inhibiting the formation of NO_2 and adversely affecting the standard and fast SCR reactions [51, 54, 55].

Chemical poison from engine oil and bio-diesel such K, P, Na and Ca have been reported to have negative impact on the performance of the SCR catalysts. The phosphorous poisoning causes metaphosphates to replace hydroxyl groups on the active isolated iron species on Fe-BEA zeolites [56]. Results show that the increased amount of K and Na contamination resulted in a linear decline of BET surface area, NH_3 storage capacity, acid sites and the subsequent NO_x reduction [57].

2.4 Modeling the Kinetics of the SCR Reactions

A numerical model aims at simulating the performance of the SCR including NO_x reduction, NH_3 storage, NH_3 slip and SCR outlet temperature in a wide range of scenarios. Models includes SCR reaction kinetics, NH_3 adsorption and desorption kinetics and the mass and heat transfer process. This section will explain the SCR

reaction mechanisms and estimation of kinetics for SCR reactions for the 1-D flow through SCR model developed at MTU by reference [9]. The 1-D SCR model considers one single channel, which is discretized into 10 finite elements from inlet to outlet. The model consists of two sites S_1 and S_2. The 1st site S_1, supports NH_3 adsorption, desorption and all the SCR reactions. Whereas, the 2nd site S_2, supports only NH_3 adsorption and desorption. NH_3 is the only species that is assumed to be stored on the catalyst surface. The exhaust flowing through the channel is known as gas phase or bulk phase. The species are transported from the gas phase to the surface phase. The SCR reactions between the stored NH_3 and the species occur on the catalyst surface. Assuming all the reactions occur on the catalyst surface, mass transfer between gas phase and the surface phase are included in the model. The equations are described in section 4.1.1 in reference [9]. Heat transfer between the bulk flow and the substrate and between the substrate and the ambient is included to simulate the SCR outlet temperatures under transient conditions [9]. However, the heat release due to the SCR reactions is negligible and was set to zero in the model.

The global chemical reactions for the urea-SCR system include urea decomposition reactions and the SCR reactions that occur on the catalytic surface [9]. A numerical model simulating the spray interaction with the exhaust gas is presented in references [58, 59, 60, 61]. The injected urea goes through a 4-step mechanism of decomposition to produce NH_3 [58] . The first step is injection of atomized, aqueous urea solution into the hot exhaust stream as shown in equation 2.1. This is followed by evaporation of water from the droplets, yielding molten urea. In the third step, pure urea thermally decomposes to equimolar amounts of ammonia and isocyanic acid as shown in equation 2.3. In the last step, isocyanic acid is hydrolyzed to NH_3 and CO_2 on the catalyst surface as given in equation 2.4. Isocyanic acid is stable in the gas phase and requires a catalytic surface to accelerate the hydrolysis reaction [9, 62]

$NH\text{-}CO\text{-}NH_2(sol) \rightarrow NH\text{-}CO\text{-}NH_2(droplets)$ Eqn. 2.1

$NH\text{-}CO\text{-}NH_2(aq) \rightarrow NH_2\text{-}CO\text{-}NH_2\ (molten) + xH_2O\ (gas)$ Eqn. 2.2

$NH\text{-}CO\text{-}NH_2(molten) \rightarrow NH_3\ (gas) + HNCO\ (gas)$ Eqn. 2.3

$HCNO\ (gas) + H_2O\ (gas) \rightarrow NH_3\ (gas) + CO_2(gas)$ Eqn. 2.4

The four steps correspond to the overall urea decomposition shown in reaction 2.5.

$NH\text{-}CO\text{-}NH_2\ (aq) + H_2O\ (gas) \rightarrow 2NH_3\ (gas) + CO_2\ (gas)$ Eqn. 2.5

However, due to complexity of the decomposition process, it was not included in the numerical simulations of the SCR chemistry. It was assumed that the urea was completely converted to NH_3 and the conversion occurred in the decomposition tube and in the first substrate of the SCR system. The stored NH_3 reacts with the species in the surface phase [9]. The NH_3 storage equations for the two sites are described in the equation 4.5 in reference [9]. $NH_{3(ads),1}$ and $NH_{3(ads),2}$ are the NH_3 molecules adsorbed on the catalytic surface of each site.

The global SCR reactions taking place on the surface phase consists of 12 reactions as shown in Table 2.1 (Table 4.1 from reference [9]). R1 and R2 represent the NH_3 adsorption and desorption on the surface of the catalyst on the 1st site. R3 and R4 represent the NH_3 adsorption and desorption on the surface of the catalyst on the 2nd site. Reactions R5 to R12 are the SCR reaction mechanisms than take place on the 1st site. R5 and R6 are the oxidation reaction of adsorbed NH_3, selectively oxidized to NO or N_2. R7 and R8 are the standard reactions which have different NH_3/NO_x stoichiometry ratio. The higher NH_3/NO_x stoichiometry ratio for R8 explains the overconsumption of NH_3. The fast and slow reactions are given in R9 and R10 respectively. R11 is a reversible reaction which considers oxidation of NO and decomposition of NO_2. R12 is N_2O formation reaction.

The reaction rate constants for the twelve reactions are described by the Arrhenius equation shown in equation 2.6. The equations for all reactions are provided in Table 2.1.

$$k = Ae^{-\frac{Ea}{RT}} \qquad \text{Eqn. 2.6}$$

Where A is the pre-exponential factor, E_a is the activation energy (J/mol), R is the universal gas constant (8.314 J/mol K) and T is the temperature (K).

Table 2.1: Reactions included in the 1-D SCR model from reference [9]

No.	**Description**	**Reaction Equation**
R1	Adsorption (Site1)	$NH_3 + S1 \rightarrow NH_{3(ads),1}$
R2	Desorption (Site 1)	$NH_{3(ads),1} \rightarrow NH_3 + S1$
R3	Adsorption (Site 2)	$NH_3 + S2 \rightarrow NH_{3(ads),2}$
R4	Desorption (Site 2)	$NH_{3(ads),2} \rightarrow NH_3 + S2$
R5	NH_3 Oxidation 1 (Site 1)	$4NH_{3(ads),1} + 3O_2 \rightarrow 2N_2 + 6H_2O$
R6	NH_3 Oxidation 2 (Site 1)	$4NH_{3(ads),1} + 5O_2 \rightarrow 4NO + 6H_2O$
R7	Standard SCR 1 (Site 1)	$4NH_{3(ads),1} + 4NO + O_2 \rightarrow 4N_2 + 6H_2O$
R8	Standard SCR 2 (Site 1)	$5NH_{3(ads),1} + 3NO + 9/4O_2 \rightarrow 4N_2 + 15/2H_2O$
R9	Fast SCR (Site 1)	$4NH_{3(ads),1} + 2NO + 2NO_2 \rightarrow 4N_2 + 6H_2O$
R10	Slow SCR (Site 1)	$4\ NH_{3(ads),1} + 3NO_2 \rightarrow 7/2N_2 + 6H_2O$
R11	NO Oxidation and NO_2 Decomposition (Site 1)	$2NO + O_2 \leftrightarrow 2NO_2$
R12	N_2O Formation (Site 1)	$6NH_{3(ads),1} + 8NO_2 \rightarrow 7N_2O + 9H_2O$

2.5 SCR Catalyst on the DPF

The sequential arrangement of DOC, DPF and SCR has the following challenges:

1) The volume of the conventional arrangement of DOC, DPF and SCR catalysts is very large (34.5 L) as shown in Table 1.2. The demand for higher NO_x reduction may require more SCR catalyst, further increasing the volume of the conventional aftertreatment system.
2) The SCR inlet temperature is insufficient during cold start when the DPF is located upstream of the SCR. This arrangement deteriorates the NO_x reduction ability of the SCR.
3) The placement of the SCR upstream of the DPF is an unfavorable condition for passive oxidation of PM accumulated in the DPF, due to reduction of NO_2 and heat loss to the ambient in the SCR.

The problem can be potentially resolved by integrating the SCR and DPF functions into one single filter, by coating catalysts on or inside the walls of the DPF. The 2-way SCR/DPF reduces the volume and mass of the aftertreatment system when compared with DPF and flow through type SCR [11, 63]. Moreover, SCR-on-filter offers potential for higher NO_x conversion efficiency due to increase in the effective reaction surface for SCR and higher substrate temperature due to passive oxidation of PM. A schematic of conventional DPF, SCR and SCR-on-DPF from reference [11] is shown in Figure 2.3.

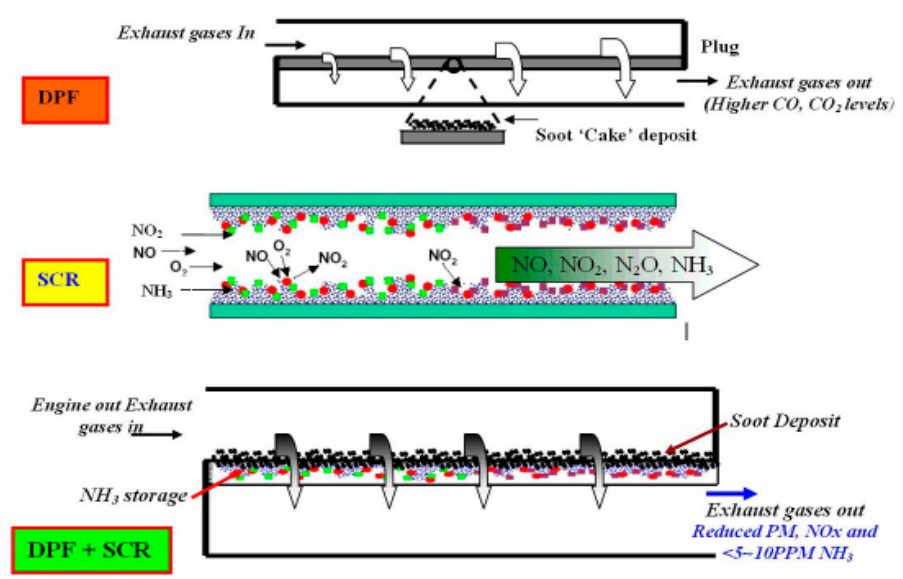

Figure 2.3: Schematic of conventional DPF, SCR and SCR-on-filter [11]

5.1 PM Oxidation

Tronconi et al. [64] performed modeling and experimental based studies to evaluate the effect of NH_3 on passive oxidation characteristics of a Cu-zeolite SCR-on filter. A comparison of modeling results for passive oxidation in the presence and absence of NH_3 is shown in Figure 2.4. The NO_2/NO_x molar feed ratio was varied from 0 to 1. In Figure 2.4a, both the CO_2 and CO peaks recorded in the presence of NH_3 are shifted to slightly lower temperatures of approximately by 50 °C, which suggests that NH_3 had positive effect on active regeneration of PM. Figure 2.4c and d, confirm that the addition of NH_3 significantly reduces the passive oxidation of PM at low temperature, since under these conditions, the fast SCR reaction (R9 in Table 2.1) and NO_2 SCR reaction (R10 in Table 2.1) successfully compete with the PM oxidation and the NH_3-SCR reactions (R9, R10 and R11 in Table 2.1) are the preferred pathway for NO_2 consumption. This phenomenon has to be carefully considered for applications which rely on passive oxidation.

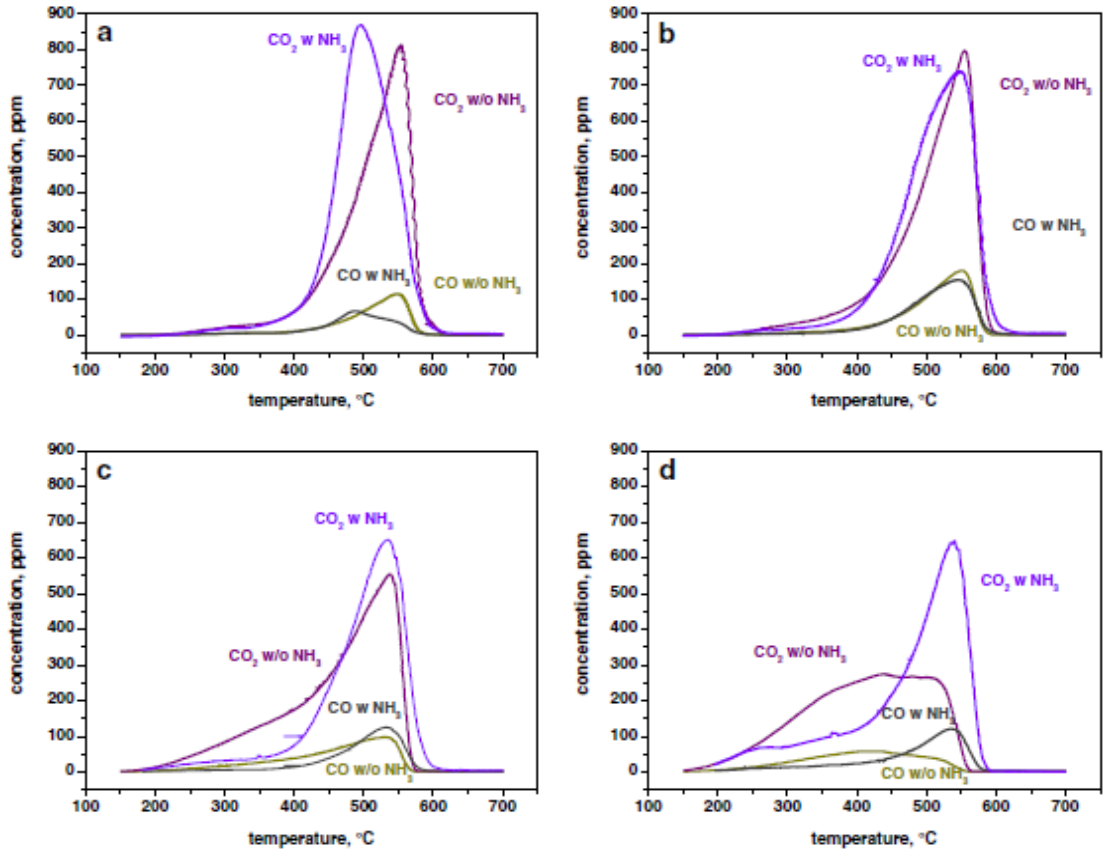

Figure 2.4: Effect of NH_3 and NO_x on the passive oxidation. GHSV=15 k/hr, H_2O=5%, O_2=8% when NH_3 is present, NH_3=500 ppm. a NO_x=0 ppm, b NO_x=500 ppm, NO_2/NO_x=0 [64]

Naseri et al. [65] compared the steady state performance of a Cu-zeolite SCR-on filter with the CPF, after loading both the filters up to 3 g/L. Passive oxidation experiments were conducted for 30 minutes at a DOC inlet temperature of 300 and 400 °C, using a 2007 MY heavy duty diesel engine. During tests with the SCR-on-filter, the engine out NO_x was 4.5 g/hp-hr, whereas for CPF tests the engine out NO_x was less than 1.0 gm/hp-hr. At 300 °C the CPF gained 10% weight (3.3 g/L for initial PM loading of 3 g/L) at the end of 30 minutes, whereas the SCR-on-filter gained 20% weight (PM loading 3.6 g/L for initial PM loading of 3 g/L) at the end of 30 minutes, with the urea injection during the 30 minutes at ANR of 1.2. The passive oxidation in SCR-on-filter was further studied with and without urea injection at the same DOC inlet temperatures. At 300 °C the SCR-

on-filter without urea gained 5% weight (3.15 g/L for initial PM loading of 3 g/L) when compared to 20% weight gain (3.6 g/L for initial PM loading of 3 g/L) with urea injection at ANR of 1.2. At 400°C the PM was oxidized by 25% (2.25 g/L for initial PM loading of 3 g/L) for no urea injection when compared to 19% PM oxidation (2.43 g/L for initial PM loading of 3 g/L) with urea injection at ANR of 1.2.

Czerwinski et al. [66] studied the passive oxidation performance of a SCR-on-filter with PM loading of 3 g/L. They observed that urea dosing significantly hinders passive oxidation. The passive oxidation efficiency decreased from 81% without urea injection to 42% with urea injection at ANR of 1.0. Similar passive oxidation trends for SCR-on-filter were observed by references [67, 68]. Enhanced PM oxidation can be achieved by calibrating the engine to a higher NO_x/PM ratio and designing the DOC to provide NO_2/NO_x ratio >0.5 [69].

2.5.2 NH_3 Storage and Oxidation

Tan et al. [70] characterized the NH_3 storage in a Cu-zeolite SCR-on-filter and the effects of PM loading and catalyst aging on the NH_3 storage through reactor experiments. The PM loading reduced the NH_3 storage over degreened SCR-on filter by 30%. However, the impact of aging on NH_3 storage was insignificant. The impact on NH_3 storage for degreened and aged SCR-on-filter was minimal up to PM loading of 1.2 g/L.

Schrade et al. [71] performed temperature programmed desorption (TPD) experiments on Cu-zeolite SCR-on-filter, with and without PM loading in the filter. The experiments were conducted for the SCR-on-filter inlet temperature range of 150 – 250 °C. They observed that the NH_3 storage for the SCR-on-filter with PM loading of 2.5 and 9 g/L was 12- 20% higher when compared to the NH_3 storage for the SCR-on-filter without PM loading.

The presence of PM has marginal influence on the NH_3 oxidation [64]. During the steady state condition, the loaded SCR-on-filter shows slower and reduced NO_x reduction and higher NH_3 slip when compared to empty SCR-on-filter, due to use of some the NO_2 for PM oxidation. To avoid NH_3 slip, it is recommended to avoid passing ANR of 0.9 [72].

2.5.3 NO_x Reduction

Understanding the NO_x reduction characteristics of the SCR-on-filter is another challenge. In a flow-through SCR, the catalyst is located on the wall while in case of SCR-on-filter, the catalyst is located inside the wall or on the wall of the inlet and outlet channel. Various research groups have concluded that the SCR-on-filter can achieve NO_x conversion efficiency close to those of flow-through SCR catalysts [10, 65, 73]. However, the PM loading on the filter and decrease in residence time affect the NO_x reduction performance of the catalyst. PM loading has minimal impact on standard SCR and fast SCR reactions and also improves NO_x conversion between 250 – 400 °C due to oxidation of PM. The competition between SCR and PM oxidation reactions for consumption of NO_2 in a SCR-on-filter is schematically illustrated in Figure 2.5 [64]. A summary of published research is described in the following paragraphs.

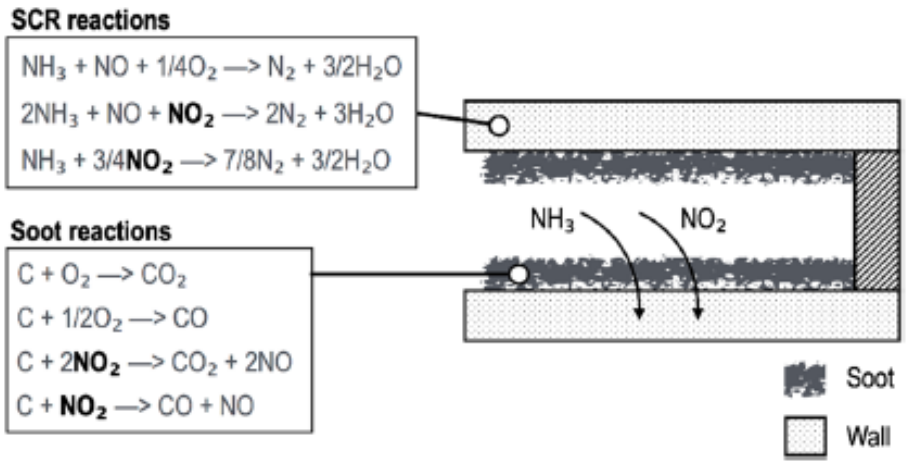

Figure 2.5: Competition between passive oxidation and SCR reactions [64]

Tang et al. [69] conducted steady state and transient tests on a 9.3L 2011MY HDD engine, to investigate the NO_x reduction performance of Cu-zeolite SCR-on-Filter. During steady state testing, with ANR of 1.0, a NO_x conversion efficiency of 90% was achieved at an exhaust temperature of 465 °C and NO_2/NO_x ratio of 0.12. The NO_x conversion dropped to 87% at an exhaust temperature of 250 °C and unfavorable NO_2/NO_x ratio of 0.74. For 1 Cold and 3 Hot NRTC tests, the cumulative NO_x

conversion of 92.6 and 95.5% was observed with a clean and pre-loaded PM to 6.2 g/L respectively, at ANR of 1.05. Computational results suggest that the kinetic rates for the SCR reactions are much faster than the NO assisted reactions of PM. This is a result of reduced local NO_2 concentrations in the PM cake layer which is due to a strong forward diffusion/flow of NO_2 [69].

Johansen et al. [74] investigated the Cu-DPF and V-DPF based SCR-on-filter with material porosity of 73 and 65%, for reactor and engine based experiments respectively. Engine tests indicate that the V-DPF shows better NO_x conversion than the Cu-DPF during the NRTC, although ammonia slip is lower for Cu-DPF due to its superior ammonia storage capacity. However, the steady state 8-mode test demonstrated that the Cu-DPF has better NO_x conversion than the V-DPF at high temperatures, although at intermediate temperature, the NO_x conversion was similar for both the catalysts as shown in Figure 2.6. Reactor tests indicate that below 300 °C, the Cu-DPF has a much higher NO_x conversion than the V-DPF. N_2O formations are similar and kept low below 450°C.

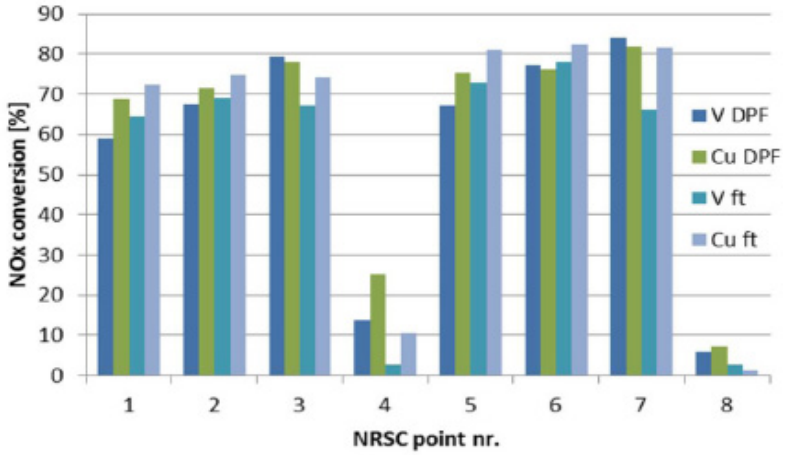

Figure 2.6: NO_x conversions for V-DPF and Cu-DPF compared to V-ft and Cu-ft during NRSC [74]

Raymond Conway et al. [75] conducted field trials on a 1998 MY Detroit Diesel S60 engine equipped with a Cu-zeolite SCR-on-filter of 26.1 L and under floor Cu-zeolite SCR of 21.8 L. They concluded that NO_x reductions of 95% can be achieved with ANR close to 1. They also observed that by reducing the SCR catalyst volume by 27%, the

NO_x reduction continued to remain between 90 – 100% depending on the inlet temperature. Kojima et al. [76] conducted experiments on a Honda 2.2L i-DTEC engine and compared the NO_x reduction performance of a 2.5 L SCR and SCR-on-filter during the steady state and FTP72. They observed that the NO_x reduction in the SCR-on-filter was 15-20% lower than the flow through SCR, below 200 °C. The difference reduced to 10 % at temperatures above 300 °C. This could be attributed to shorter residence time in the SCR-on-filter when compared to the SCR, since the catalyst is coated inside the wall in the case of SCR-on-filter. They also found that at temperatures below 200 °C, the PM loading of 3 g/L decreased the NO_x conversion efficiency of SCR-on-filter by 5-10% when compared to no PM loading.

Rappe et al. [77] conducted experiments on a Cu-zeolite catalyst based SCR-on-filter with a 2003 VW Jetta TDI engine. They observed that the SCR-on-filter provides >90% NO_x conversion without PM loading in the SCR-on-filter at ANR of 1.0, for inlet temperatures between 250 – 400 °C and NO_2/NO_x ratio between 0.45 – 0.50. However, the NO_x conversion decreased for the NO_2/NO_x ratios above or below 0.50. The NO_x conversion of the SCR-on-filter with PM loading of 4 g/L improves by 8 – 10 % for inlet temperatures below 300°C and NO_2/NO_x ratio 0.6. Conversely, for a NO_2/NO_x ratio of 0.45, the NO_x conversion decreases for the inlet temperatures between 250 – 350°C. A summary of the representative experimental studies is described in Table 2.2.

Table 2.2: Summary of experimental studies with SCR-on-DPF

Organizations	Year	Experimental Setup	Major Conclusions	Reference
Politecnico di Milano Aristotle University	2015	Reactor tests on Cu-zeolite SDPF.	• PM loading improves the NO_x conversion efficiency between 250-400 °C. • PM has marginal influence on the NH_3 oxidation, standard SCR and fast SCR activity. • NH_3 significantly reduces the passive oxidation of PM at low temperature.	[64]
UAS, TTM, AEEDA, BAFU	2015	3.0 L Iveco engine equipped with a DOC and SDPF. Steady state and transient experiments were performed.	• For SCRF® loaded to 3 g/L, the passive regeneration decreases from 81% without urea injection to 42% with urea injection. • NO_x conversion efficiency decreased to 40-45% in WHTC against 75% in ETC at ANR of 0.9.	[66, 72]
University of Wisconsin KIMM	2015	Cu-zeolite SCR Filter with porosity of 45 % and 60 g/L was evaluated on an engine setup	• Soot deposition around the catalyst surface impedes transport process, thus lowers SCR reaction rates. Participation of NO_2 is more in SCR reactions than PM oxidation. • Energy released from PM oxidation affects the SCR reactions and vice versa.	[63]
Haldor Topsoe A/S	2014	Cu-DPF and V-DPF with 65% porosity and 139 and 129 g/L was tested on 13 L engine downsized to 7 L	• During WHTC, V-DPF shows lower NO_x conversion and higher NH_3 slip than Cu-DPF. • During NRTC, V-DPF shows higher NO_x conversion and ammonia slip than Cu-DPF. • Soot balance point temperature is unaffected without and with urea dosing.	[74]
Johnson Matthey	2014	9L engine with 5.6 gm/hp-hr engine-out NO_x equipped with DOC, SCRF®, SCR and HPS SCR	• During hot FTP, SCR+SCR (total vol. 17 L) showed NO_x conversion of 83% in comparison to 88% for SCRF®+SCR (total vol. 25.5 L) and 91% for SCRF®+HPS SCR. • NO_x conversion during cold FTP was 77% for SCRF®+HPS SCR and was improved by 19% with thermal management and NH_3 pre-saturation.	[78]

2.6 Modeling of SCR Catalyst on the DPF

The simulation model is a useful and reliable tool to design and optimize the aftertreatment devices. It allows investigation of wide range of scenarios in a time and cost effective way. It also provides insight into the kinetics of the reactions and the internal states of the catalyst which cannot be measured using the experimental setup. One of the main objectives of the modeling studies is to understand the interaction between the SCR reactions and the PM oxidation, since SCR reactions occur on the surface, whereas, PM is deposited inside the wall and on the cake layer. There is also the need to understand the temperature and PM distribution along with the filtration efficiency that is related to the PM in the wall and the resulting pressure drop across the filter. A summary of the modeling studies is presented in Table 2.2.

Yang et al. [63] considered that the deposition of PM on the surface deteriorates the mass transport of the species from gas stream to the catalyst surface, which in turn weakens the SCR reactions. The model also assumes that the passive oxidation of PM changes the NO_2/NO_x ratio, which can have positive or negative impact on SCR reactions, depending on the NO_2/NO_x ratio being higher or lower than 0.5 respectively. However, if the reaction rate for NO_2 assisted oxidation of PM is much lower than the reaction rate for SCR reactions, then passive oxidation will have minimum impact on the SCR reactions. The energy released by oxidation of PM is another factor that influences the SCR reactions [63]. The substrate temperature increases with the oxidation of PM, which promotes the SCR reactions.

Strots et al. [79] and Schrade et al. [71] demonstrated that the PM reaction model and the SCR kinetics sub-model are sufficient to model the interactions between the SCR and PM oxidation reactions observed in SCR-on-filter substrates. The PM reaction model [71] consists of PM oxidation by NO_2 and oxygen, both pathways producing CO and CO_2. Oxidation of CO on the SCR catalyst is also included in the model. The SCR sub-model includes NH_3 storage on two sites, reaction between NH_3 stored on the catalyst with the NO and NO_2 in the exhaust stream. The oxidation of NH_3 and NO as well as formation

and reactions of N_2O are also included in the SCR in the model. A summary of the representative modeling studies is described in Table 2.3.

The next chapter describes the experimental setup, instrumentation and test matrix used for the experimental study of the NO_x reduction and NH_3 storage in the production-2013-SCR and the SCRF®, with and without PM loading in the SCRF®.

Table 2.3: Summary of modeling studies on SCR-on-filter

Organizations	Year	Major Conclusions	Reference
University of Wisconsin, KIMM	2015	• Developed by combining DPF and SCR model. Filtration, pressure drop, flow field, temperature field and two-layer models included. • PM oxidation by NO_2 and O_2 and eight SCR reactions were included. • Passive oxidation changes effective NO_2/NO_x ratio, which has an impact on SCR reactions	[63]
Politecnico di Milano, Aristotle University,	2015	• Model developed by [Colombo] was modified for Cu-zeolite SDPF. Integration of SCR reactions into the DPF model in AxiSuite. • NO promotion of NH_3 oxidation was disregarded over Cu zeolites. • Spillover of NH_3 onto redox sites was eliminated. • N_2O reactivity with NO and NH_3 were disregarded	[64]
Johnson Matthey	2012	• Model created by combining SCR reactions with the CPF. • Mass, momentum and energy balance for gas in inlet and outlet channel. • Diffusion through washcoat is neglected. PM in filter wall is not considered. • PM oxidation by NO_2 and O_2. 9 SCR reactions included in the model. • Model was validated for LD and HD engine data.	[67]
IAV, GmbH	2014	• Aftertreatment and vehicle models created in Simulink-based simulation environment, VeLoDyn. Catalyst models were converted from AxiSuite in reference [73] into Simulink S-functions in reference [84]. • The DPF model was replaced by the SCR/DPF catalyst model and SCR catalyst volume was adjusted. Active DPF regeneration was not used • AdBlue injection control matches the NH_3 storage and reactivity of the SCR. • Thermal losses to environment and cooling caused by AdBlue are included for realistic temperature profile.	[79, 71]

Chapter 3. Experimental Setup, Instrumentation and Test Procedures

This chapter explains the test cell setup for the ISB 2013 engine, the production aftertreatment system and the SCRF®, including the instrumentation and the test procedures for various aftertreatment configurations. The steady state engine experiments were conducted to evaluate the NO_x reduction and NH_3 storage performance of the production-2013-SCR and the SCRF® in the Heavy Duty Diesel Laboratory on the campus of Michigan Technological University.

The overall experimental program to study the Baseline System and the SCRF® is shown in Figure 3.1. The Baseline System is the production aftertreatment system supplied by Cummins and it consists of a DOC, a CPF and a SCR (production-2013-SCR).

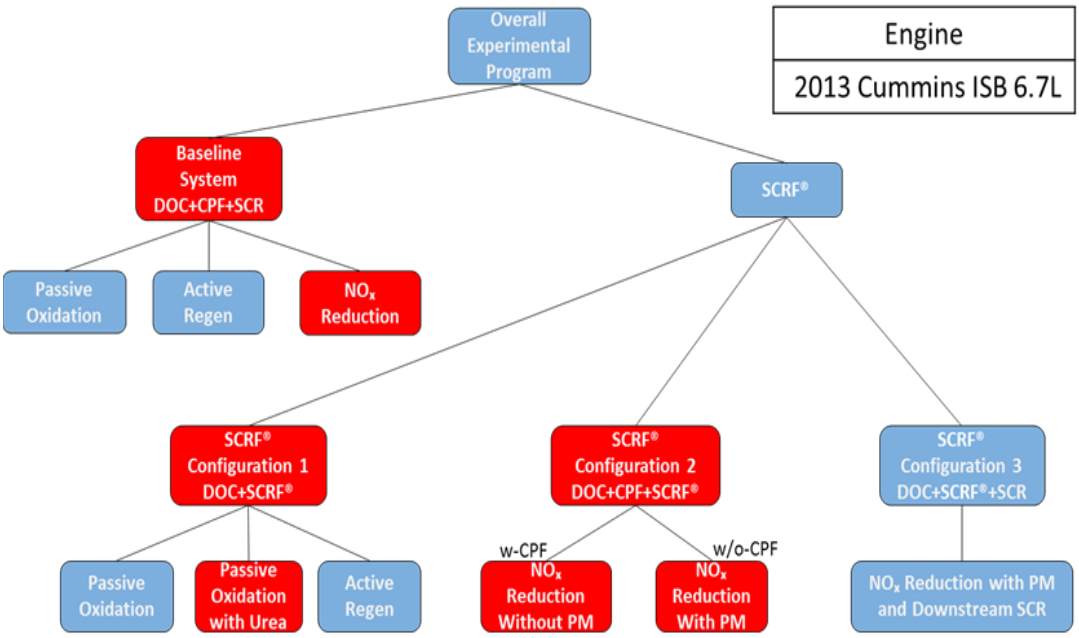

Figure 3.1: Overall experimental program

The PM oxidation, PM loading and PM filtration performance of the CPF and the NO_x reduction and NH_3 storage performance of the production-2013-SCR were determined from the experiments conducted on the Baseline System. The experimental PM data obtained from the Baseline System, presented in the thesis [3], were used to calibrate the MTU 1-D CPF model [80] and the NO, NO_2 and NH_3 data were used to calibrate the MTU 1-D SCR model [9]. The MPF model in reference [13] has been used to develop a SCR-F model and it will be used to calibrate the baseline data and configuration 1, 2 and 3 data as shown in Figure 3.1.

The configuration-1 was performed to study the PM oxidation, PM loading and PM filtration performance of the SCRF®, with and without urea injection in the SCRF®. The configuration-2 was performed to study the NO_x reduction and NH_3 storage performance of the SCRF®, without PM and with 2 and 4 g/L of PM in the SCRF®. The purpose of configuration-3 is to study the NO_x reduction performance of the SCRF® and the SCR together and evaluate the effect of ANR >1.0 on the NO_2 assisted PM oxidation of the SCRF®. The experimental data collected for the SCRF® will be used to develop and calibrate the SCR-F model being developed at Michigan Tech. The model would be used to simulate the PM filtration efficiency, pressure drop, PM oxidation kinetics, SCR reaction kinetics and substrate temperatures for the SCRF®. The configurations highlighted in red in Figure 3.1 are the main focus of this thesis.

3.1 Engine Test Cell Setup

The test cell setup was done to measure, monitor and record the various parameters which determine the performance of the diesel aftertreatment components. A picture of the test cell is shown in Figure 3.2. The layout of the engine, Baseline System (production aftertreatment components), sensors and sampling locations within the test cell are shown in Figure 3.3. The engine exhaust flows through a 4-inch diameter exhaust pipe, from where it can be directed either into the trap line, which has the aftertreatment components, or directly to the building exhaust through the bypass line. The path of exhaust flow is selected by opening or closing the pneumatic butterfly valve mounted in each exhaust line. In the trap line, the exhaust gas flows through a 25 kW exhaust heater

which can be used to raise the temperature of the gas entering the aftertreatment system. This enables the evaluation of the aftertreatment system in a controlled and elevated temperature range without changing engine operating conditions [9].

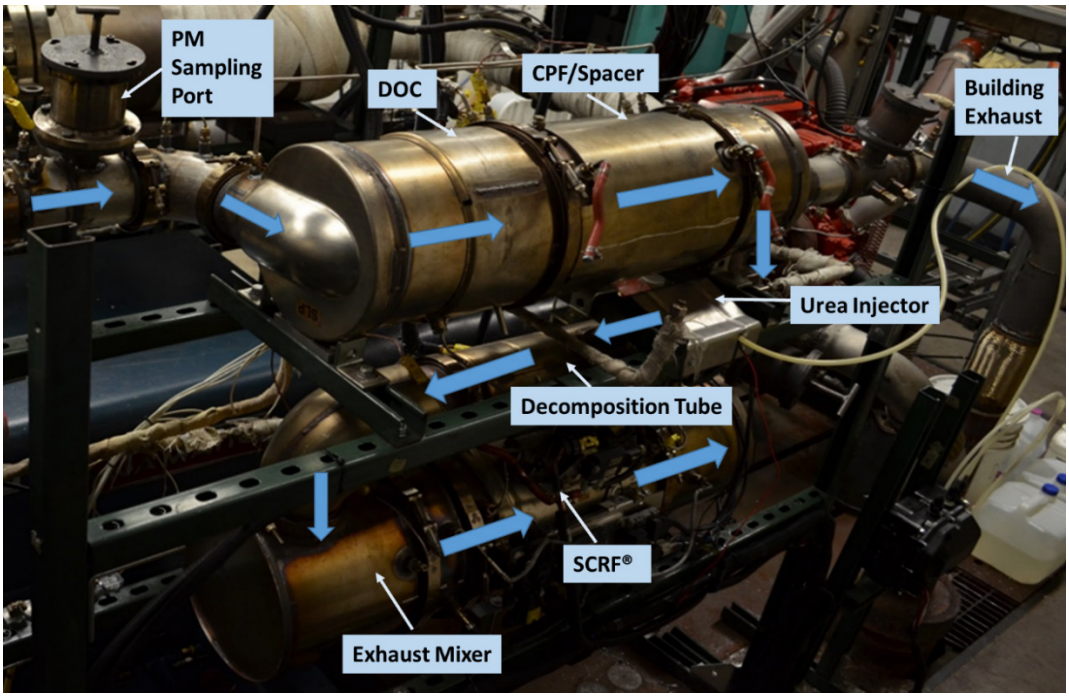

Figure 3.2: A picture from the heavy duty diesel lab at MTU

The exhaust flows through the DOC, where the HC, CO and NO are oxidized to H_2O, CO_2 and NO_2. The next component in the production set-up is the CPF where PM is filtered and oxidized. Then the exhaust flows through the decomposition tube on which the DEF injector is mounted. The next component is a mixer to ensure homogenous mixing of the DEF decomposition products/droplets and the exhaust gas. After this, exhaust flows through the two SCR-A substrates (production-2013-SCR) and then to the building exhaust through another mixer downstream of the SCR substrates. The mixer downstream of the production-2013-SCR ensured proper mixing for tailpipe emission measurements by the IMR-MS, and the NO_x and the NH_3 sensors. The production aftertreatment system has one SCR-A substrate (only SCR catalyst present) followed by one SCR-B substrate (SCR and oxidation catalyst present). However, the SCR-B substrate was replaced by SCR-A substrate in this experimental study, to obtain the NH_3

slip data out of the two SCR-A substrates, which was necessary in order to collect data to calibrate the MTU 1-D SCR model.

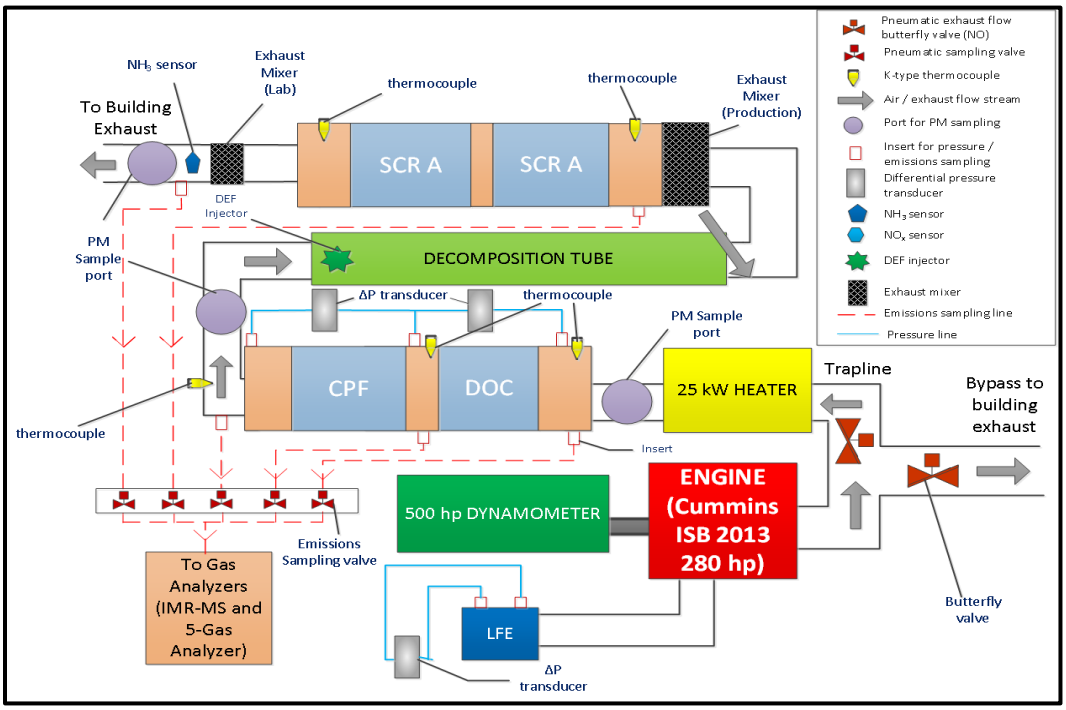

Figure 3.3: Schematic of test cell with the production engine and aftertreatment system and the instrumentation [3]

The passive oxidation experiments with urea injection were performed with the SCRF® in configuration-1 as shown in Figure 3.1. One of the objectives of this configuration was to study the effect of NO_x reduction in the SCRF® on the NO_2 assisted PM oxidation kinetics of the SCRF®. During the passive oxidation experiments with urea injection, conducted in configuration-1, the CPF was replaced with the spacer and the two SCR-A substrates were replaced with the SCRF® and the spacer as shown in Figure 3.4. The NO_x reduction experiments with the SCRF®, with and without PM loading in the SCRF® were performed in configuraton-2, as shown in Figure 3.1. The schematic for configuration-2 is shown in Figure 3.5. During the NO_x reduction experiments without PM loading, the CPF was placed upstream of the SCRF®, to filter the PM entering into the SCRF®. During the NO_x reduction experiments with PM loading, the CPF upstream of the SCRF® was replaced with the spacer. The test procedures for experiments conducted in configurations 1 and 2 are explained later in the chapter.

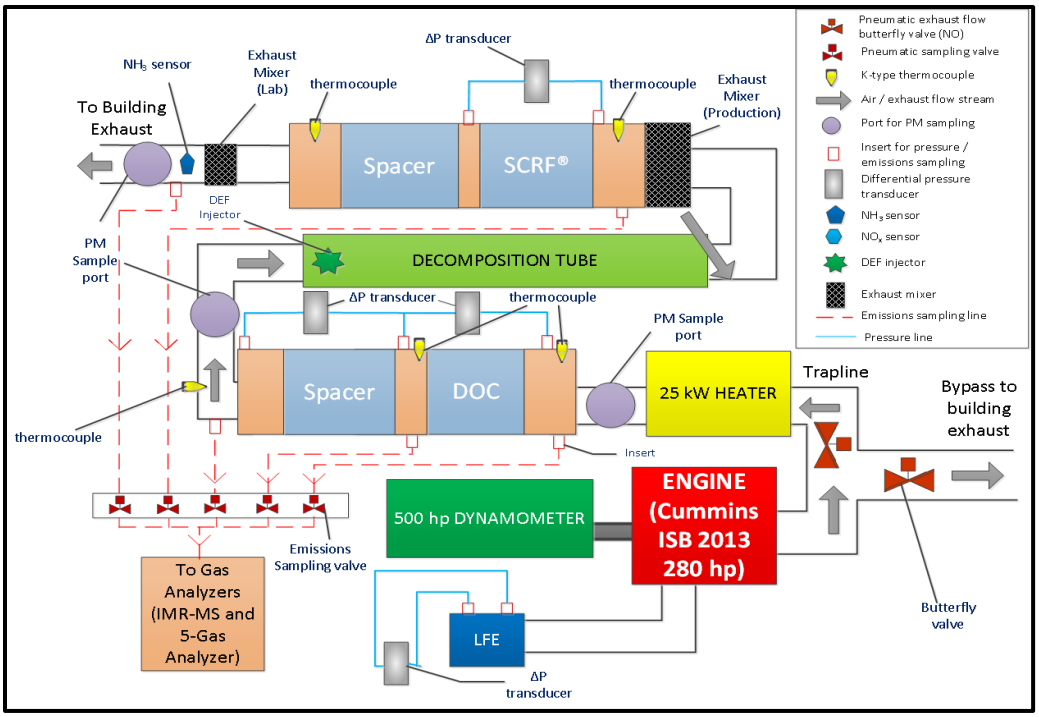

Figure 3.4: Schematic of test cell with the production engine and the SCRF® and the instrumentation for configuration-1 [3]

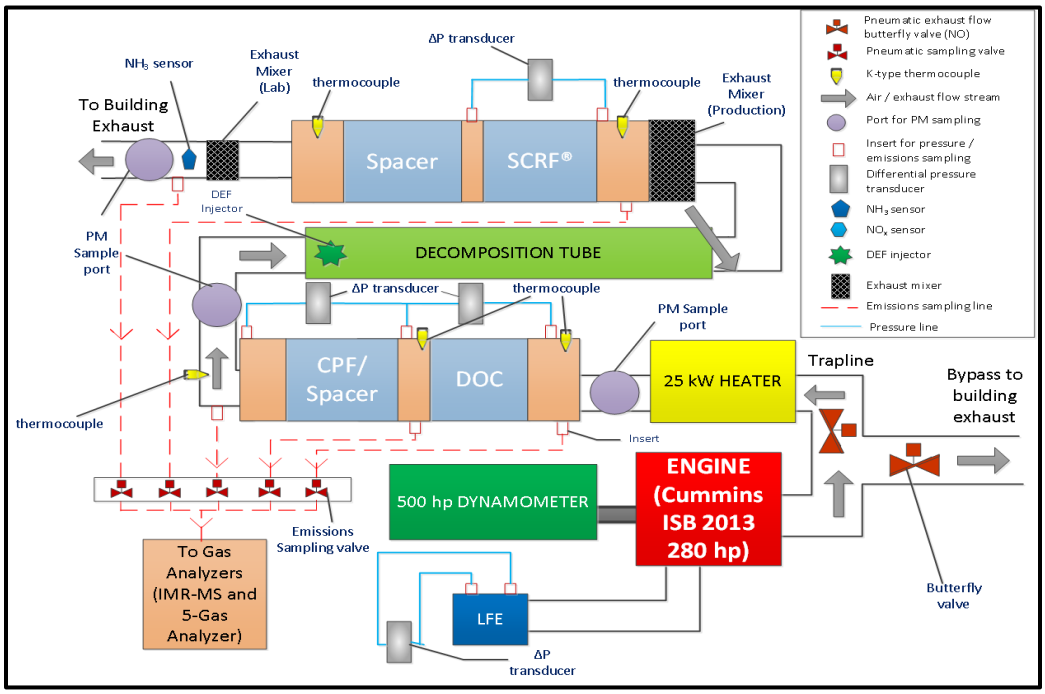

Figure 3.5: Schematic of test cell with the production engine and the SCRF® (with and without the upstream CPF) and the instrumentation for configuration-2 [3]

3.2 Engine and Dynamometer

A Cummins 2013 ISB (280 hp) engine that conforms to the U.S EPA 2013 emission regulations was used in the research. The specifications of the engine are provided in Table 3.1. An engine control module governs the engine and sub-systems such as the common rail fuel injection system, the DEF dosing system and the EGR system.

Table 3.1: Specifications of the Cummins ISB 2013 engine

Model	Cummins ISB 208 kW (280 hp)
Year of Manufacture	2013
Cylinders	6, inline
Bore &Stroke	107 x 124 mm
Displacement	409 in^3 (6.7 L)
Aspiration	Turbocharged
Aftercooling	Cummins Charge Air Cooler
Turbocharger	Variable Geometry Turbocharger (Holset)
Rated Speed and Power	2400 RPM and 209 kW
Peak Torque	895 N·m @1600 RPM
EGR system	Electronically controlled and cooled

The engine was coupled to an eddy current dynamometer which regulates the speed and the load on the engine. The specifications are provided in Table 3.2. The dynamometer was controlled by a Digalog Model 1022A controller and can be operated in the 'constant speed' and 'constant load' modes using the controller. However, during the engine testing, the dynamometer controller was set to the 'constant speed' mode and the throttle was operated to regulate the load on the engine. Throttle (rheostat) varies the fuel flow rate supplied to the engine to apply the desired load on the engine.

Table 3.2: Dynamometer specifications

Manufacturer	Dynamatic
Model Number	AD8121
Peak Power (kW)	373@ 1750-7000RPM
Peak Torque (N-m)	2035@1750RPM

3.3 Fuel Properties

The ULSD that conforms to EPA regulations was used to conduct the experimental tests in this research. The fuel properties from reference [3] are reported in Table 3.3, since the same fuel was used for the experiments.

Table 3.3: Specifications of the fuel used for engine testing from reference [3]

Fuel Type	ULSD -2
API. Gravity at	35.4
SP. Gravity at	0.848
Viscosity at	2.999
Total Sulfur	7
Initial Boiling	184
Final Boiling	363
Cetane Index	48.7
Water Content	34
Higher Heating	45.68
Lower Heating	42.89
H/C[1]	1.833

[1] These values were obtained from reference [81], since similar fuel was used

3.4 Aftertreatment System

The Cummins production aftertreatment system and the SCRF® from Johnson Matthey and Corning were used to conduct the experiments. The production aftertreatment system included a DOC, a CPF, and two SCR-A substrates. The specifications of the production aftertreatment system and the SCRF® are given in Table 3.4.

To reduce the variation in the performance of the catalysts, a de-greening procedure was performed for all the aftertreatment components, prior to conduction of the reported tests. The test cycle recommended by Cummins was used to perform the de-greening procedure. During the de-greening procedure, the engine was run at 1400 RPM and 820 N-m for 12 hours with active regeneration for 30 mins, starting off after 4 hours and recurring every 2 hours after that. The exhaust conditions during the de-greening procedure are given in Table 3.5.

Table 3.4: Specifications of the ISB 2013 production aftertreatment system and the SCRF®

Substrate	**DOC**	**CPF**	**2 * SCR-A**	**SCRF®**
Material	Cordierite	Cordierite	Cordierite	Cordierite
Diameter (inch)	9.0	9	10.5	10.5
Length (inch)	4	10	12[1]	12
Cell Geometry	Square	Square	Square	Square
Total Volume (L)	4.17	10.40	17.04	17.04
Open Volume (L)	3.5	7.3	14.4	10.2
Cell Density /in^2	400	200	400	200
Cell Width (mil)	46	59	46	55
Filtration Area (in^2)	NA	8858	NA	11370
Open Frontal Area (in^2)	26.92	22.15	73.29	25.9
Channel Wall Thickness	4	12	4	16
Wall density (g/cm^3)	0.91	1.53	0.91	-
Porosity (%)	35	59	35	50
Mean Pore Size (µm)	NA	15	NA	16
Number of in cells	25447	6362	34636	8659
Weight of substrate +	5155	14377	14088	18140

Table 3.5: Diesel engine aftertreatment de-greening procedure

Speed	**Load**	**Exhaust Flow Rate**	**SCRF® Inlet Temp**	**Post-Fuel Dosing**	**Duration**
[RPM]	**[N-m]**	**[kg/min]**	**[°C]**	**[mg/stroke]**	**[Hours]**
1400	830	6.5	450	0.0	4.0
			602	23.0	0.5
			451	0.0	2.0
			606	23.0	0.5
			448	0.0	2.0
			603	23.5	0.5
			451	0.0	2.0
			601	24.0	0.5
				Total Hours	12.0

3.5 Test Cell Measurements and Data Acquisition

3.5.1 Exhaust Mass Flow Rate

The exhaust mass flow rate is considered as the sum of air and fuel flow rates. The air flow rate was calculated from the pressure drop (in intake air flow) measured using a pressure transducer across the Meriam Instruments Laminar Flow Element (LFE). The pressure drop value was used to calculate the intake air standard volumetric flow rate which was then converted to the mass flow rate using density of air at the standard conditions (20°C and 1 atm pressure). The fuel mass flow rate was measured by a model CMFS015M319N2BAECZZ Micro Motion Coriolis Meter. The specifications of the flow meter are given in Table 3.6.

Table 3.6: Coriolis meter specifications

Manufacturer	Micro Motion		
Model	CMFS015M319N2BAECZZ		
Measurement	Flowrate	Density	Temperature
Units	[%]	[kg/m^3]	[°C]
Accuracy	± 0.10	± 0.5	± 1.0
Repeatability	± 0.05	± 0.2	± 0.2

3.5.2 Temperature

The temperature sensors were installed at various locations in the exhaust system, and in the CPF and the SCRF® to record the radial and axial gas temperature distribution. K-type thermocouples manufactured by Omega were used to measure the temperature. The details of the thermocouples used are given in Table 3.7. The thermocouple layout in the CPF and the SCRF® are given in Figures 3.6 and 3.7. Twenty thermocouples, namely S1 – S20 were instrumented in the SCRF®. The thermocouples S1 – S10 were inserted into the SCRF® through the inlet channels of the SCRF® and the thermocouples S11 – S20 were inserted into the SCRF® through the outlet channels of the SCRF®.

Table 3.7: Specifications of the thermocouples used in the aftertreatment system

Manufacturer	Type	Diameter	Length	Part Number	Accuracy	Location
[-]	[-]	[in.]	[in.]	[-]	[%]	[-]
Omega	K	0.020	12	K-MQSS-020-U-12	± 2.2 °C	CPF
Omega	K	0.020	16	K-MQSS-020-U-16	± 2.2 °C	CPF
Omega	K	0.020	12	K-MQSS-020-U-12	± 2.2 °C	SCRF®
Omega	K	0.020	16	K-MQSS-020-U-16	± 2.2 °C	SCRF®
Omega	K	0.125	6	K-MQSS-125-U-6	± 2.2 °C	Exhaust, Air Intake, Coolant

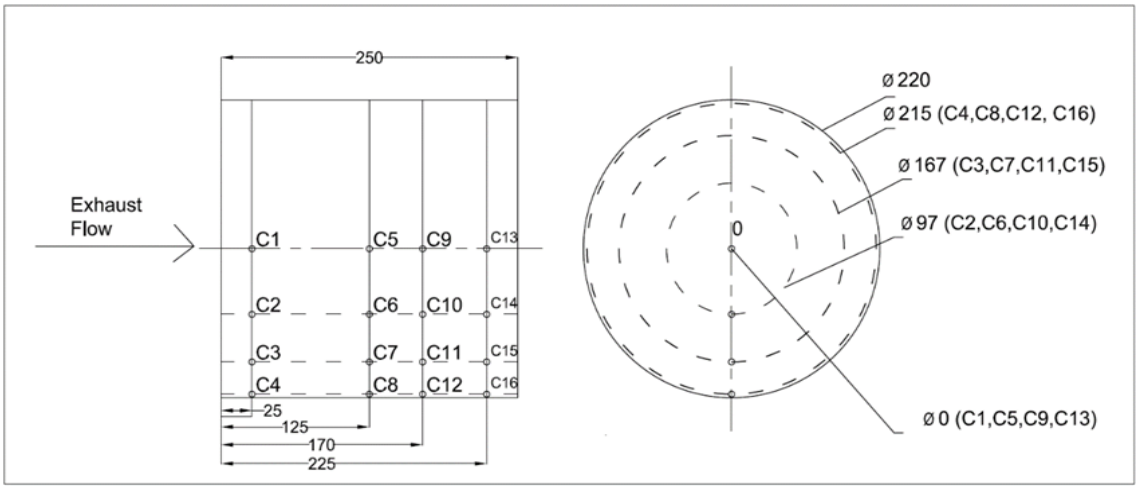

Figure 3.6: Thermocouple arrangement in the CPF (adapted from reference [3])

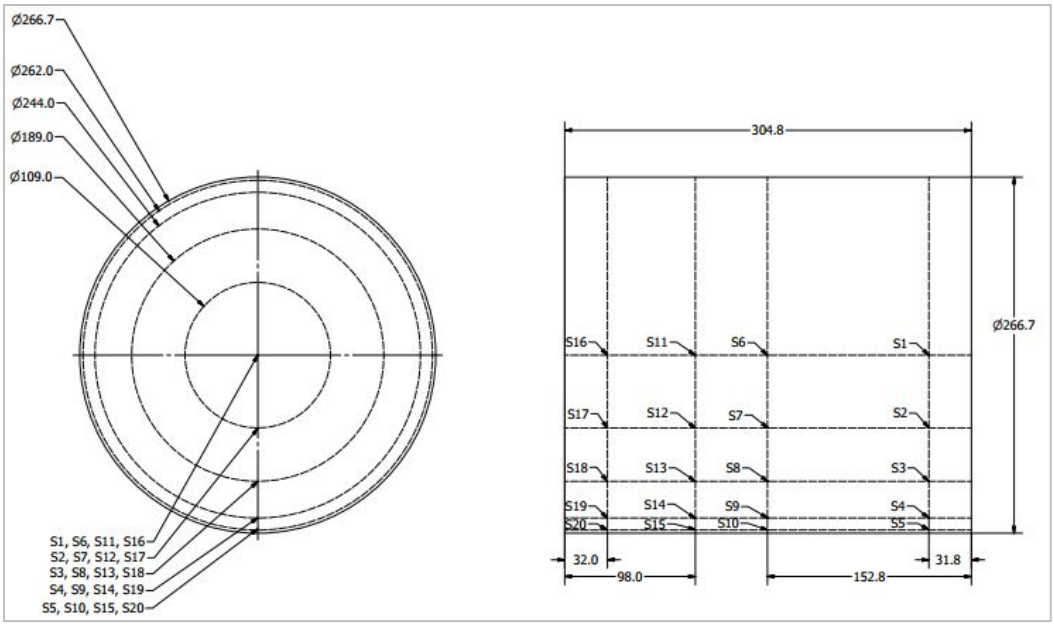

Figure 3.7: Thermocouple arrangement in the SCRF®

3.5.3 Pressure

The pressure drop data across the LFE, DOC, CPF, SCR and SCRF® was continuously measured and recorded by several differential pressure transducers. The barometric pressure was measured by an absolute pressure transducer. The specifications of the transducers are given in Table 3.8

Table 3.8: Specifications of pressure transducers

Parameters	**Barometric Pressure**	**LFE**	**DOC**	**CPF**	**SCRF®**
Sensor Make	Omega Engineering	Omega Engineering	Omega Engineering	Omega Engineering	Omega Engineering
Model Number	PX419-26B5V	PX429-10DWU-10V	PX429-2.5DWU-10V	PX409-2.5DWU-5V	PX429-5DWU-10V
Type	Absolute	Differential	Differential	Differential	Differential
Range	26.00-32.00	0-10	0-2.5	0-2.5	0-5
Units	in. Hg	in. H_2O	PSID	PSID	PSID
Accuracy, Linearity, Hysteresis	±0.08% FS	±0.08% FS	±0.08% FS	±0.08% FS	±0.08% FS
Output Voltage	0-5 Vdc	0-10 Vdc	0-5 Vdc	0-10 Vdc	0-10 Vdc

Note: FS indicates full scale reading

3.5.4 Data Acquisition

The data acquisition hardware consists of two National Instruments (NI) DAC chassis (NI cDAQ-9178). Multiple NI modules were plugged in to collect the engine speed, load, temperature and pressure data from the various locations. The details of data acquisition system are given in Table 3.9. A NI LabVIEW program was used to log the data and display it on the desktop computer for continuous data monitoring during the test. The specifications of the various modules are described in reference [9, 1].

Table 3.9: Details of the data acquisition system

Module	**Measurement**	**Quantity**
NI 9263	Analog Output ±10 V	1
NI 9239	Analog Input 10 V range	2
NI 9237	Analog Input ±25 mV/V (Bridge)	1
NI 9213	Thermocouple	4
NI 9472	24 V, Digital Output	1
NI 9205	Analog Input upto ± 10 V (Single ended, differential)	1
NI 9401	Digital Input / Output	1

A PCAN service tool was connected to the desktop computer via USB, to obtain the data from the engine via CAN communication (J1939 protocol). The proprietary software from Cummins Inc., Calterm, was used record and monitor the data from the engine ECM. Calterm was also used to control the post-fuel dosing, urea dosing, throttle position and fuel rail pressure.

3.5.5 Gaseous Emissions

The gaseous emissions during the NO_x reduction tests were measured using a V&F Airsense ion molecule reaction mass spectrometer (IMR-MS). The details of MS and calibration gases used to calibrate the MS are given in Table 3.10. The procedure to operate and calibrate the MS is described in Appendix A. N_2O measurement is also important for NO_x reduction experiments on the SCR and the SCRF®, but due to

interference caused by the same molecular mass of N_2O and CO_2 (44 amu), accurate measurements were not possible with the MS [9].

Table 3.10: Specifications of IMR-MS and calibration gases

Components	Detection Level at 100 ms	Monitoring Mass	Ionization Gas	Span Gas	Span gas concentration	Accuracy
[-]	[ppb]	[amu]	[-]	[-]	[ppm]	[%]
NO	100	30	Mercury	NO, N_2	797	± 1
NO_2	50	46	Mercury	NO_2, Air	495	± 2
NH_3	120	17	Mercury	NH_3, N_2	103.8	± 2

The exhaust gases from different locations were sampled by the MS through the stainless steel sampling lines which were heated to 190 °C. Heating the sampling lines avoided the condensation of water vapor in the exhaust gas and the adsorption of gaseous emissions on the sampling lines [9].

Two UniNO_x-sensors were installed on the production aftertreatment system, one each at the engine outlet and the SCR outlet, which measured NO_x concentrations in the exhaust gas and the displayed the values through Calterm. The sensor consists of zirconia based multilayer sensing element made by NGK Insulators and a control unit made by Continental. A Delphi make sensor was also installed at the outlet of the SCR/SCRF® to measure NH_3 slip. The specifications of the sensors are given in Table 3.11.

Table 3.11: Specification NO_x and NH_3 sensor on production aftertreatment system

Component	Range	Resolution	Accuracy	Voltage Range	Operating Temperature
[-]	[-]	[ms]	[%]	[V]	[°C]
NO_x Sensor	0-1500 ppm	0.1 ppm	±10	12-32	100-800
NH_3 Sensor	0-1500 ppm	0.1 ppm	±10	13.5-32	200-500
λ Sensor, O_2 (linear)	12 - 21%	0.10%	±0.3 - ±1.4	24	100-800

3.5.6 Particulate Matter (PM)

The concentration of PM was measured by performing hot sampling (without dilution) from the engine exhaust flow using a dry gas meter and a manual sampling train (Made by Anderson Instruments Inc.). The PM was deposited by passing the sampled raw exhaust through an A/E type glass fiber filter. The PM concentration in the engine exhaust was determined by recording the pre and post sampling weights of the glass fiber filter. The detailed information about PM sampling procedure and the instrument is given in reference [3, 7].

3.5.7 Weighing Balance for SCRF®

PM was deposited in the SCRF® during passive oxidation tests (configuration1) and NO_x experimental tests (configuration 2) with PM loading of 2 and 4 g/L in the SCRF®. The PM loading was performed in stages, and to determine the PM retained in the SCRF®, it was weighed four times during a test for configuration 1 and three times for configuration 2, which is discussed in detail in sections 3.6.5 and 3.6.6. The weight of the SCRF® was used to determine the PM mass retained during that stage of the test [3] and the procedure used to calculate the PM mass is described in section 3.6.7. The specifications of the weighing balance are given in Table 3.12. The detailed procedure to weigh the SCRF® is discussed in reference [3].

Table 3.12: Specifications of the weighing balance used to weigh the SCRF®

Manufacturer	Ohaus
Model	Ranger
Capacity	35,000 g
Certified Readability	± 1.0 g
Readability	± 0.1 g
Linearity	± 0.3 g

3.6 Test Matrices and Test Procedures

The primary objective of conducting the NO_x reduction tests on the production-2013-SCR and the SCRF® is to acquire the data to calibrate the 1-D SCR model (developed at MTU) and the SCR-F model (being developed at MTU). The inlet and outlet

SCR/SCRF® measurements of exhaust temperature, exhaust flow rate, NO, NO_2 and NH_3 concentrations at a variety of test conditions were required to calibrate the models. In addition, the gas temperature in the substrate and the pressure drop across the SCRF® were also needed for calibration of the SCR-F model. Hence, the engine test conditions were selected to cover a wide range of SCR/SCRF® inlet exhaust temperature, space velocity, NO_x and NO_2/NO_x ratio.

3.6.1 Test Matrix for Configuration 1

The schematic of several stages in the test procedure of a passive oxidation (PO) test with urea dosing is shown in Figure 3.8. The test procedure was adopted by modifying the procedures developed by references [3, 82].

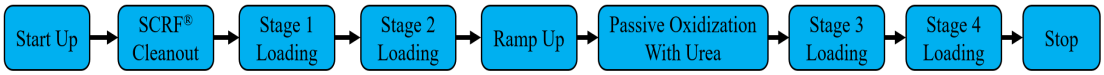

Figure 3.8: Stages of a passive oxidation test with urea dosing with configuration 1 [1]

The first two stages are loading stages where the SCRF® is loaded with PM to a target value of 2 ± 0.2 g/L. The loaded PM is oxidized in the PO stage, during which the urea dosing is performed. PO stage is followed by Stage 3 and Stage 4, which provide the post oxidation filter loading characteristics. The detailed procedure for passive oxidation test with urea dosing in described in reference [1]. The passive oxidation with urea dosing was obtained for five different Test Points and two repeat points. The test matrix for passive oxidation with urea injection is given in Table 3.13.

The primary objective of this configuration was to determine the kinetics of NO_2 assisted passive oxidation (PO) of PM in the SCRF®, without and with urea dosing during the PO. The urea dosing was performed to study the effect of NO_x reduction on passive oxidation of PM in the SCRF® and vice-versa. The NO_x reduction data obtained from the passive oxidation with urea dosing was analyzed and will be discussed in Chapter 4.

Table 3.13: Test matrix for passive oxidation with urea dosing with configuration 1 [1]

Test Point	Speed	Load	Exhaust Flowrate	SCRF® Space Velocity	SCRF® Inlet Temp.	PM into SCRF®	NO_2 into SCRF®	NO_x into SCRF®
[-]	[RPM]	[N.m]	[kg/min]	[k/hr]	[°C]	[mg/scm]	[ppm]	[ppm]
A	1300	302	5.6	16.8	265	2.3	304	590
C	1402	544	6.8	20.2	340	2.8	301	689
E	1199	653	7.0	20.8	344	2.2	653	1635
B	900	456	3.6	10.6	266	1.8	821	1867
B Rpt	902	449	3.7	11.0	256	1.7	758	1798
D	2099	594	12.3	36.8	368	3.0	171	505
D Rpt	2098	594	12.5	37.4	365	3.1	191	497

3.6.2 Test Matrix for NO_x Experimental Tests (Production-2013-SCR and Configuration 2)

Eight Test Points were selected that span the SCR/SCRF® inlet temperature from 200 to 450°C with space velocity and NO_x ranging from 12.0 to 45.2 k/hr and 300 to 1700 ppm respectively. The Test Points were chosen based on the engine maps for the ISB 2013 engine and were validated by running the engine at the specified speed-load and collecting the exhaust and gaseous emission data. The Test Points and important exhaust parameters for the NO_x reduction tests with the SCR and the SCRF® in configuration 2 are given in Table 3.14. The Test Points at temperatures lower than 200 °C were not selected to avoid potential urea deposition on the catalyst and the exhaust pipe. Seven Test Points were completed for the production SCR, excluding Test Point 7 (due to malfunctioning of the urea dosing system). The NO_x reduction performance of the SCRF® was evaluated without and with 2 and 4 g/L PM loading in the SCRF®. The Test Points marked with "*" in Table 3.14 (Test Points 1, 3, 6 and 8) were run and were selected on the basis of the range of the SCRF® inlet temperatures, space velocities and inlet NO_x concentrations.

Table 3.14: Test matrix for NO_x reduction tests for the production-2013-SCR and the SCRF® with configuration 2

Test Point	Speed	Torque	Exhaust Flow rate	SCRF® Inlet Temperature	SCRF® Std. Space Vel.	SCRF® Inlet NO_x	SCRF® Inlet NO_2/NO_x	SCRF® Inlet NO_2
[-]	[RPM]	[N-m]	[kg/min]	[˚C]	[k/hr]	[ppm]	[-]	[ppm]
1*	1200	203	4.9	208	14.6	492	0.61	301
2	1650	203	6.5	231	19.4	306	0.6	184
3*	2200	325	10.0	310	29.9	341	0.64	217
4	2100	377	0.4	331	28.1	372	0.62	230
5	1660	529	7.8	353	23.3	662	0.54	356
6*	1200	580	6.4	354	19.1	1712	0.54	922
7	2100	750	13.0	404	38.8	546	0.44	242
8*	2400	813	16.0	455	47.8	596	0.39	233

3.6.3 Baseline Condition and Aftertreatment Clean-out

The engine was run at 1660 RPM and 475 N-m, hereafter referred as the "baseline condition", to ensure repeatability of the instrumentation and the engine. To start a test, the engine was slowly ramped up from the idling condition to the baseline condition. After the engine had stabilized, exhaust emission samples were collected at UDOC and DDOC to check the repeatability. Then the CPF inlet temperature was raised to 600 ± 10 °C by in-cylinder post fuel injection to oxidize PM deposited in the CPF/SCRF® and desorb the NH_3 adsorbed on the SCR/SCRF® during the previous test. This is called the "aftertreatment clean-out". Fuel dosing was stopped after the pressure drop across the CPF/SCRF® had stabilized indicating that the rate of oxidation of PM is equal to the rate of PM being deposited on the CPF/SCRF®. This phenomenon is also known as the balance point. A similar procedure was also performed by previous researchers at MTU [3, 9, 7, 83, 84].

3.6.4 NO_x Experimental Tests: SCR

The NO_x reduction test procedure for the SCR was modified and adapted from reference [9]. It consists of three steps. In the first two steps, baseline condition and aftertreatment cleanout were performed to have a common start state for the experiments. In the third step, the engine was run at the NO_x reduction Test Point and stabilized. The emission

samples were collected at UDOC, DDOC, USCR and DSCR to measure NO, NO_2 and NH_3. Then the urea dosing cycle was performed and gaseous emission samples were sampled across the SCR to measure the SCR performance. The urea dosing cycle for the production-2013-SCR is shown in Figure 3.9. The urea injection was varied to achieve the targeted ANR of 0.3, 0.5, 0.8, 1.0, 1.2, 1.0 repeat, 0.8 repeat and 1.2 repeat. The ANR was varied from 0.3 to 1.2 to collect data to calibrate the SCR kinetics for modeling and predicting NO, NO_2 and NH_3 concentrations at the SCR outlet. The ANR 1.0 repeat and 0.8 repeat were performed to validate the repeatability of the production-2013-SCR performance. The ANR 1.2 repeat was performed to collect data to calculate the NH_3 storage on the production-2013-SCR.

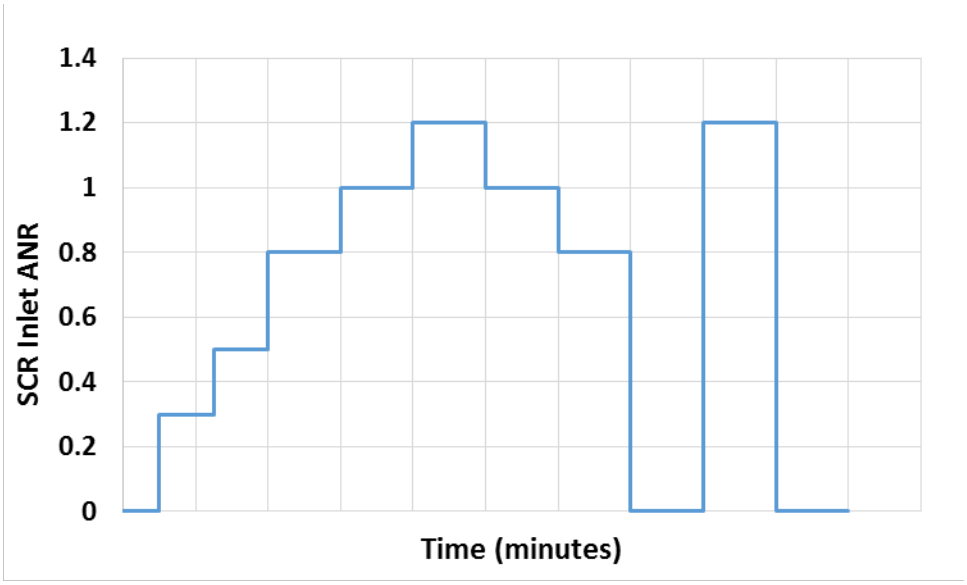

Figure 3.9: Urea dosing cycle for the production-2013-SCR

3.6.5 NO_x Experimental Tests: SCRF® - without PM Loading – Configuration 2

The test procedure to perform the NO_x reduction in the SCRF®, without PM loading, was similar to the test procedure for the production-2013-SCR. The emission data were collected at the baseline condition to check the repeatability and then the aftertreatment clean-out was performed by increasing the SCRF® inlet temperature to 600 ± 10 °C.

After that, the engine was stabilized at the NO_x reduction Test Point. The Test Points in Table 3.11, highlighted with "*" were run for the SCRF®. Then the urea dosing cycle was performed and gaseous emissions were sampled at the inlet and outlet of the SCRF®. The schematic NO_x reduction tests on the SCRF® without PM loading is shown in Figure 3.10. The production CPF used during the baseline tests was placed upstream of the SCRF® as shown in Figure 3.5, which filtered the PM produced by the engine and ensured minimum PM deposition in the SCRF®.

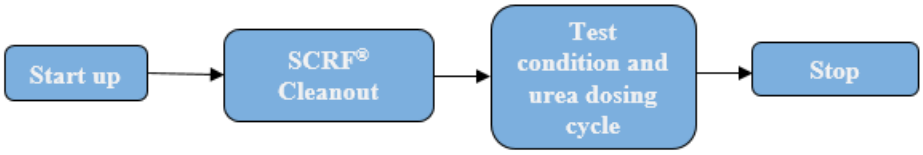

Figure 3.10: Schematic for NO_x reduction test on SCRF® without PM Loading

The urea dosing cycle was modified to reduce the test duration. Since 0.3 and 0.5 ANR are not performed during the actual engine operation in a vehicle, they were removed to modify the urea dosing cycle. The modified urea dosing cycle helped to maintain constant PM in the SCRF® during the tests with the target PM loading of 2 and 4 g/L. The modified urea dosing cycle is shown in Figure 3.11. The urea injection was varied to achieve the targeted ANR of 0.8, 1.0, 1.2 and 1.2 repeat. The ANR was varied from 0.8 to 1.2 to collect data to calibrate the SCR kinetics for the SCRF® to be used in the SCR-F model calibration. The ANR 1.2 repeat was performed to collect data to calculate the NH_3 storage on the SCRF®, with 0, 2 and 4 g/L PM loading.

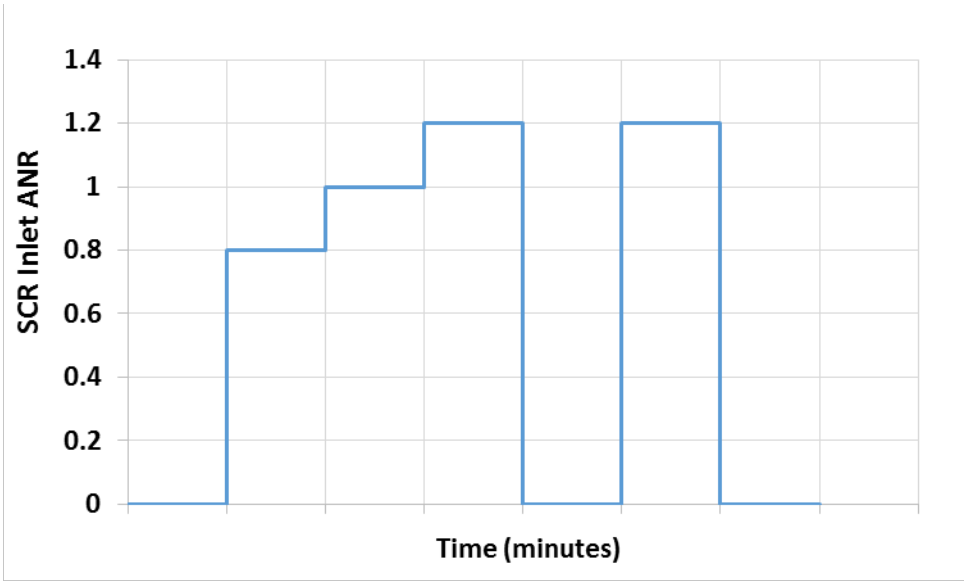

Figure 3.11: Modified urea dosing cycle for the SCRF®

3.6.6 NO_x Experimental Tests: SCRF® - with PM Loading (2 g/L) – Configuration 2

During these tests, the SCRF® was loaded to 2.0 ± 0.2 g/L of PM in two stages, namely Stage 1 and Stage 2. The test procedure started with the baseline condition and the aftertreatment clean-out.

Stage 1 Loading (S1): After the completion of the clean-out procedure, the engine speed and load were changed to 2400 RPM and 200 N-m at a fuel rail pressure reduced from 1500 to 1050 bar (30% reduction). This stage is called Stage 1 (S1) and the engine operating point is called Loading condition. The purpose of this stage is to stabilize the SCRF® inlet temperature at the Loading condition, since the weight of the wall flow filter varies with the temperature of the filter. The S1 was run for 30 minutes and then the engine was shut down to weigh the SCRF®.

Stage 2 Loading (S2): On completion of the SCRF® weighing procedure, aftertreatment components were assembled and the engine was warmed up using the exhaust bypass line (Figure 3.3). After the engine stabilized at the Loading condition, the exhaust flow was

switched to the trap line (Figure 3.3) and the Stage 2 Loading (S2) duration was started. The purpose of this stage is to load the SCRF® to the targeted PM loading of 2.0 ± 0.2 g/L. The Stage 2 Loading (S2) was run for 330 minutes and at the end the engine was shut down to weigh the SCRF®. The detailed S1 and S2 procedures are available in reference [3, 1]. The exhaust parameters are given in Table 3.15.

Table 3.15: Exhaust parameters during the Loading Condition

Speed	Load	Exhaust Flowrate	SCRF® Inlet Temperature	SCRF® Inlet NO_2	SCRF® Inlet PM	NO_2:PM Mass Ratio
[RPM]	[N-m]	[kg/min]	[°C]	[ppm]	[mg/scm]	[NO_2/PM]
2400	200	11.2	274	72	11.2	11.6

The Test Points 1 and 3 have low SCRF® inlet temperature (218 and 304°C), hence less PM would be oxidized during the urea dosing cycle than Test Points 6 and 8. There will be higher PM oxidation at Test Point 6 and Test Point 8 due to higher SCRF® inlet temperature (350 to 450°C). Hence, to accumulate PM during the NO_x reduction test condition, the CPF upstream of SCRF® was needed to be replaced with a spacer. To have consistency in the test procedure, the CPF was removed during all the data collection for the Test Points. The schematic diagram for these tests is given in Figure 3.12.

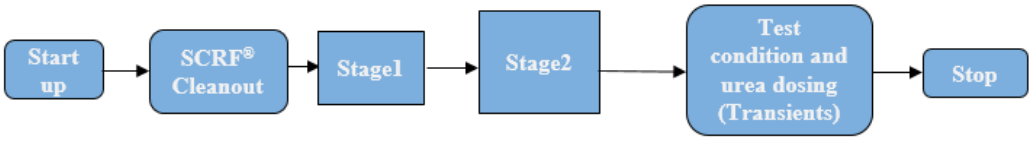

Figure 3.12: Schematic for effect of PM Loading on SCRF® NO_x reduction

Test Point - W/PM Stage: The pressure drop across the SCRF® for the Test Point 1 is plotted in Figure 3.13. The SCRF® was loaded with PM in Loading Stages S1 and S2. Then the test condition for NO_x reduction is run which is labeled as Test Point 1-W/PM. During the Test Point 1-W/PM the urea dosing cycle (Figure 3.11) was performed continuously and the test condition was completed without adding PM to the SCRF®,

since the rate of PM addition and the rate of PM oxidation are about equal. It can be observed that the pressure drop is constant during the NO_x reduction test condition which indicates that the PM in the SCRF® is constant. During the Test Point 1-W/PM stage, emission samples were collected at UDOC and USCRF® in the beginning and then switched to DSCRF® to measure the NO, NO_2 and NH_3 concentrations during the urea dosing cycle. The USCRF® and DSCRF® values were used to evaluate the performance of the SCRF®. The same test procedure was followed for Test Point 3-W/PM.

The pressure drop across the Test Point 8 is plotted in Figure 3.14. It can be observed that during Test Point 8-W/PM-I, Test Point 8-W/PM-II and Test Point 8-W/PM-III, the pressure drop curves across the SCRF® is steep, which is due to the high PM oxidation rate. Hence, it was decided to run the loading condition to redeposit PM in the SCRF® to maintain PM loading close to 2 g/L. These stages are labeled as Repeat Loading-I and Repeat Loading-II. During the Test Point 8-W/PM-I, emission samples were collected at UDOC, DDOC, USCRF® and DSCRF®. The same test procedure was followed for Test Point 6 with PM.

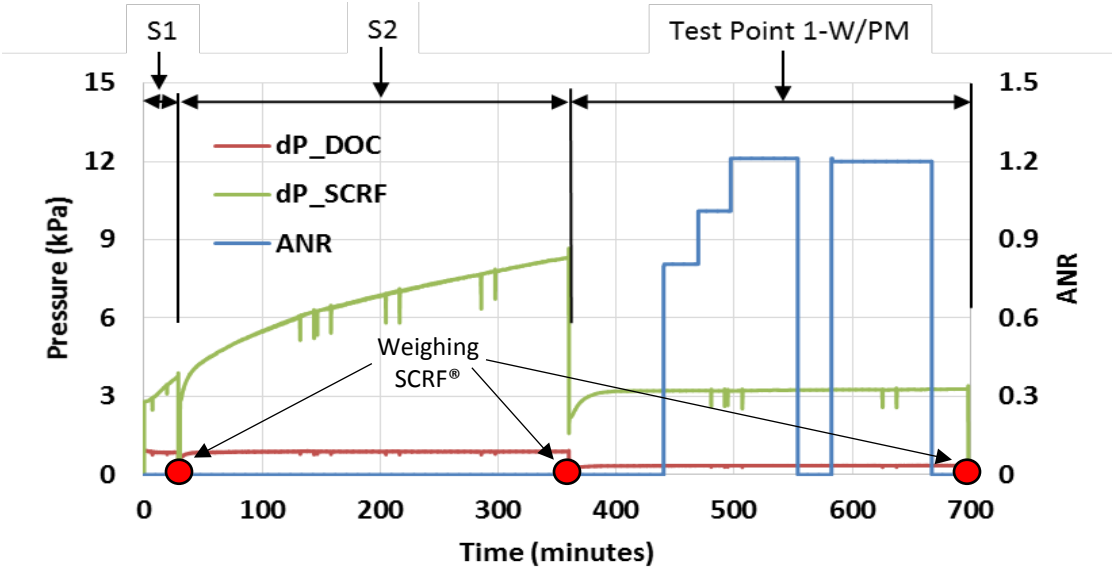

Figure 3.13: Delta Pressure across the SCRF® for Configuration 2 - Test Point 1 with PM

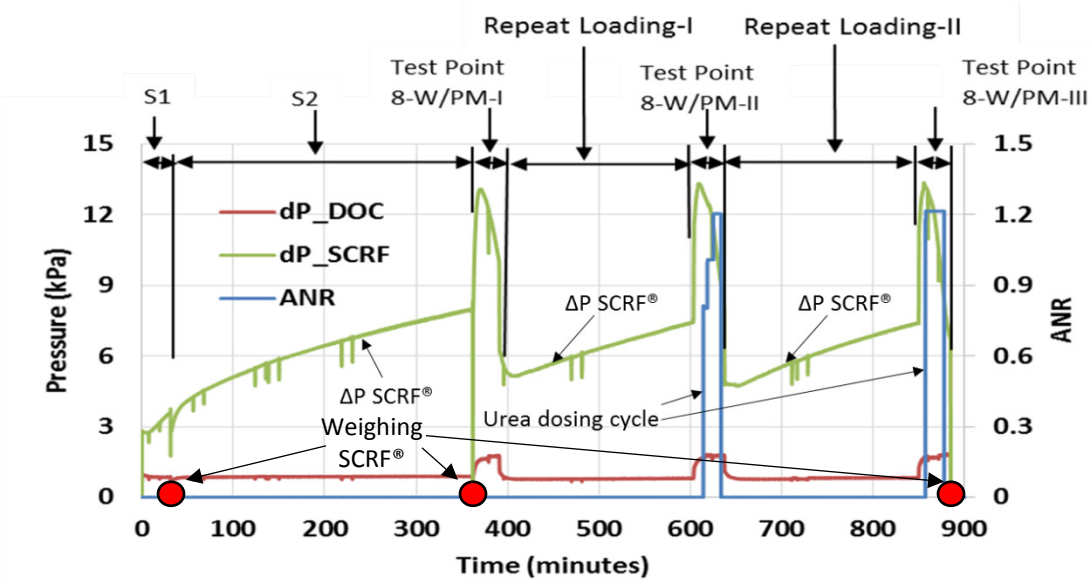

Figure 3.14: Delta Pressure across the SCRF® for Configuration 2 - Test Point 1 with PM

3.6.7 NO_x Experimental Tests: SCRF® - with PM Loading (4 g/L) – Configuration 2

The engine operating conditions for the Loading condition were modified to accumulate the targeted PM loading of 4 g/L in the SCRF®. The exhaust parameters of the modified loading condition are given in the Table 3.16. The fuel rail pressure was reduced by 50 % for 4 g/L of PM loading in comparison to 30% for 2 g/L. The reduced rail pressure was 750 bar.

Table 3.16: Engine and exhaust parameters of the Loading Condition

PM Loading	Speed	Load	Exhaust Flow Rate	SCRF® Inlet Temperature	SCRF® Inlet NO_2	SCRF® Inlet PM	NO_2:PM Mass Ratio
[g/L]	[RPM]	[N.m]	[kg/min]	[ºC]	[ppm]	[mg/scm]	[NO_2/PM]
2	2400	200	11.2	274	72	11.2	11.6
4	2400	201	11.1	292	40	20.8	3.6

The test procedure for NO_x reduction tests in SCRF® with the PM loading of 4 g/L was similar to the tests with the PM loading of 2 g/L. The Test Points 1 and 3 had two PM loading stages (S1 and S2) followed by the urea dosing cycle. The Test Points 6 and 8 had four PM loading stages (S1, S2, Repeat Loading-I and Repeat Loading-II) with intermediate urea dosing cycle.

3.6.8 Calculation of PM Mass Retained and Nitrogen Balance

The following terms and equations are used in the analysis of the data. The terms used in the equations are described below with a brief description.

PM Mass Retained

The SCRF® substrate was weighed three times during the NO_x experimental tests with PM loading of 2 and 4 g/L in configuration 2 as shown in Figures 3.13 and 3.14. The SCRF® mass measurements include the mass of the substrate and the PM retained in the filter. These mass measurements and PM concentrations at the inlet and outlet of the SCRF® are used to calculate the PM mass retained in the SCRF® ($PM_{Retained}$) at the end of each stage. The equations used to calculate the $PM_{Retained}$ are described in the following section. The equations and assumptions are discussed in more detail in Appendix C of reference [1].

C_{in} The average PM concentration in the exhaust in mg/scm at the inlet of the SCRF® for the stage.

PM_{In} Mass of PM in grams produced by the engine and flows into the substrate during the stage. The mass of PM that goes into the SCRF® is calculated based on the flowrate of exhaust, PM concentration, and the time of the stage.

$$PM_{In} = C_{In} * \frac{Exhaust\ Flow\ Rate}{\rho_{Std}} * \frac{Stage\ Duration}{1000} \qquad \text{Eqn. 3.1}$$

Where C_{in} is in mg/scm, exhaust flow rate is in (kg/min), stage duration is duration of the stage in (minutes) and ρ_{std} is exhaust density taken to be 1.18 kg/m3 (at 25°C and 101.3 kPa).

PM_{Out} Mass of PM out of the SCRF® as a result of substrate filtration in grams. This includes PM that was filtered but not oxidized

$$PM_{Out} = (1 - \eta_f) * PM_{In} \quad \text{Eqn. 3.2}$$

Where η_f is the Filtration efficiency of the SCRF®. Only one downstream concentration is taken during the test in stage 2, so an assumption is made that the filtration efficiency remains roughly constant after the cake layer forms. Appendix C in reference [1] discusses the assumption for filtration efficiency of stage 1. The efficiency of the stage is given by:

$$\eta_f = \frac{C_{In} - C_{Out}}{C_{In}} \quad \text{Eqn. 3.3}$$

PM_{Start} Mass of PM in the filter at the beginning of the stage in grams.

$PM_{Retained}$ Mass of PM retained in the substrate at the end of the stage in grams. PM retained is a cumulative value, meaning the mass of PM at the end of the stage includes what was loaded from the previous stages.

$PM_{Available}$ The theoretical total PM in grams that is or will be available for oxidation during the stage.

$$PM_{Available} = m_{Start} + PM_{In} \quad \text{Eqn. 3.4}$$

$PM_{Oxidized}$ Mass of PM oxidized during the stage in grams. It comes from the overall stage balance.

$$PM_{Oxidized} = PM_{Start} + PM_{In} - PM_{Out} - PM_{Retained} \quad \text{Eqn. 3.5}$$

$\%PM_{Oxidized}$ The percentage of mass oxidized during the stage.

$$\%PM_{Oxidized} = \frac{PM_{Oxidized}}{PM_{Available}} * 100 \quad \text{Eqn. 3.6}$$

$PM_{Loading}$ The cumulative loading of PM divided by the open volume of the SCRF® with units of g/L. The values are considered at the end of the stage.

$$PM_{Loading} = \frac{PM_{Retained}}{V_{Substrate}} \quad \text{Eqn. 3.7}$$

Nitrogen Balance

Inlet NH_3 The NH_3 concentration in ppm at the inlet of the SCRF®.

$$Inlet\ NH_3 = \frac{DEF\ Flow\ Rate * \rho_{DEF} * 0.325 * 2 * MW_{Exhaust\ Gas} * 1.02}{Exhaust\ Flow\ Rate * MW_{Urea}} \quad \text{Eqn. 3.8}$$

Where, DEF flow rate is obtained from Calterm (ml/s), ρ_{DEF} is density of DEF taken to be 1080 ($kg/m^{3)}$ under room condition. The urea concentration of the DEF is 32.5% by weight. Molecular weight of the urea molecule is 60 (g/gmol) and molecular weight of the exhaust is 28.96 (g/gmol). 1.02 denotes the 2% correction applied to the DEF flow rate recorded by Calterm, since the actual injection verified by conducting bucket test at various DEF flow rates is 2% higher than the measurements obtained from Calterm (See Appendix C).

ANR, also described as Target ANR is the ratio of the NH_3 concentration (ppm) to the NO_x concentration (ppm) at the inlet of the SCRF®.

$$ANR = \frac{Inlet\ NH_3}{Inlet\ NO_x} \quad \text{Eqn. 3.9}$$

Inlet NH_3 concentration was calculated using Equation 3.8 and inlet NO_x concentration was obtained by adding inlet NO and NO_2 concentrations measured using MS.

The NO_x conversion efficiency was calculated using inlet and outlet NO_x concentrations (ppm) as indicated in equation 3.10.

$$NO_x\ Conversion\ efficiency\ (\%) = \frac{Inlet\ NO_x - Outlet\ NO_x}{Inlet\ NO_x} * 100 \quad \text{Eqn.3.10}$$

Nitrogen Balance was performed using the NO, NO_2 and NH_3 concentrations (ppm) at the inlet and outlet of the SCRF® to validate the data consistency. The nitrogen balance of 100 ± 10 % was considered to be a good agreement since the concentration of N_2O and

isocyanic acid and cyanuric acid (by products of incomplete urea decomposition) were not measured.

$$Nitrogen\ Balance\ (\%) = \{1 - \frac{Inlet\ NH_3 - [(Inlet\ NO_x - Outlet\ NO_x) + NH_3\ Slip]}{Inlet\ NH_3}\} * 100 \quad \text{Eqn. 3.11}$$

Where all the concentrations are in ppm. The inlet and outlet NO_x were measured using the MS and the NH_3 slip out of the SCRF® was measured using the sensor.

The values for various parameters such as the emission concentrations, PM concentrations, temperatures and exhaust flow rates recorded during the experiments were analyzed and the results will be discussed in detail in Chapter 4.

Chapter 4. Results and Discussion

This chapter discusses the data and the results of the NO_x reduction tests conducted with the production-2013-SCR and the SCRF®. The NO_x reduction and NH_3 storage performance of the production-2013-SCR was evaluated at seven Test Points (Table 3.14) as discussed in Chapter 3. This chapter also presents the results of 1-D SCR model calibration and comparison of the experimental and the simulation results for the seven test runs with the production-2013-SCR.

The NO_x reduction performance of the SCRF® was evaluated with 2 and 4 g/L PM and without PM at four different Test Points in configuration 2 (total twelve tests) and with PM at five different Test Points (Table 3.13) in configuration 1 (total seven tests including two repeat Test Points. The NO_x reduction performance and the NH_3 storage in the SCRF® and the production SCR are compared to study the difference in the performance of the SCRF® and the production-2013-SCR.

4.1 NO_x Reduction in Production-2013-SCR (Baseline)

The engine operating conditions and the important exhaust parameters during the seven NO_x reduction tests for the production-2013-SCR1 are given in Table 4.1. The Test Points are arranged in the increasing order of SCR inlet temperature. It is seen that the Test Point 1 has the lowest SCR inlet temperature and the lowest standard space velocity, while Test Point 8 has the highest SCR inlet temperature and the highest standard space velocity. The NO_2/NO_x ratio varies between 0.22 and 0.48.

The analysis of NO and NO_2 values across the production-2013-SCR without urea injection are given in Table 4.2. The delta NO and NO_2 values were calculated by subtracting the SCR outlet from the SCR inlet values as indicated in equations 4.1 and 4.2. Ideally, change in concentration of NO across the SCR (without urea injection) must be equal and opposite to the change in concentration of NO_2 across the SCR (without urea injection), i.e. $\Delta NO = -(\Delta NO_2)$. In Table 4.2 it is observed that the SCR outlet NO_2 concentration has increased and SCR outlet NO concentration has decreased for all the

Test Points, which indicates that the Cu-zeolite SCR catalyst has a tendency to oxidize up to 20% of upstream NO to NO_2.

$$\text{Delta NO} = \text{SCR Inlet NO} - \text{SCR Oulet NO} \quad \text{Eqn. 4.1}$$

$$\text{Delta } NO_2 = \text{SCR Inlet } NO_2 - \text{SCR Outlet } NO_2 \quad \text{Eqn. 4.2}$$

Table 4.1: Engine and exhaust conditions at SCR inlet for NO_x reduction tests

Test Point	Speed	Load	Exhaust Flow Rate	SCR Inlet Temp.	Std. Space velocity	SCR Inlet NO_x	SCR Inlet NO_2/NO_x
	[RPM]	[Nm]	[kg/min]	[°C]	[k/hr]	[ppm]	[-]
1	1200	204	4.4	219	12.0	648	0.27
2	1650	189	6.3	238	17.1	279	0.37
3	2201	324	9.7	307	26.4	291	0.31
4	2100	376	9.7	327	26.5	342	0.46
5	1659	531	7.8	354	21.3	552	0.41
6	1198	575	6.2	352	16.9	1730	0.40
8	2400	826	16.4	447	44.7	542	0.18

Table 4.2: NO and NO_2 concentrations across the production-2013-SCR without urea injection

Test Point	SCR Inlet Temp.	SCR Inlet NO	SCR Outlet NO	Δ NO	SCR Inlet NO_2	SCR Outlet NO_2	Δ NO_2	Out/In NO_2
[-]	[°C]	[ppm]	[ppm]	[ppm]	[ppm]	[ppm]	[ppm]	[-]
1	219	470	439	31	178	189	-11	1.06
2	238	177	173	3	102	107	-4	1.04
3	307	199	184	16	91	109	-17	1.19
4	327	185	172	12	158	173	-15	1.10
5	354	325	286	40	227	253	-27	1.12
6	352	1045	926	119	685	847	-162	1.24
8	447	443	416	26	99	115	-16	1.17

The NO, NO_2 and NH_3 concentrations and the NO_x reduction performance of the production-2013-SCR at an ANR of 1.0 are given in Table 4.3. It is observed that the NO_x conversion efficiency increases with increase in the SCR inlet temperature until 350°C and decreases thereafter. NO_x conversion efficiency higher than 95% was observed in the range of 300 to 350°C. At temperatures below 250°C, the urea to NH_3 conversion is not complete (<80%) and at temperatures above 400°C, the oxidation of NH_3 to N_2 and NO is expected to be significant (>50%). Since N_2 (formed by R5 in Table 2.1), N_2O and isocyanic acid are not considered in the nitrogen balance equation (calculated using Equation 3.11), nitrogen balance lower than 90% were observed for Test Points 1 and 8.

Table 4.3: NO_x reduction performance of the production-2013-SCR at target ANR of 1.0

Test Point	**SCR Inlet Temp.**	**NO, [ppm]**		**NO_2, [ppm]**		**NH_3, [ppm]**		**ANR**	**NO_x Conv. Efficiency**	**Nitrogen Balance**
[-]	**[°C]**	**In**	**Out**	**In**	**Out**	**In**	**Out**	**[-]**	**[%]**	**[%]**
1	219	439	116	189	0	604	13	0.96	82	87
2	238	178	50	110	1	268	2	0.96	82	86
3	307	186	23	111	0	332	33	1.12	92	93
4	327	181	6	167	0	318	0	0.93	96	106
5	354	315	6	255	7	546	0	0.99	99	99
6	352	926	69	847	2	1720	9	0.97	96	97
8	447	425	87	121	0	584	67	1.07	84	90

Table 4.4: NO_x reduction performance of the production-2013-SCR at target ANR of 1.2

Test Point	**SCR Inlet Temp.**	**NO, [ppm]**		**NO_2, [ppm]**		**NH_3, [ppm]**		**ANR**	**NO_x Conv. Efficiency**	**Nitrogen Balance**
[-]	**[°C]**	**In**	**Out**	**In**	**Out**	**In**	**Out**	**[-]**	**[%]**	**[%]**
1	219	439	87	189	0	728	177	1.16	86	99
2	238	178	23	110	0	324	44	1.16	92	93
3	307	186	22	111	0	400	107	1.34	92	96
4	327	181	0	167	0	385	61	1.13	100	105
5	354	315	0	255	0	655	91	1.19	100	98
6	352	926	13	847	0	2078	222	1.17	99	95
8	447	425	75	121	0	704	150	1.29	86	88

Similar trends were observed at ANR of 1.2 as given in Table 4.4. The NO_x conversion efficiency is almost 100% in the SCR inlet temperature range of 300 – 350 °C at ANR of 1.2. The NO_x conversion efficiency for seven Test Points with the production-2013-SCR, at ANRs of 1.0 and 1.2 are shown in Figure 4.1. 5–10% improvement in NO_x conversion efficiency was observed for all the Test Points (except Test Point 3) with an increase in the ANR from 1.0 to 1.2. The NO, NO_2 and NH_3 concentrations and the NO_x reduction performance of the production-2013-SCR at ANR of 0.3, 0.5, 0.8, 1.0-repeat, 0.8-repeat and 1.2-repeat are given in Appendix D.

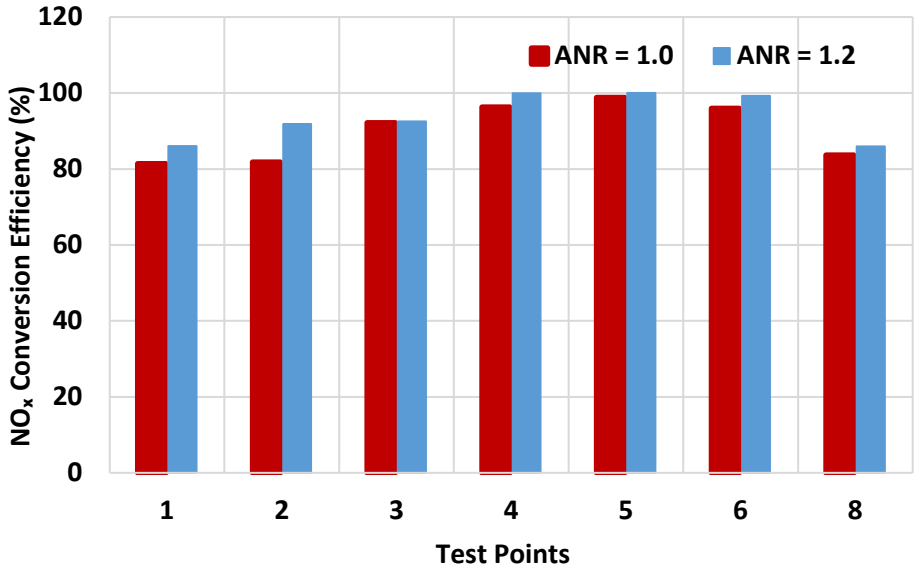

Figure 4.1: NO_x conversion efficiency of production-2013-SCR for steady state conditions at target ANR 1.0 and 1.2

The NH_3 slip for the seven Test Points with the production-2013-SCR, at ANR 1.0 and 1.2 are shown in Figure 4.2. The NH_3 slip for the various Test Points is less than 50 ppm at ANR 1.0, except of the Test Point 8, which is high space velocity and high temperature test condition. However, the NH_3 slip increases significantly at ANR 1.2. The increase in the NH_3 slip at ANR 1.2 was observed to be ~ 20 % of the inlet NO_x.

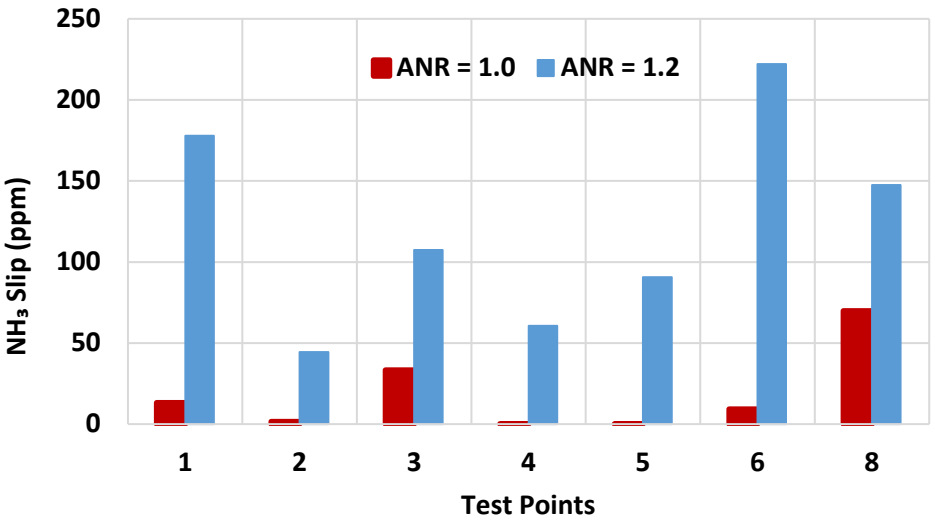

Figure 4.2: NH_3 slip in production-2013-SCR for steady state conditions at target ANR 1.0 and 1.2

4.2 1-D SCR Model Calibration Results

The experimental data obtained from the seven NO_x reduction tests with the production-2013-SCR were used to calibrate the 1-D SCR model developed by reference [9] and Dr. Parker at Michigan Tech. The 1-D SCR model used in this study is discussed in section 2.4 of this thesis. This section describes the model parameters for the production-2013-SCR and the comparison of the simulation of SCR outlet concentrations of NO, NO_2 and NH_3 data to the experimental data.

The comparison of the model parameters required to calibrate the model to engine experimental data for the production-2013-SCR and production-2010-SCR [9] is shown in Table 4.5. It can be seen that the storage capacity Ω1 is comparable for the production-2013-SCR and production-2010-SCR. However, the storage capacity Ω2 for the production-2013-SCR is ~ 10% higher than Ω2 for the production-2010-SCR. The pre-exponential parameters for R1, R2, R7 and R9 were changed to calibrate the model to the engine experimental data obtained with the production-2013-SCR. The model calibration procedure is described in Appendix D.

Table 4.5: 1-D SCR model calibration parameters

Parameter	Calibration to ISB2010 engine data *	Calibration to ISB2013 engine data Test Points 2-8	Calibration to ISB2013 engine data Test Point 1	References * [18,43,129,130]	Unit
Ω1	4.36 E+01	4.31 E+01	4.50 E+01	1.20E+02	$gmol/m^3$
Ω2	3.60 E+01	4.07 E+01	5.51 E+01	-	$gmol/m^3$
A_ads1	1.08 E+00	1.18 E+00	1.01 E+01	-	$m^3/gmol \cdot s$
E_ads1	-10.2 ± 4.04	-10.2 ± 4.04	-10.2 ± 4.04	0	kJ/gmol
A_des1	3.22 E+04	5.0 E+04	3.22 E+04	-	1/s
E_des1	67.5 ± 12.1	67.5 ± 12.1	67.5 ± 12.1	96.1, 97.5	kJ/gmol
A_ads2	2.11 E+01	2.11 E+01	2.11 E+01	-	$m^3/gmol \cdot s$
E_ads2	-7.60 ± 1.12	-7.60 ± 1.12	-7.60 ± 1.12	-	kJ/gmol
A_des2	9.58 E+05	9.58 E+05	9.58 E+05	-	1/s
E_des2	72.4 ± 10.9	72.4 ± 10.9	72.4 ± 10.9	-	kJ/gmol
A_NH_3oxi1	2.33 E+05	2.33 E+05	2.33 E+05	-	1/s
E_NH_3oxi1	91.1 ± 9.18	91.1 ± 9.18	91.1 ± 9.18	177, 63.8	kJ/gmol
A_std	7.18 E+07	1.23 E+08	9.08 E+07	-	$m^3/gmol \cdot s$
E_std	77.3 ± 7.92	77.3 ± 7.92	77.3 ± 7.92	48.7, 88.0, 89.1	kJ/gmol
A_std2	6.17 E+06	6.17 E+06	6.17 E+06	-	$m^3/gmol \cdot s$
E_std2	68.4 ± 7.28	68.4 ± 7.28	68.4 ± 7.28	-	kJ/gmol
A_slo	7.13 E+09	7.13 E+09	7.13 E+09	-	$m^3/gmol \cdot s$
E_slo	109 ± 9.21	109 ± 9.21	109 ± 9.21	58.3, 136.3	kJ/gmol
A_fst	1.76 E+08	1.55 E+08	9.50 E+06	-	$m^6/gmol^2 \cdot s$
E_fst	45.2 ± 9.55	45.2 ± 9.55	45.2 ± 9.55	113, 32.1, 77.1	kJ/gmol

The results from calibrated model were compared with the experimental data. The comparison of NO and NO_2 concentrations at SCR outlet is given in the Table 4.6 and 4.7 respectively. The model has been calibrated to within ± 20 ppm for both the gases. The values highlighted in green have high difference due to inconsistency in the experimental data. The comparison of NH_3 concentration at SCR outlet is given in the Table 4.8. The model has been calibrated to within ± 30 ppm for NH_3 slip (measured using NH_3 sensor).

Table 4.6: Results from calibrated model – NO concentration at SCR outlet (ppm)

Experiment Name	Test 1			Test 2			Test 3			Test 4			Test 5			Test 6			Test 7		
Temp (°), SV (k/hr)	219, 12.0			238, 17.2			307, 26.0			327, 27.0			354, 22.0			352, 17.0			447, 44.7		
ANR	Expt.	Model[1]	Diff.	Expt.	Model	Diff.	Expt.	Model	Diff.	Expt.	Model	Diff.	Expt.	Model	Diff.	Expt.	Model	Diff.	Expt.	Model	Diff.
0.0	439	439	0	173	173	1	184	184	0	172	172	0	286	285	1	926	926	0	416	416	0
0.3	347	353	-6	142	140	2	139	134	5	122	120	2	203	205	-2	647	675	-28	336	335	1
0.5	289	289	0	113	110	3	105	98	7	86	86	0	142	152	-10	474	504	-30	252	270	-18
0.8	217	200	17	82	71	11	50	38	12	40	36	4	61	73	-12	244	251	-7	124	162	-38
1.0	117	104	13	50	42	8	23	13	10	6	8	-2	6	21	-15	69	70	-1	87	100	-13
1.2	88	76	12	23	17	6	22	4	18	0	2	-2	0	5	-5	13	1	12	75	56	19
1.0	110	101	9	30	24	6	24	11	13	6	8	-2	3	22	-19	85	17	68[2]	89	100	-11
0.8	144	119	25	67	43	24	49	40	9	40	35	5	70	75	-5	274	246	28[2]	131	160	-29

[1] – For Test Point 1, model was calibrated using calibration parameters specific to Test Point 1 (as shown in Table 4.5)
[2] - The value highlighted appears to be an error in measurement of NO concentrations

Table 4.7: Results from calibrated model – NO_2 concentration at SCR outlet (ppm)

Experiment Name	Test 1			Test 2			Test 3			Test 4			Test 5			Test 6			Test 7		
Temp (°), SV (k/hr)	219, 12.0			238, 17.2			307, 26.0			327, 27.0			354, 22.0			352, 17.0			447, 44.7		
ANR	Expt.	Model[1]	Diff.	Expt.	Model	Diff.	Expt.	Model	Diff.	Expt.	Model	Diff.	Expt.	Model	Diff.	Expt.	Model	Diff.	Expt.	Model	
0.0	189	189	0	107	107	-1	109	109	0	173	173	0	253	249	4	847	847	0	115	115	0
0.3	125	118	7	78	74	4	67	61	6	127	121	6	179	166	13	578	594	-16	53	42	11
0.5	78	65	13	51	46	5	38	30	8	92	85	7	122	112	10	405	421	-16	12	10	2
0.8	32	26	6	23	13	10	3	1	2	41	34	7	38	32	6	139	162	-23	1	0	1
1.0	0	2	-2	1	1	0	0	0	0	7	6	1	0	2	-2	2	10	-8	0	0	0
1.2	0	0	0	0	0	0	0	0	0	0	1	-1	0	0	0	0	0	0	0	0	0
1.0	0	0	0	0	0	0	0	0	0	4	5	-1	0	1	-1	1	0	1	0	0	0
0.8	0	0	0	2	0	2	1	1	0	33	32	1	33	30	3	124	161	-37[2]	0	0	0

[1] – For Test Point 1, model was calibrated using calibration parameters specific to Test Point 1 (as shown in Table 4.5)
[2] - The value highlighted appears to be an error in measurement of NO_2 concentrations

Table 4.8: Results from calibrated model – NH_3 concentration at SCR outlet (ppm)

Experiment Name	Test 1			Test 2			Test 3			Test 4			Test 5			Test 6			Test 7		
Temp (°), SV (k/hr)	219, 12.0			238, 17.2			307, 26.0			327, 27.0			354, 22.0			352, 17.0			447, 44.7		
ANR	Expt.	Model[1]	Diff.	Expt.	Model	Diff.	Expt.	Model	Diff.	Expt.	Model	Diff.	Expt.	Model	Diff.	Expt.	Model	Diff.	Expt.	Model	Diff.
0.0	0	0	0	0	0	0	0	0	0	0	1	-1	0	0	0	0	0	0	0	0	0
0.3	0	0	0	1	0	1	0	0	0	0	0	0	0	0	0	0	0	0	0	2	-2
0.5	1	0	1	1	0	1	0	0	0	0	0	0	0	0	0	0	0	0	0	4	-4
0.8	1	0	1	1	1	0	0	5	-4	0	0	0	0	0	0	0	0	0	15	19	-4
1.0	13	1	13	2	2	0	33	36	-3	0	13	-13	0	11	-11	9	1	8	70	65	5
1.2	178	158	20	44	43	1	107	107	0	61	65	-4	91	81	10	222	207	15	148	115	33
1.0	39	42	-3	12	19	-7	35	36	-1	1	9	-8	6	8	-2	5	13	-8	68	66	2
0.8	6	0	6	3	2	1	1	3	-2	0	0	0	0	0	0	0	0	0	13	33	-20

Comparison of the simulation results and experimental measurements for NO, NO_2 and NH_3 concentrations at the SCR outlet are shown in Figure 4.3, 4.4 and 4.5 respectively. From Figures 4.3 and 4.4 it is observed that the difference between the simulation results and experimental measurements for NO and NO_2 concentration is less than 20 ppm for all the Test Points at ANR 0.8, 1.0 and 1.2. From Figure 4.5 it can be observed that the measured (using NH_3 sensor) and simulated values are in good agreement for NH_3 slip out of the SCR, as the difference between the simulation results and experimental measurements is less than 30 ppm for all the Test Points at ANR 1.0 and 1.2.

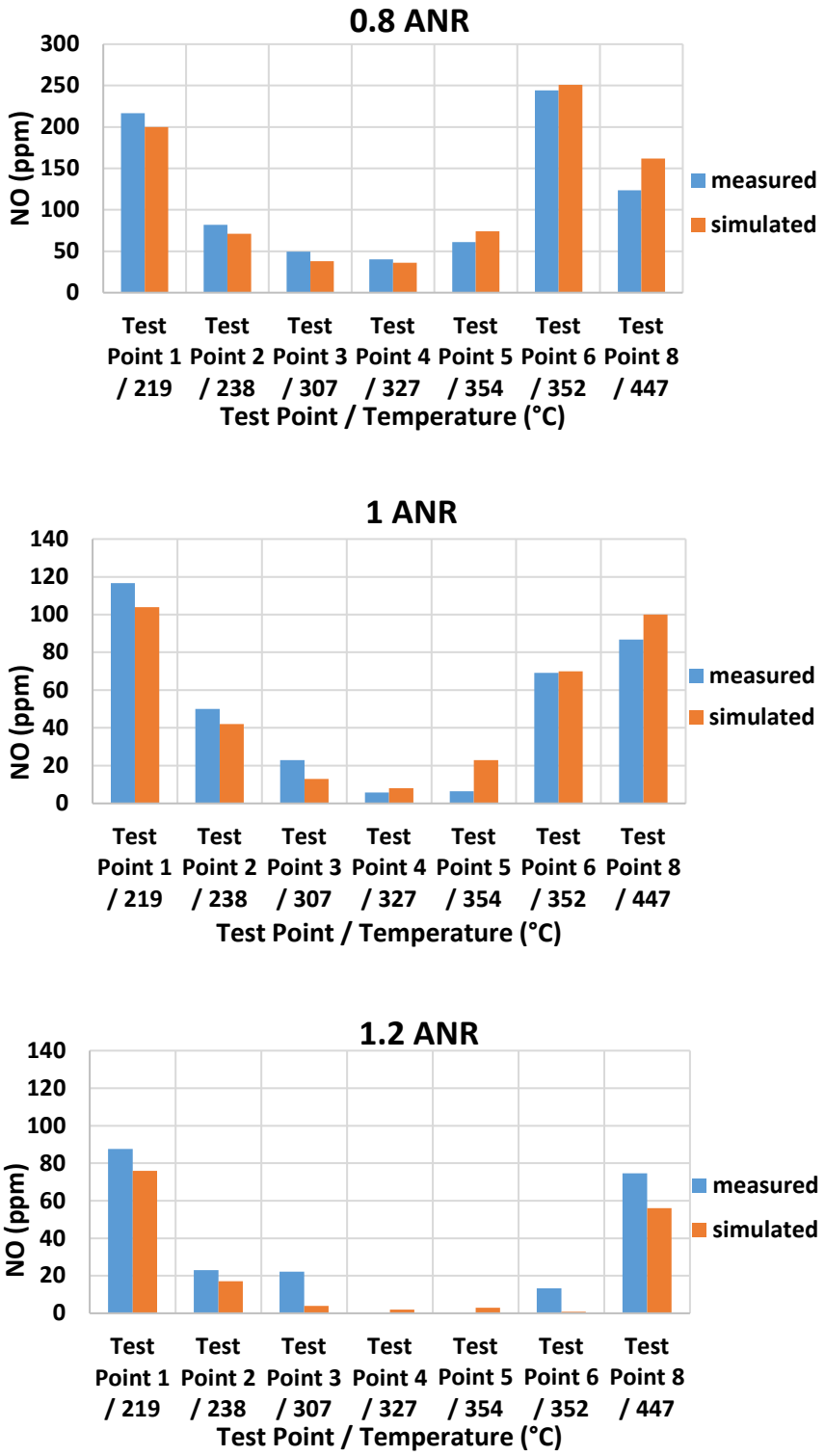

Figure 4.3: Comparison of SCR outlet NO concentrations for various Test Points

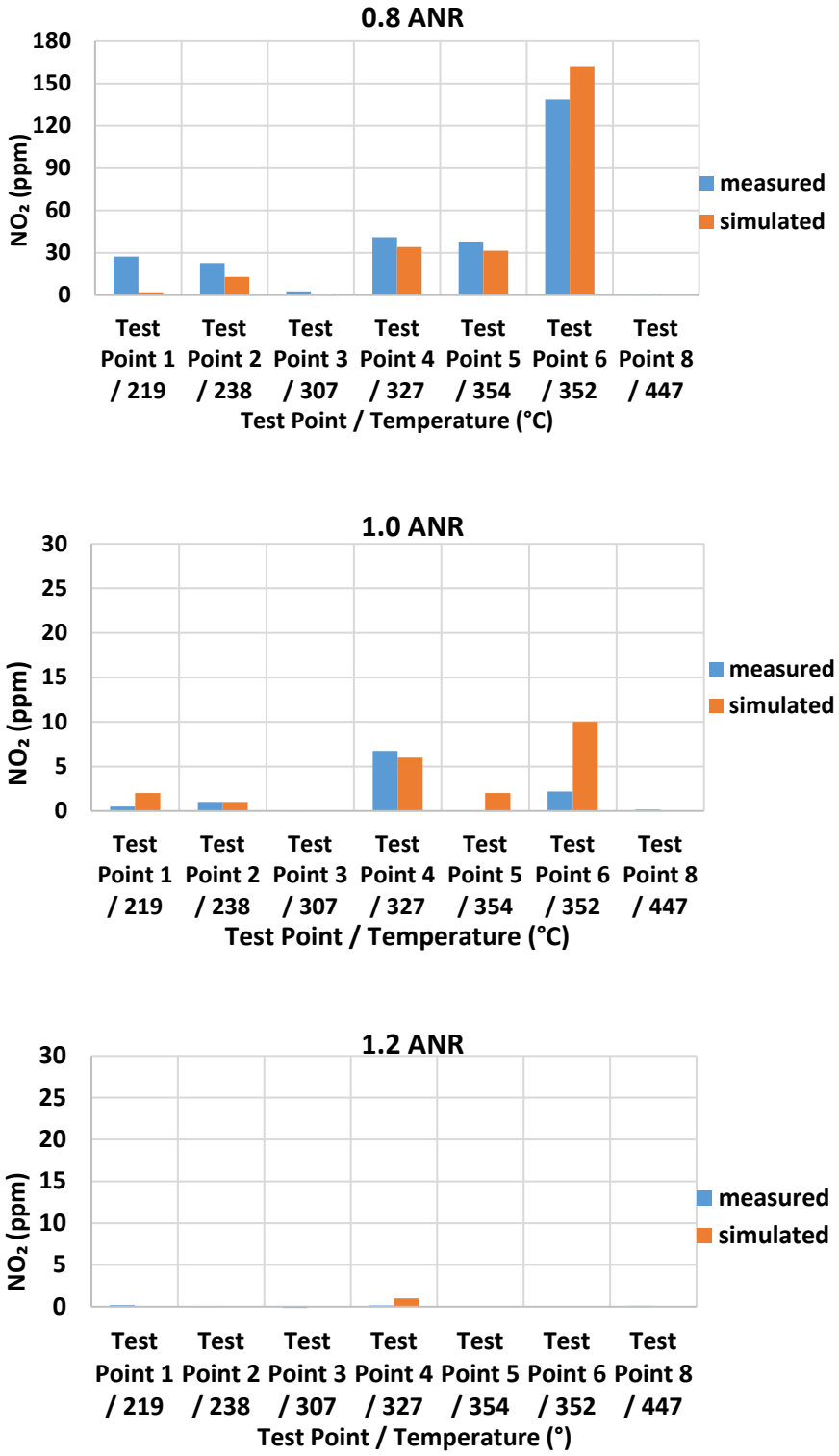

Figure 4.4: Comparison of SCR outlet NO_2 concentrations for various Test Points

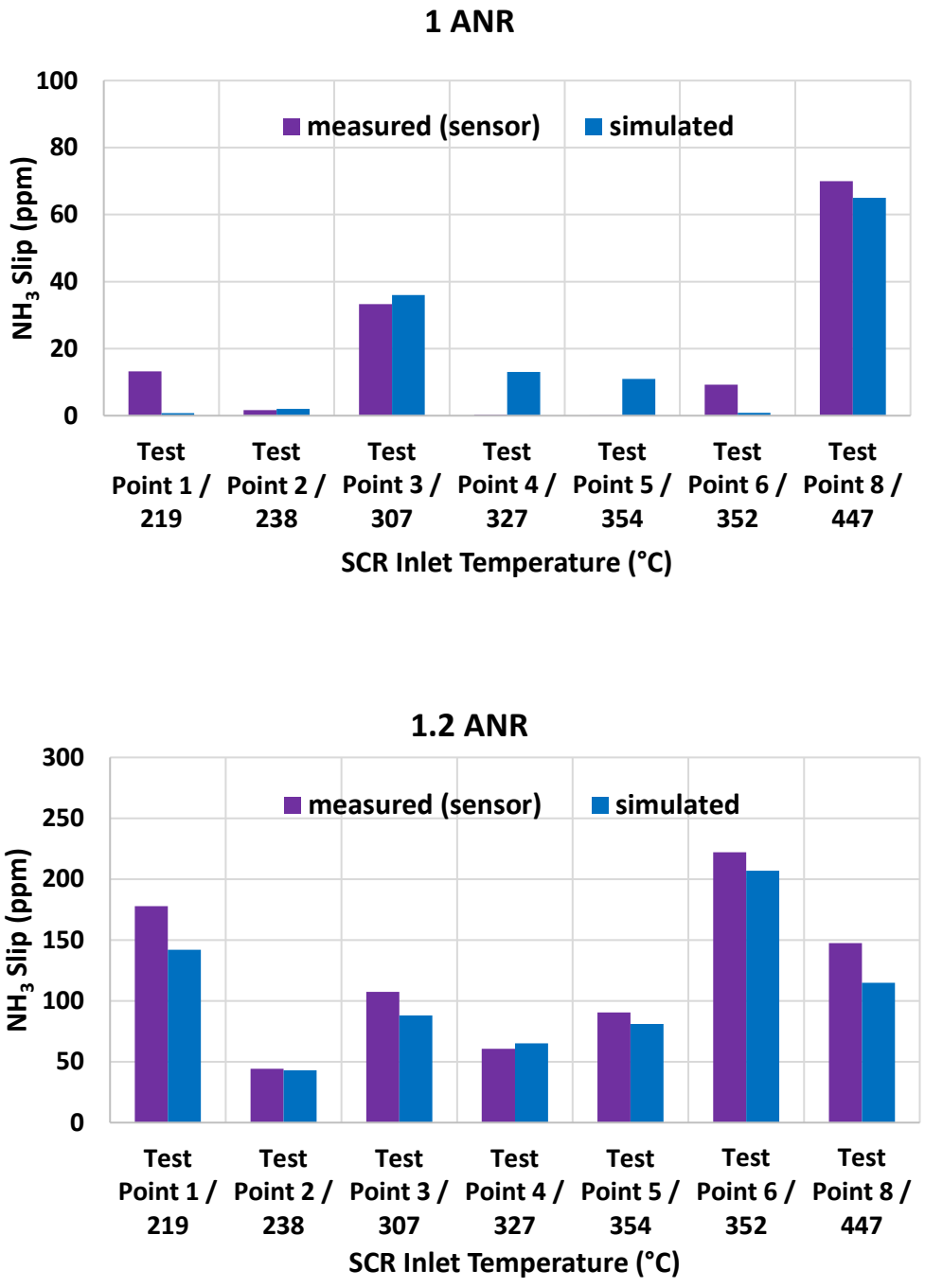

Figure 4.5: Comparison of NH_3 slip concentrations for various Test Points

Comparison the simulation of SCR outlet concentrations of NO, NO_2 and NH_3 data to the experimental data for the Test Point 4 (SCR inlet temperature of 327°C, SV of 26.7 k/hr) and Test Point 1 (SCR inlet temperature of 218°C, SV of 12.0 k/hr) are given in Figures 4.6 and 4.7. The simulation results for the other Test Points are described in Appendix D.

The top plot of the Figure 4.6 shows the SCR inlet concentrations of NO, NO_2 and NH_3. The bottom three plots of the Figure 4.6 show the SCR outlet concentrations of NO, NO_2, NO_x and NH_3 compared between the model simulation and the experimental results. The bottommost plot of the Figure 4.6 compares the NH_3 measured using the MS, the production sensor and the simulated values from the SCR model. Since there was a delay in the measurement of NH_3 slip using the MS and disagreement in the nitrogen balance during a few test runs, NH_3 values measured using the sensor were used for all the calculations.

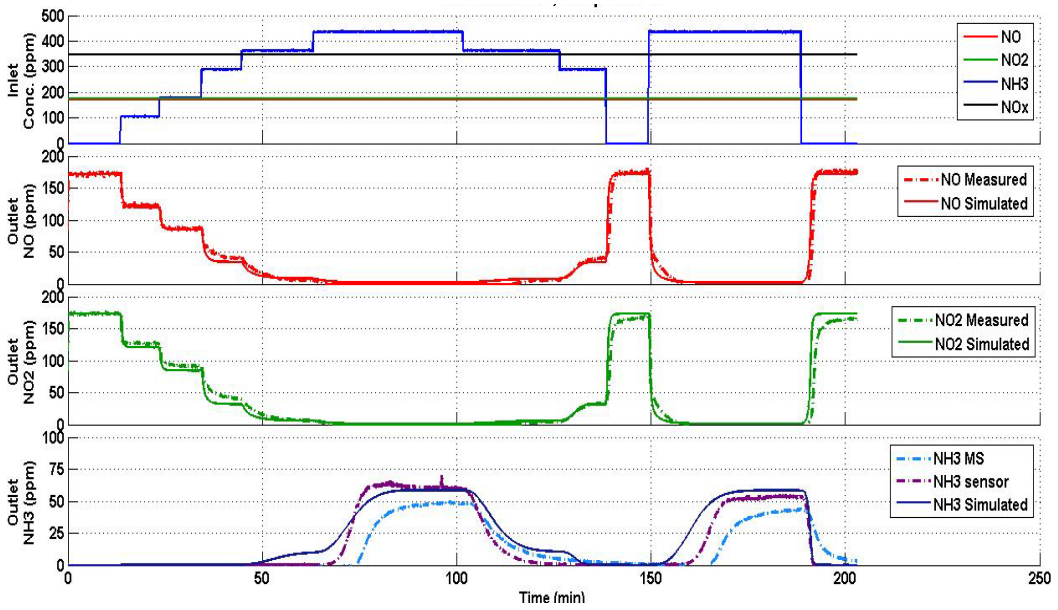

Figure 4.6: Comparison of the SCR outlet gaseous concentrations between simulation results and experimental measurements for Test Point 4 (SCR inlet temperature 327°C, SV 26.7 k/hr) using urea dosing cycle (Figure 3.9)

It can be observed that for Test Point 4, the maximum simulation error under the steady state urea injection condition is less than 10 ppm for NO and NO_2 and less than 15 ppm for NH_3. The simulation results follow the overall trend of the experimental measurements for NO and NO_2, under both steady state and transient urea injection.

However, from Figure 4.7 it can be observed that with the unique set of model parameters, NO_2 values simulated by the model are significantly lower than the NO_2 values measured during the experiment. Hence, for Test Point 1, a different set of parameters was used which is described in Table 4.5. The comparison of results with different parameters for Test Point 1 are shown in Figure 4.8. It can be observed that the difference for NO and NO_2 species has decreased during the steady state and the transient urea dosing conditions.

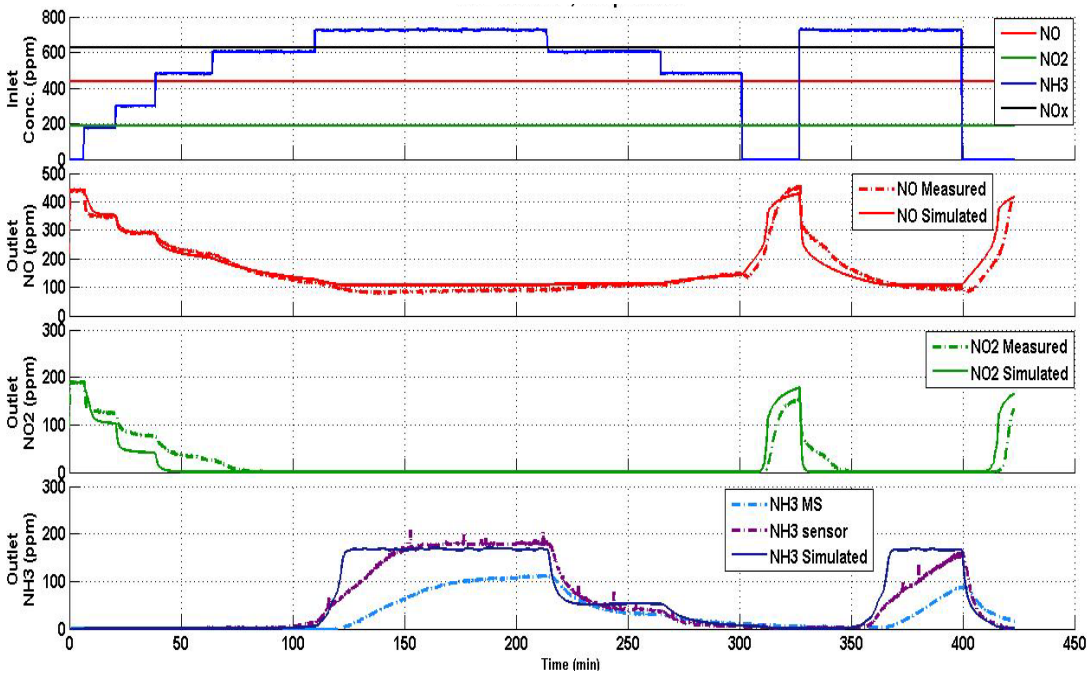

Figure 4.7: Comparison of the SCR outlet gaseous concentrations between simulation results and experimental measurements for Test Point 1 (SCR inlet temperature 218°C, SV 12.0 k/hr) using urea dosing cycle (Figure 3.9)

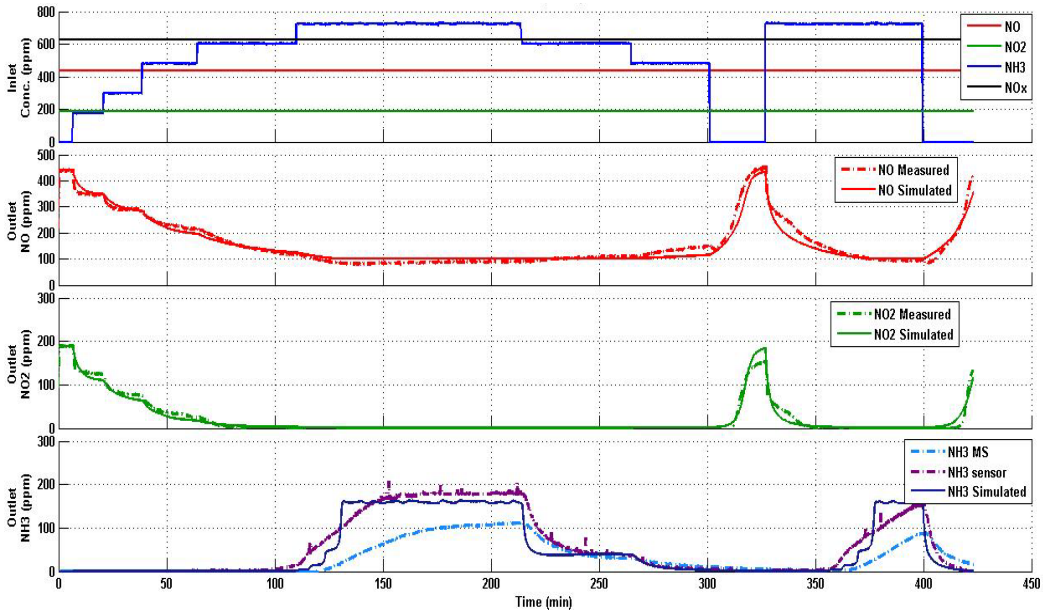

Figure 4.8: Comparison of the SCR outlet gaseous concentrations between simulation results and experimental measurements for Test Point 1 (SCR inlet temperature 218°C, SV 12.0 k/hr), using different parameters as shown in Table 4.5

4.3 SCRF® Experimental Data: Configuration 1 (Passive Oxidation with Urea Injection)

This section discusses the results and analysis of the experimental data obtained from seven passive oxidation tests conducted with urea injection as a part of the configuration 1. The purpose of the passive oxidation tests was to study the effect of the NO_x reduction reactions on the kinetics of the NO_2 assisted passive oxidation and to obtain experimental data for calibrating the SCR-F model.

The NO, NO_2 and NO_x concentrations at the inlet and outlet of the SCRF® and the NO_x conversion efficiency for the seven passive oxidation tests with urea dosing are given in Table 4.9. In Table 4.9, PM_{Start} is the PM deposited in the SCRF® at the beginning of passive oxidation stage, $PM_{Available}$ is the total PM mass available for oxidation during passive oxidation stage and $PM_{Retained}$ is the PM retained in the SCRF® at the end of the passive oxidation stage, as discussed in section 3.6.7 and reference [1]. PM_{Start},

$PM_{Available}$, $PM_{Retained}$ for stage 1, stage 3 and stage 4 are given in reference [1]. From Table 4.9 it is observed that for Test Points A, B and B Rpt, $PM_{Oxidized}$ (explained in section 3.6.7) is less than 30 % and for Test Points C, D, D Rpt and E, $PM_{Oxidized}$ is less than 50%. Hence, during the seven passive oxidation tests with urea injection conducted in configuration 1, the NO_x reduction performance of the SCRF® was studied with PM in the SCRF® varying between 2 – 1 g/L (calculated using PM_{Start} and $PM_{Retained}$ in Table 4.9). The NO_x conversion efficiency for Test Point A and B is approximately 90% and for Test Points D, D-repeat and E, it is approximately 95% as shown in Figure 4.9. These results are in agreement with the results obtained from the production-2013-SCR (discussed in section 4.1). The nitrogen balance for Test Points A, B and B-repeat are around 90% since all the urea is not converted to ammonia at 250 – 260°C. The Test Point B-repeat has NO_x conversion efficiency of 99%, since 1.10 ANR was maintained instead of 1.0. Similarly, the Test Point C has NO_x conversion efficiency of 88%, since 0.89 ANR was maintained during the test instead of 1.0. The NH_3 slip for all the Test Points is below 20 ppm. It can be concluded that the SCRF® with PM loading of 2 g/L, has NO_x conversion efficiency comparable to the production-2013-SCR in the temperature range of 250 to 350°C. The Test Point B-repeat also indicates that the SCRF® has the potential to achieve high NO_x conversion efficiency (98 – 99 %) at ANR greater than 1.0, with NH_3 slip less than 20 ppm. The additional data needed to calibrate the SCR-F model, pressure drop across the SCRF® and temperature distribution in the SCRF®, obtained from configuration 1 (passive oxidation with urea injection) are discussed in the reference [1].

Table 4.9: Emission concentrations and NO_x conversion efficiency during passive oxidation tests with urea injection – Configuration 1 [1]

Test Points	Exhaust Flow Rate	SCRF® Inlet Temp.	SCRF® Inlet NO	SCRF® Inlet NO_2	SCRF® Inlet NO_x	SCRF® Inlet NO_2/NO_x Ratio	SCRF® Outlet NO	SCRF® Outlet NO_2	SCRF® Outlet NO_x	NO_x Conv. Eff.	ANR	NH_3 Slip	Nitrogen Balance	PM_{Start}	$PM_{Available}$	$PM_{Retained}$	$PM_{Oxidized}$
[-]	[kg/min]	[°C]	[ppm]	[ppm]	[ppm]	[-]	[ppm]	[ppm]	[ppm]	[%]	[-]	[ppm]	[%]	[gm]	[gm]	[gm]	[%]
A	5.6	265	286	304	590	0.52	51	4	55	91	1.03	12	90	29.2	35.2	32.0	11
C	6.8	340	387	301	689	0.44	83	3	86	88	0.89	0	98	33.5	34.2	23.2	36
E	7.0	344	798	653	1450	0.45	78	2	80	94	1.01	5	94	32.2	32.3	20.4	39
B	3.6	266	789	821	1610	0.51	137	9	146	91	1.01	1	90	30.3	30.6	22.9	28
B Rpt	3.7	256	822	758	1580	0.48	10	0	10	99	1.10	6	90	28.1	28.5	25.0	16
D	12.3	368	297	153	450	0.34	16	0	16	96	1.01	17	100	30.6	34.5	19.8	45
D Rpt	12.5	365	306	191	497	0.38	24	2	26	95	0.99	17	99	25.7	30.2	16.9	45

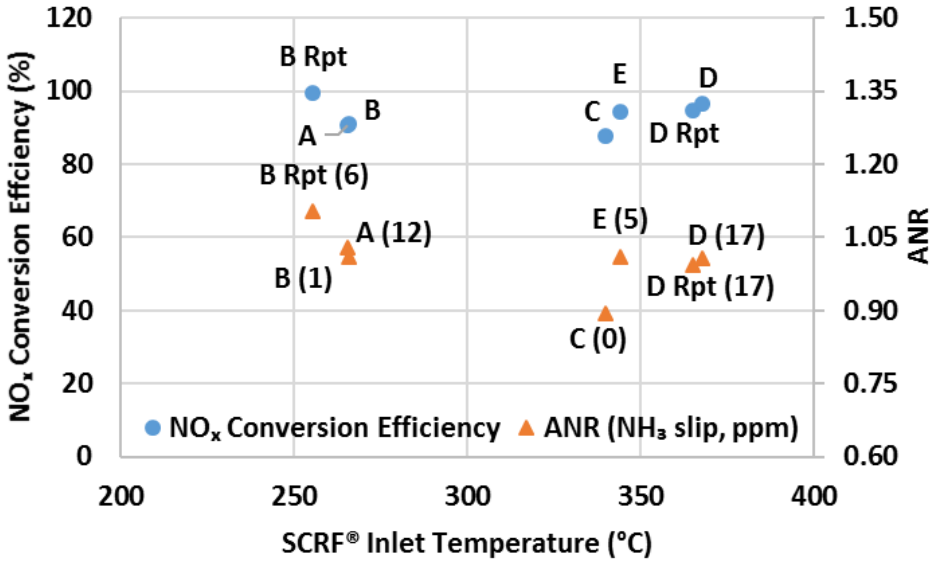

Figure 4.9: NO_x conversion efficiency of the SCRF® – Configuration 1

4.4 SCRF® Experimental Data: Configuration 2 (NO_x Reduction with 0, 2 and 4 g/L PM Loading)

The purpose of these tests was to determine the NO_x reduction performance, NH_3 slip and NH_3 storage for the SCRF® with and without PM in the SCRF® as a function of ANR. The engine conditions and the exhaust parameters at the inlet of the SCRF®, for the twelve NO_x reduction tests with the SCRF® are given in Table 4.10. It can be observed that the engine speed and load were consistent during the four Test Points without PM and with 2 and 4 g/L PM in the SCRF®. Hence the space velocities, SCRF® inlet temperatures, NO_2/NO_x ratios were also consistent at the SCRF® inlet. The four Test Points represent the range of SCRF® inlet temperatures from 200 to 450°C, space velocities from 13 to 48 k/hr, NO_x concentration from 300 to 1600 ppm and NO_2/NO_x ratio from 0.2 to 0.5. The SCRF® inlet conditions described in Table 4.10 are also in agreement with the production-2013-SCR inlet conditions given in Table 4.1.

Table 4.10: Engine exhaust conditions at SCRF® inlet for NO_x reduction Test Points

Parameter	PM Loading	Test Point			
		1	3	6	8
Speed [RPM]	SCRF® - 0 g/L	1199	2200	1202	2401
	SCRF® - 2 g/L	1200	2101	1200	2398
	SCRF® - 4 g/L	1200	2203	1200	2401
Load [Nm]	SCRF® - 0 g/L	201	330	580	826
	SCRF® - 2 g/L	208	329	588	820
	SCRF® - 4 g/L	203	331	587	818
Exhaust Flow [kg/min]	SCRF® - 0 g/L	5.0	10.7	6.9	17.0
	SCRF® - 2 g/L	5.0	9.9	6.8	17.6
	SCRF® - 4 g/L	5.0	10.9	6.8	17.7
SCRF® Inlet Temperature [°C]	SCRF® - 0 g/L	218	304	345	443
	SCRF® - 2 g/L	206	305	340	438
	SCRF® - 4 g/L	207	302	343	446
SCRF® Std. Space Vel. [k/hr]	SCRF® - 0 g/L	13.7	29.1	18.8	46.3
	SCRF® - 2 g/L	13.7	27.0	18.6	48.0
	SCRF® - 4 g/L	13.5	29.8	18.6	48.2
SCRF® Act. Space Vel. [k/hr]	SCRF® - 0 g/L	24.5	60.2	42.0	115.2
	SCRF® - 2 g/L	22.6	53.8	39.3	117.9
	SCRF® - 4 g/L	22.7	56.4	35.7	99.6
SCRF® Inlet NO [ppm]	SCRF® - 0 g/L	345	158	795	411
	SCRF® - 2 g/L	403	161	844	424
	SCRF® - 4 g/L	452	198	793	415
SCRF® Inlet NO_2 [ppm]	SCRF® - 0 g/L	213	121	674	140
	SCRF® - 2 g/L	203	131	744	125
	SCRF® - 4 g/L	141	143	588	115
SCRF® Inlet NO_x [ppm]	SCRF® - 0 g/L	558	279	1468	551
	SCRF® - 2 g/L	607	292	1588	548
	SCRF® - 4 g/L	594	341	1381	530
Upstream NO_2/NO_x	SCRF® - 0 g/L	0.38	0.43	0.46	0.25
	SCRF® - 2 g/L	0.34	0.45	0.47	0.23
	SCRF® - 4 g/L	0.26	0.42	0.43	0.22
Engine Out PM [mg/scm]	SCRF® - 0 g/L	N/A	N/A	N/A	N/A
	SCRF® - 2 g/L	2.14	4.30	3.59	7.39
	SCRF® - 4 g/L	1.97	4.93	2.85	4.97

N/A - Engine out PM concentrations not measured for tests without PM in the SCRF®

The NO_2/NO_x ratio at the inlet of the SCRF® is dependent on the NO to NO_2 conversion efficiency of the DOC, which in turn is dependent on the DOC inlet temperature and

space velocity of the exhaust, flowing through the DOC. The NO conversion efficiency of the DOC is defined in equation 4.3.

$$\text{NO Conversion Efficiency (\%)} = \frac{\text{DOC Inlet NO} - \text{DOC Outlet NO}}{\text{DOC Inlet NO}} * 100 \qquad \text{Eqn. 4.3}$$

The NO and NO_2 concentrations at the inlet and outlet of the DOC during the twelve NO_x reduction tests are given in Table 4.11. The exhaust conditions and the NO conversion efficiency of the DOC are given in the Table 4.12. The NO conversion efficiency was maximum in the range of 300 to 350°C which is in agreement with the trend for NO conversion efficiency observed by reference [7]. However, the NO conversion efficiency for Test Point 1, without PM in the SCRF®, was observed to be 40 %, which is 10 – 20 % higher than the results obtained from the Test Point 1 with PM loading in the SCRF®. This could be due to inconsistency in the NO data obtained from the mass spectrometer.

Table 4.11: NO and NO_2 concentration at the inlet and outlet of DOC during NO_x reduction stage – configuration 2

Test Point	NO [ppm]						NO_2 [ppm]					
	SCRF® – 0 g/L		SCRF® – 2 g/L		SCRF® – 4 g/L		SCRF® – 0 g/L		SCRF® – 2 g/L		SCRF® – 4 g/L	
	In	Out	In	Out	In	Out	In	Out	In	Out	In	Out
1	575	345	581	403	515	411	5	213	2	203	37	141
3	257	160	288	161	324	198	18	120	0	131	1	124
6	1336	795	1484	743	1483	793	18	674	4	644	14	588
8	542	411	556	424	507	415	1	140	2	125	8	115

Table 4.12: DOC exhaust conditions and NO conversion efficiency during NO_x reduction stage – configuration 2

Test Point	DOC Inlet Temperature [°C]			SCRF® Space Velocity [k/hr]			NO Conversion Efficiency [%]		
	SCRF®-0	SCRF®-2	SCRF®-4	SCRF®-0	SCRF®-2	SCRF®-4	SCRF®-0	SCRF®-2	SCRF®-4
1	221	218	214	56	56	55	40	31	20
3	306	315	316	119	111	121	38	44	39
6	346	355	362	77	76	76	40	43	46
8	439	442	449	189	196	197	24	24	18

4.4.1 Experimental Data

The NO, NO_2 and NH_3 slip concentrations downstream of the SCRF® and NO_x conversion efficiency of the SCRF® relative to the ANR for various Test Points, with and without PM loading in the SCRF® are shown in Figures 4.10, 4.11, 4.12 and 4.13. From Figure 4.10 it can be observed that for Test Point 1, with and without PM loading, <10 ppm of NO_2 is remaining downstream of the SCRF® at ANR >0.8. The NO concentrations decrease from ~130 ppm to <20 ppm when ANR is increased from 0.8 to 1.2.The NO_x conversion efficiency of the SCRF® increases from ~75 % at ANR 0.8 to ~90 % at ANR 1.0 due to availability of more ammonia to react with NO_x in the exhaust gases. The NO_x conversion efficiency of the SCRF® with 2 and 4 g/L of PM loading was observed to be 2 – 3 % higher than the NO_x conversion efficiency of the SCRF® without PM loading, at ANR 0.8 and 1.0.

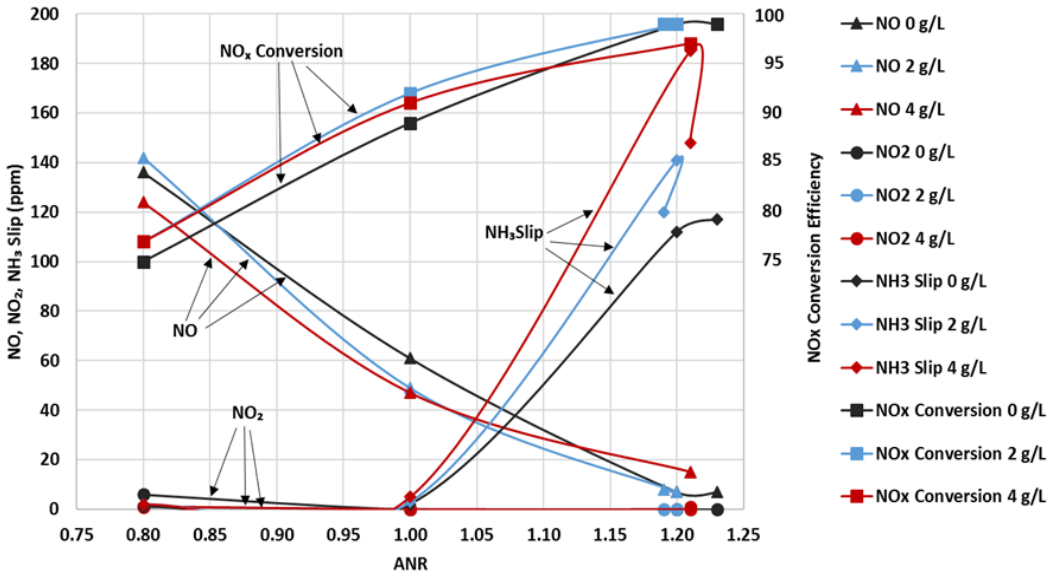

Figure 4.10: NO, NO_2 NH_3 slip downstream of the SCRF® and NO_x conversion efficiency at various ANR for Test Point 1, with and without PM in the SCRF® (SCRF® inlet temperature = 201 °C and SV = 13.7 k/hr)

The NH_3 slip <10 ppm was observed up to ANR 1.0, with and without PM loading in the SCRF®. However, the NH_3 slip increased to 100 -150 ppm at ANR 1.2 due to excess ammonia availability in the SCRF®. A reduction in the NO_x conversion efficiency of the

SCRF® with PM loading was observed at ANR 1.2. This is evident from the change in the slope of the NO_x conversion trend of the SCRF® with PM loading (Blue and Red lines). The NO_x conversion efficiency at ANR 1.2 was the least for the SCRF® with PM loading of 4 g/L. Hence, at ANR 1.2, the SCRF® with PM loading of 4 g/L had the highest NH_3 slip from the SCRF®.

The trends for NO and NO_2 concentrations downstream of the SCRF® for Test point 3 with and without PM loading were similar to Test Point 1. The NO and NO_2 concentrations decreased to <20 ppm with increase in ANR from 0.8 to 1.0. The NO_x conversion efficiency increased from ~82 % at ANR 0.8 to ~96 % at ANR 1.0. The actual ANR for the test with 4 g/L PM loading was higher than the targeted ANR, as indicated by the red line (0.8, 1.0 and 1.2). Hence, 2 – 3 % higher NO_x conversion efficiency was observed. The NH_3 slip <10 ppm were observed at ANR 1.0. However, the NH_3 slip increased to 60 ppm at ANR 1.2.

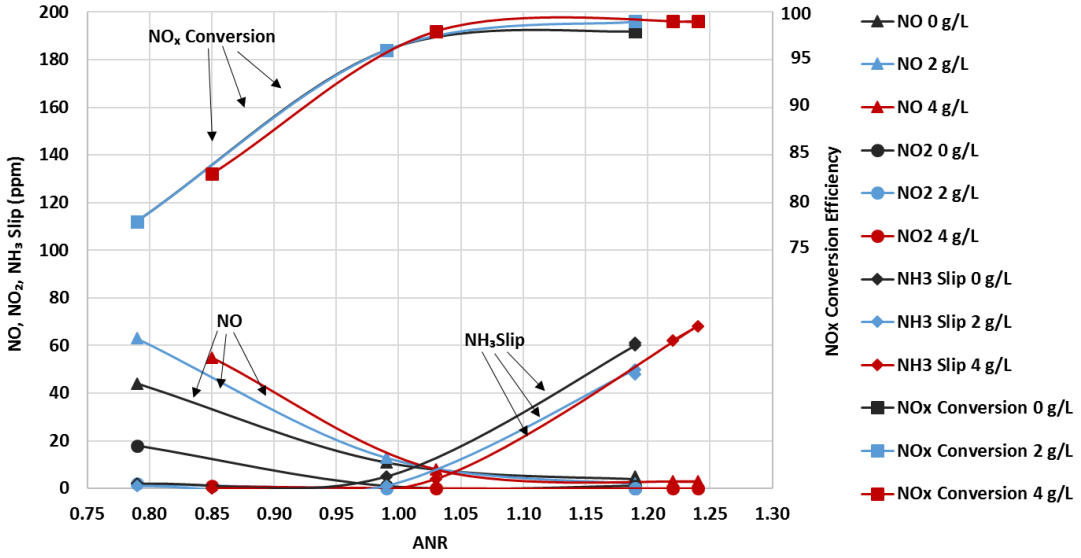

Figure 4.11: NO, NO_2 NH_3 slip downstream of the SCRF® and NO_x conversion efficiency at various ANR for Test Point 3, with and without PM in the SCRF® (SCRF® inlet temperature = 304 °C and SV = 29.1 k/hr)

Figures 4.12 and 4.13 show the NO, NO_2 and NH_3 slip concentrations downstream of the SCRF® and NO_x conversion efficiency of the SCRF® relative to the ANR for Test Points 6 and 8 respectively, with and without PM loading in the SCRF®. From Figure 4.12 it is observed that ~100 ppm NO and ~150 ppm NO_2 concentrations were present downstream of the SCRF at ANR 0.8 for Test Point 6 without PM loading. However, the concentrations decreased to <10 ppm for Test Point 6 with 2 and 4 g/L PM loading at ANR 0.8. This is due to the consumption of NO_2 via NO_2 assisted oxidation of PM. From Figures 4.12 and 4.13 it is observed that the NO_x conversion for the test without PM loading (black line) is 3 – 4 % higher that the tests with 2 and 4 g/L PM loading in the SCRF®. This could be attributed to decrease in the effective NO_2/NO_x ratios on the SCRF® catalyst due to consumption of NO_2 via NO_2 assisted oxidation of PM. The NO_x conversion efficiency for Test point 8 with PM loading is observed to be ~87 % at ANR 1.0 and ~92 % at ANR 1.2, which is 6 – 7 % lower than the corresponding NOx conversion efficiency for Test Points 3 and 6.

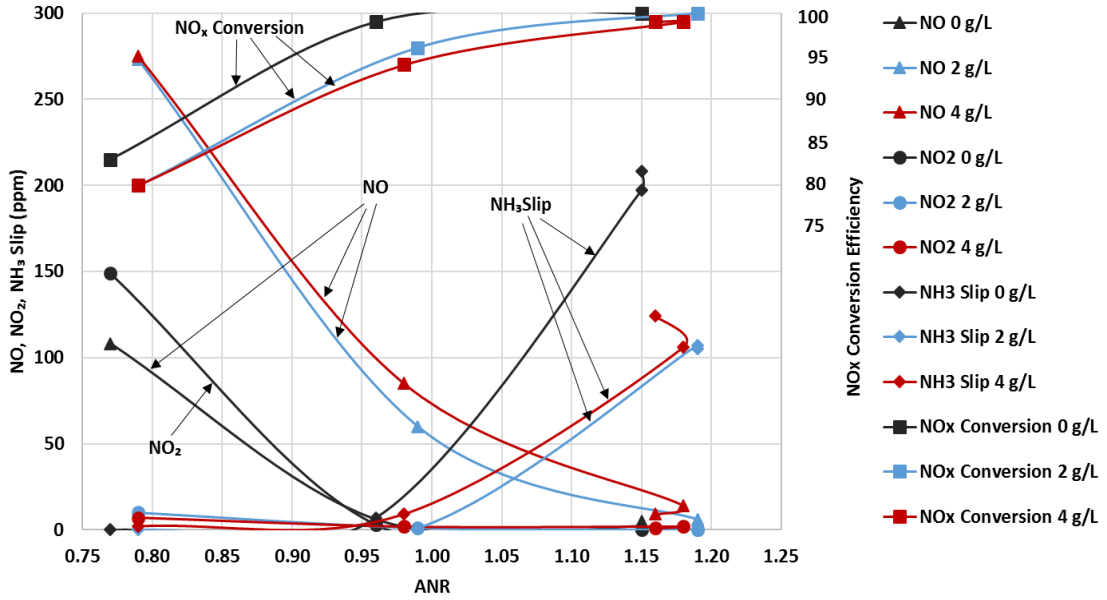

Figure 4.12: NO, NO_2 NH_3 slip downstream of the SCRF® and NO_x conversion efficiency at various ANR for Test Point 6, with and without PM in the SCRF® (SCRF® inlet temperature = 345 °C and SV = 18.8 k/hr)

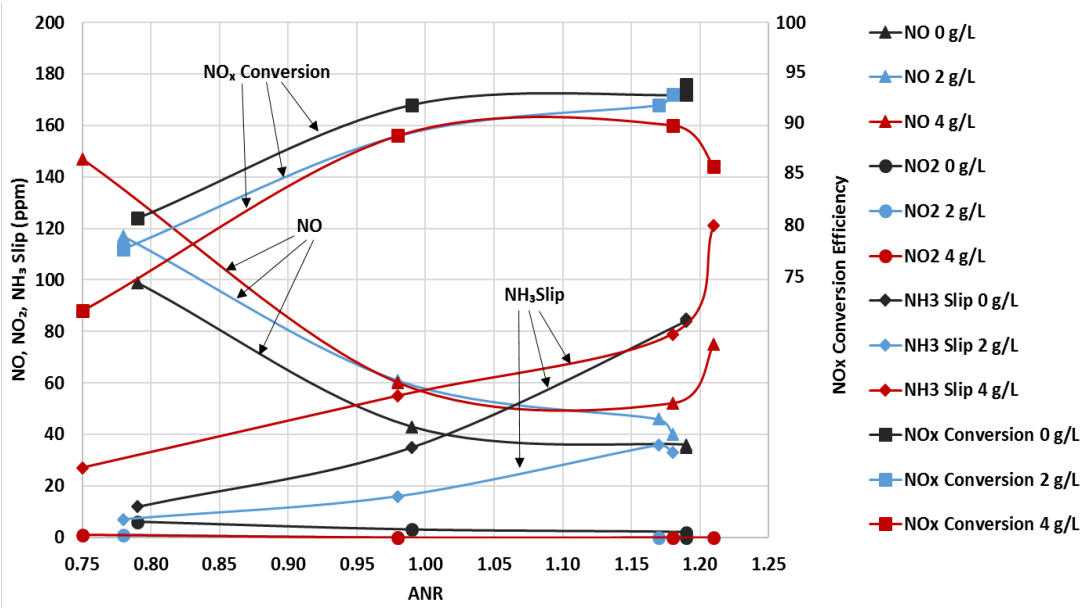

Figure 4.13: NO, NO_2 NH_3 slip downstream of the SCRF® and NO_x conversion efficiency at various ANR for Test Point 8, with and without PM in the SCRF® (SCRF® inlet temperature = 443 °C and SV = 46.3 k/hr)

4.4.2 Analysis of Data

The analysis of NO and NO_2 concentrations at 0 ANR (without urea injection) for the SCRF® without PM loading and with 2 and 4 g/L of PM loading are given in Tables 4.13, 4.14 and 4.15 respectively. From Table 4.13 it can be observed that the NO and NO_2 concentrations at the SCRF® inlet and outlet remain unchanged for all the Test Points, without PM loading in the SCRF®. This indicates that the SCRF® has negligible tendency to oxidize NO to NO_2. However, the production-2013-SCR showed up to 20 % conversion of NO to NO_2 across the two SCR-A brick, without urea injection.

Table 4.13: NO and NO_2 concentrations at the inlet and outlet of the SCRF® at 0 ANR without PM loading in the SCRF®

Test Point	SCRF® Inlet Temp.	SCRF® Inlet NO	SCRF® Outlet NO	Delta NO	SCRF® Inlet NO_2	SCRF® Outlet NO_2	Delta NO_2	SCRF® Inlet NO_x	SCRF® Outlet NO_x	Ratio of In/Out NO_2
[-]	[°C]	[ppm]	[ppm]	[ppm]	[ppm]	[ppm]	[ppm]	[ppm]	[ppm]	[-]
1	213	345	352	-7	213	200	13	558	552	0.94
3	301	158	160	-2	121	116	5	279	276	0.96
6	345	795	808	-13	674	688	-14	1469	1496	1.02
8	443	411	415	-4	140	139	1	551	554	0.99

From Table 4.14 and 4.15 it can be observed that the ratio of the SCRF® outlet NO_2 to the SCRF® inlet NO_2 decreases with the increase in the SCRF® inlet temperature (Test Points are arranged in the increasing order of the SCRF® inlet temperature) and increase in PM loading in the SCRF®. This can be attributed to the consumption of NO_2 via NO_2 assisted oxidation of PM, as indicated by the reactions in equations 4.4 and 4.5. The higher proportion of NO_2 available at the SCRF® inlet is consumed through the NO_2 assisted oxidation of PM, as the substrate temperature and PM in the filter increases. The NO_2 is converted to NO by oxidation of PM, hence the coherent increase of NO concentration at the SCRF® outlet was also observed as indicated in Table 4.12 and 4.13.

$$C + NO_2 \rightarrow CO + NO \qquad \text{Eqn. 4.4}$$

$$C + 2NO_2 \rightarrow CO_2 + 2NO \qquad \text{Eqn. 4.5}$$

Table 4.14: NO and NO_2 concentrations at the inlet and outlet of the SCRF® at 0 ANR with 2 g/L PM loading in the SCRF®

Test Point	SCRF® Inlet Temp.	SCRF® Inlet NO	SCRF® Outlet NO	Delta NO	SCRF® Inlet NO_2	SCRF® Outlet NO_2	Delta NO_2	SCRF® Inlet NO_x	SCRF® Outlet NO_x	Ratio of In/Out NO_2
[-]	[°C]	[ppm]	[ppm]	[ppm]	[ppm]	[ppm]	[ppm]	[ppm]	[ppm]	[-]
1	206	403	387	16	203	205	-2	606	592	1.01
3	305	161	198	-37	131	88	43	292	286	0.67
6	340	743	963	-220	644	424	220	1387	1387	0.66
8	438	424	457	-33	125	52	73	549	509	0.42

Table 4.15: NO and NO_2 concentrations at the inlet and outlet of the SCRF® at 0 ANR with 4 g/L PM loading in the SCRF®

Test Point	SCRF® Inlet Temp.	SCRF® Inlet NO	SCRF® Outlet NO	Delta NO	SCRF® Inlet NO_2	SCRF® Outlet NO_2	Delta NO_2	SCRF® Inlet NO_x	SCRF® Outlet NO_x	Ratio of In/Out NO_2
[-]	[°C]	[ppm]	[ppm]	[ppm]	[ppm]	[ppm]	[ppm]	[ppm]	[ppm]	[-]
1	207	452	401	51	141	116	25	593	517	0.82
3	302	198	249	-51	124	75	49	322	324	0.60
6	341	793	1151	-358	588	231	357	1381	1382	0.39
8	446	415	502	-87	115	22	93	530	524	0.19

The consumption of NO_2, through NO_2 assisted oxidation of PM, changes the NO_2/NO_x ratio across the catalyst. The NO_2/NO_x ratios at the inlet and outlet of the SCRF® without urea injection (0 ANR) are given in Table 4.16. Since the ANR is 0, NO_2 consumption through SCR reactions is zero and the changes in the NO_2/NO_x ratios are only due to consumption of NO_2 through NO_2 assisted oxidation of PM. Figure 4.14 shows the NO_2/NO_x ratios at the inlet and outlet of the SCRF® at 0 ANR. It can be observed that the SCRF® inlet and outlet NO_2/NO_x ratio remains unchanged for Test Point 1, since the SCRF® inlet temperature is approximately 200°C and NO_2 assisted oxidation of PM is negligible at that temperature. However, as the SCRF® inlet temperature increases for 2 and 4 g/L data, the difference between the inlet and outlet NO_2/NO_x ratios increases due to consumption of NO_2 through NO_2 assisted oxidation of PM. As the PM loading in the SCRF® increases from 2 to 4 g/L for the same Test Point, the difference between the inlet and outlet NO_2/NO_x ratios increases further indicating higher proportion of NO_2 being consumed through NO_2 assisted oxidation of PM, with increase in PM loading from 2 to 4 g/L. Due to NO_2 consumption, the effective NO_2/NO_x ratio at the reaction site on the substrate of the SCRF® could be much lower than the NO_2/NO_x ratios at the SCRF® inlet. Hence, effective NO_2/NO_x ratio should be considered while analyzing the NO_x reduction performance of the SCRF®.

Table 4.16: NO_2/NO_x ratios at the inlet and outlet of the SCRF® at 0 ANR

Test Point	SCRF® Inlet Temp. [°C]	SCRF® - 0 g/L		SCRF® - 2 g/L		SCRF® - 4 g/L	
		Inlet NO_2/NO_x	Outlet NO_2/NO_x	Inlet NO_2/NO_x	Outlet NO_2/NO_x	Inlet NO_2/NO_x	Outlet NO_2/NO_x
1	213	0.38	0.36	0.34	0.35	0.24	0.22
3	301	0.43	0.42	0.45	0.31	0.42	0.23
6	345	0.46	0.46	0.47	0.31	0.43	0.17
8	443	0.25	0.25	0.23	0.1	0.22	0.04

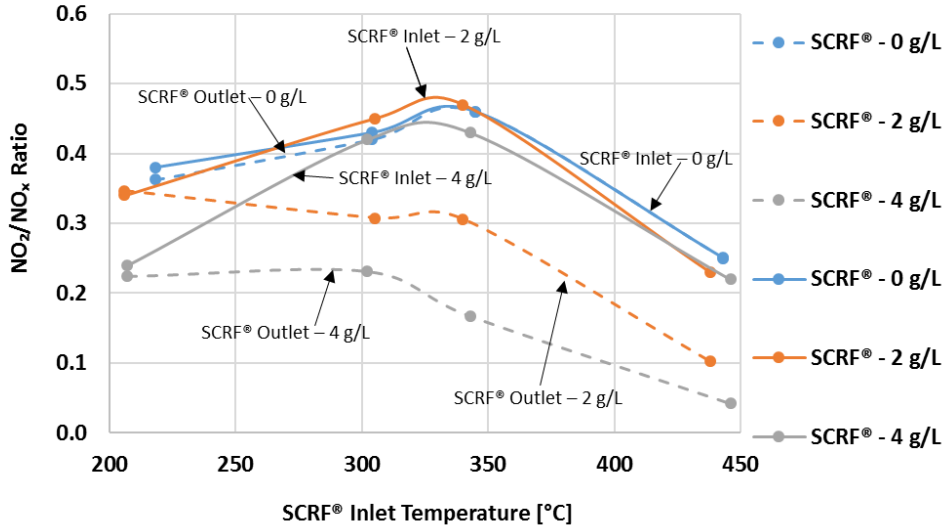

Figure 4.14: NO_2/NO_x ratios at the inlet and outlet of the SCRF® at 0 ANR

Table 4.17 and 4.18 provide the NO, NO_2 and NH_3 concentrations downstream of the SCRF® and the NO_x conversion efficiency of the SCRF® at ANR of 0.8. It can be observed that the NO_x conversion efficiency improved by 2 – 4% for Test Point 1 and 3, with increase in the PM loading. However, for Test Point 6 and 8, NO_x conversion efficiency reduced by 5 – 10%, with increase in PM. The NO_x conversion efficiency for all the Test Points is shown in Figure 4.15. From Figure 4.16 it can be observed that less than 10 ppm NH_3 slip was observed downstream of the SCRF® except for Test Point 8, which is in agreement with the values observed for the production-2013-SCR, described in the section 4.1.

Table 4.17: NO, NO_2 and NH_3 concentrations at inlet and outlet of the SCRF® at ANR 0.8

Test Point	NO [ppm]						NO_2 [ppm]						NH_3 [ppm]					
	SCRF®-0		SCRF®-2		SCRF®-4		SCRF®-0		SCRF®-2		SCRF®-4		SCRF®- 0		SCRF®- 2		SCRF®- 4	
	In	Out	In	Out	In	Out	In	Out	In	Out	In	Out	In	Out	In	Out	In	Out
1	345	136	403	142	411	124	213	6	203	1	141	1	446	1	486	2	481	2
3	158	44	161	63	198	55	121	18	131	2	124	1	220	2	231	1	274	0
6	795	108	743	273	793	275	674	149	644	10	588	7	1125	0	1096	0	1093	2
8	411	99	424	117	415	147	140	6	125	1	115	1	438	12	426	7	399	27

Table 4.18: NO_x conversion efficiency of the SCRF® at ANR 0.8

Test Point	ANR			NO_x conversion efficiency [%]			Nitrogen Balance [%]		
	SCRF®-0	SCRF®-2	SCRF®-4	SCRF®-0	SCRF®-2	SCRF®-4	SCRF®-0	SCRF®-2	SCRF®-4
1	0.80	0.80	0.80	75	77	79	94	96	99
3	0.79	0.79	0.85	78	78	82	99	99	97
6	0.77	0.79	0.79	83	80	80	108	101	101
8	0.79	0.78	0.75	81	78	72	105	103	102

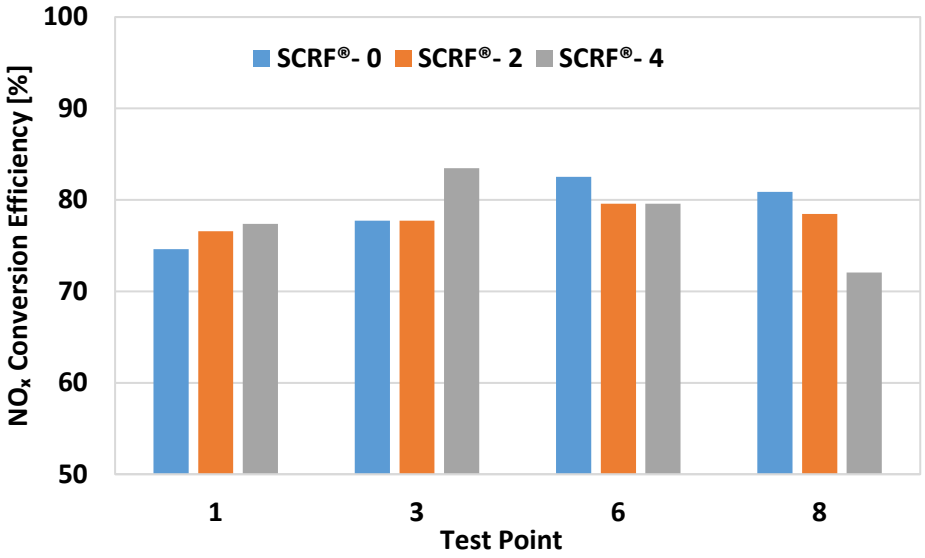

Figure 4.15: NO_x conversion efficiency of the SCRF® with and without PM at ANR 0.8

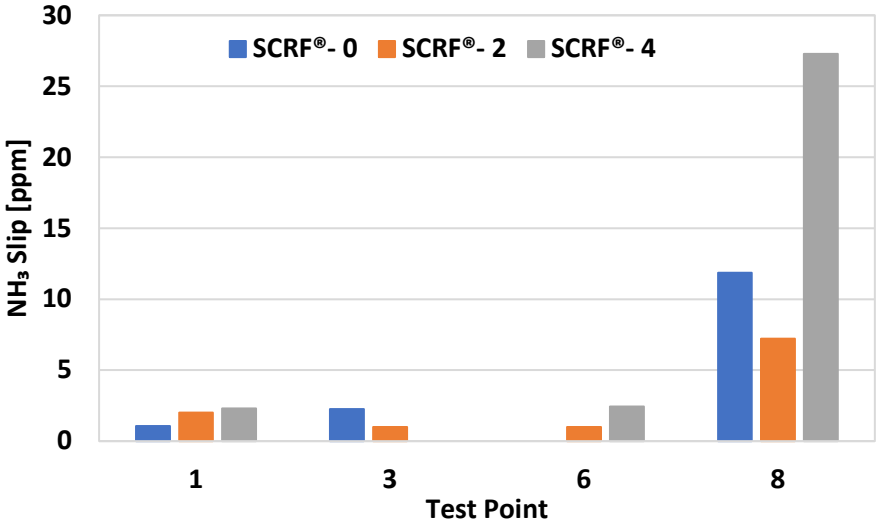

Figure 4.16: NH_3 Slip from the SCRF® with and without PM at ANR 0.8

Table 4.19 and 4.20 provide the NO, NO_2 and NH_3 concentrations downstream of the SCRF® and the NO_x conversion efficiency of the SCRF® at ANR of 1.0. Since the SCRF® inlet NO_2/NO_x ratios were lower than 0.5, most of NO_2 at the inlet of the SCRF® is reduced at ANR of 1.0. Table 4.20 and Figure 4.17 indicate that the NO_x conversion was not affected significantly by PM loading in the SCRF®, at SCRF® inlet temperatures below 300°C (Test Point 1 and 3). The NO_x conversion efficiency for Test Point 1 without PM loading is observed to be lower (89 %) due to insufficient stabilization time for measurement of the concentrations at the outlet of the SCRF®. The NO_x conversion efficiency for Test Point 3 with 4 g/L PM loading is observed to be higher by 2% due to higher ANR (1.03). However, increase in the PM deposition affected the NO_x conversion efficiency of the SCRF®, at SCRF® inlet temperatures above 350°C (Test Point 6 and 8). This could be attributed to the reduced effective NO_2/NO_x ratio in the SCRF®, as described in Table 4.16, since a significant amount of NO_2 is consumed through the passive oxidation pathway. Hence, the lower effective NO_2/NO_x ratio reduces the NO_x conversion for Test Point 6 and 8. The SCRF® inlet ANR was maintained very close to 1.0 and the nitrogen balance for all the tests is also very close to 100%, indicating that the urea injection, NO_x conversion and ammonia slip phenomenon are in agreement.

Tables 4.21 and 4.22 provide the NO, NO_2 and NH_3 concentrations downstream of the SCRF® and the NO_x conversion efficiency of the SCRF® at ANR of 1.2. Table 4.22 shows that most of the NO_x is reduced in the SCRF® at ANR of 1.2 and the NO_x conversion efficiency is above 99% for all the Test Points except Test Point 8. As described in Table 4.10, Test Point 8 is a high temperature (450°C) and high SV and (48 k/hr) Test Point. Oxidation of NH_3 to N_2 and NO is a dominant reaction at temperatures above 400°C, the NO_x conversion efficiency is poor. Also the Nitrogen balance is poor for this condition since N2 and N_2O are not considered in the nitrogen balance estimation.

Table 4.19: NO, NO_2 and NH_3 concentrations at inlet and outlet of the SCRF® at ANR 1.0

Test Point	NO [ppm]						NO_2 [ppm]						NH_3 [ppm]					
	SCRF®-0		SCRF®-2		SCRF®-4		SCRF®-0		SCRF®-2		SCRF®-4		SCRF®- 0		SCRF®- 2		SCRF®- 4	
	In	Out	In	Out	In	Out	In	Out	In	Out	In	Out	In	Out	In	Out	In	Out
1	345	61	403	49	411	47	213	0	203	0	141	0	558	2	609	3	600	5
3	158	11	161	13	198	8	121	1	131	0	124	0	275	5	289	1	331	4
6	795	6	743	60	793	85	674	3	644	1	588	2	1404	7	1370	1	1360	9
8	411	43	424	61	415	60	140	3	125	0	115	0	548	35	536	16	522	55

Table 4.20: NO_x conversion efficiency of the SCRF® at ANR 1.0

Test Point	ANR			NO_x conversion efficiency [%]			Nitrogen Balance [%]		
	SCRF®-0	SCRF®-2	SCRF®-4	SCRF®-0	SCRF®-2	SCRF®-4	SCRF®-0	SCRF®-2	SCRF®-4
1	1.00	1.00	1.00	89	92	92	89	92	93
3	0.99	0.99	1.03	96	96	98	99	97	96
6	0.96	0.99	0.98	99	96	94	104	97	96
8	0.99	0.98	0.98	92	89	89	99	94	101

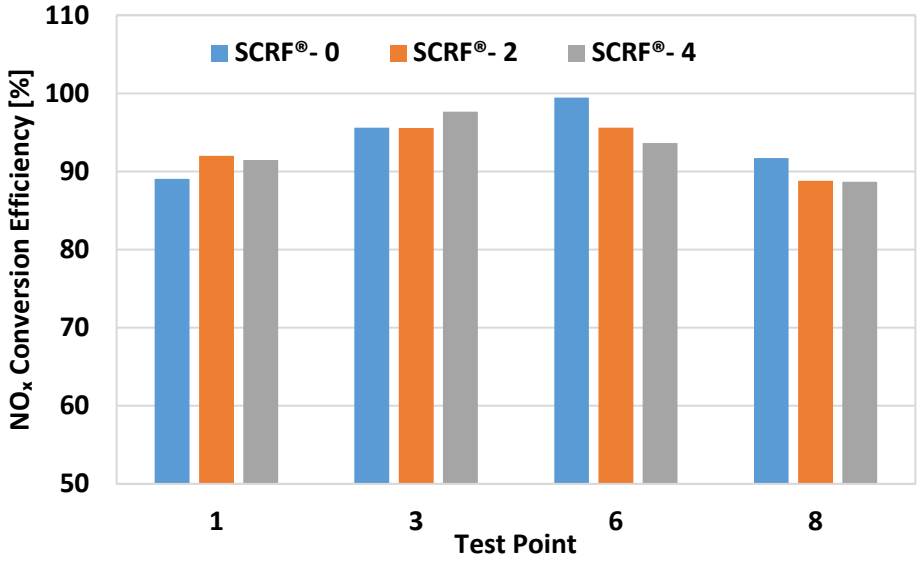

Figure 4.17: NO_x conversion efficiency of the SCRF® with and without PM at ANR 1.0

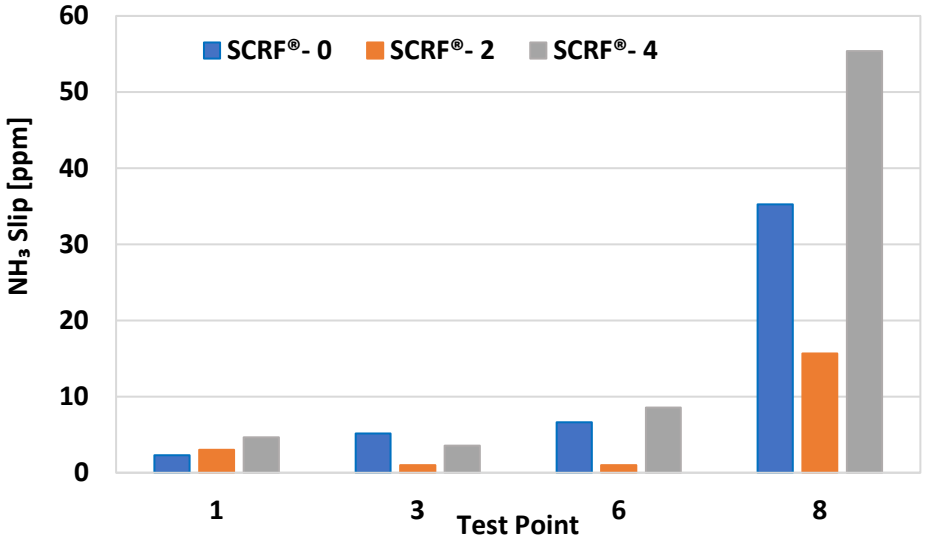

Figure 4.18: NH_3 Slip from the SCRF® with and without PM at ANR 1.0

Table 4.21: NO, NO_2 and NH_3 concentrations at inlet and outlet of the SCRF® at ANR 1.2

Test Point	NO [ppm]						NO_2 [ppm]						NH_3 [ppm]					
	SCRF®-0		SCRF®-2		SCRF®-4		SCRF®-0		SCRF®-2		SCRF®-4		SCRF®- 0		SCRF®- 2		SCRF®- 4	
	In	Out	In	Out	In	Out	In	Out	In	Out	In	Out	In	Out	In	Out	In	Out
1	345	7	403	7	411	15	213	0	203	0	141	0	669	112	730	141	722	185
3	158	4	161	2	198	3	121	1	131	0	143	0	331	60	347	50	398	68
6	795	2	743	6	793	14	674	-1	644	0	588	2	1685	197	1644	107	1633	106
8	411	36	424	46	415	52	140	2	125	0	115	0	657	84	640	36	626	79

Table 4.22: NO_x conversion efficiency of the SCRF® at ANR 1.2

Test Point	ANR			NO_x conversion efficiency [%]			Nitrogen Balance [%]		
	SCRF®-0	SCRF®-2	SCRF®-4	SCRF®-0	SCRF®-2	SCRF®-4	SCRF®-0	SCRF®-2	SCRF®-4
1	1.20	1.20	1.21	99	99	98	99	103	100
3	1.19	1.19	1.24	98	99	99	101	98	97
6	1.15	1.19	1.18	100	100	99	99	91	90
8	1.19	1.17	1.18	93	92	90	91	84	89

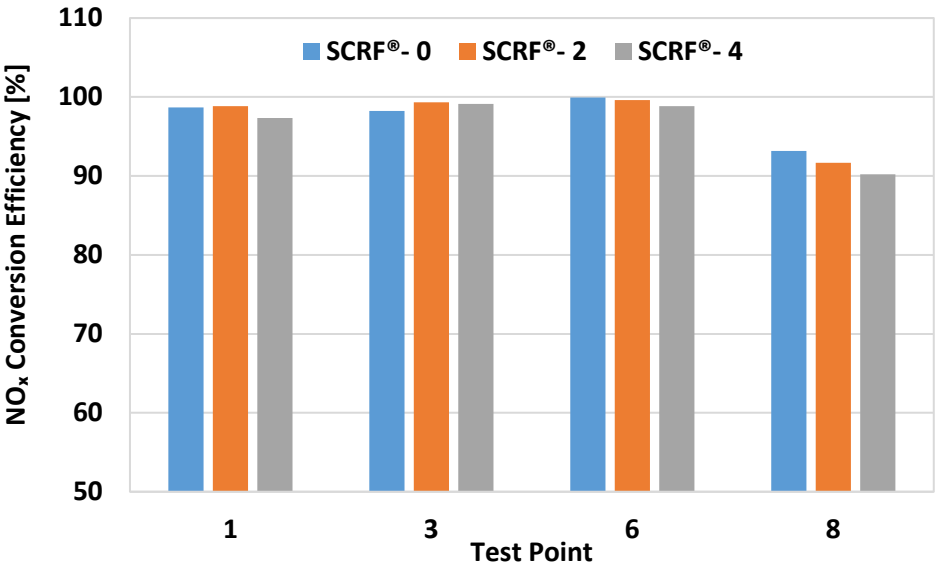

Figure 4.19: NO_x conversion efficiency of the SCRF® with and without PM at ANR 1.2

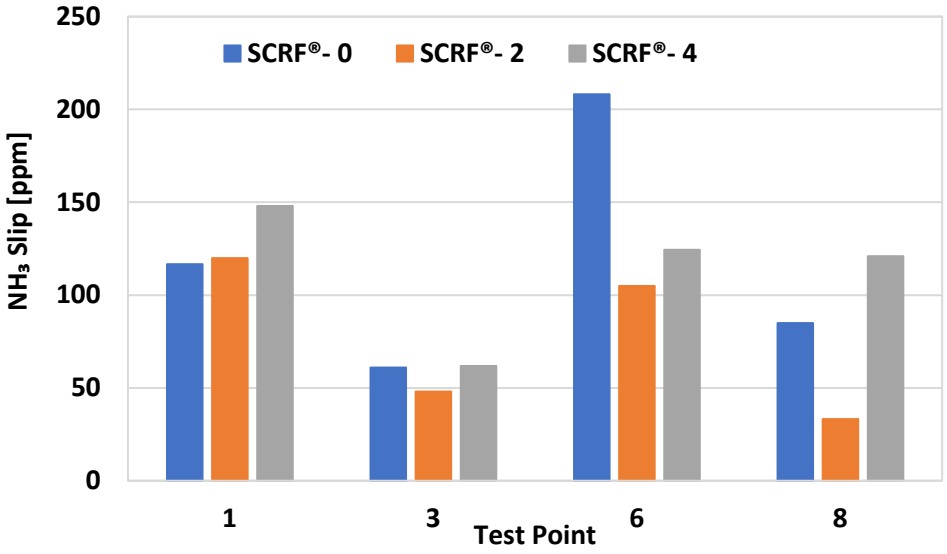

Figure 4.20: NH_3 Slip from the SCRF® with and without PM at ANR 1.2

Pressure Drop across the SCRF®

To understand the performance of the SCRF®, the pressure drop across the SCRF® for various tests was investigated. The pressure drop across the SCRF® and $PM_{Retained}$ at the end of the stages for Test Point 1 and 6 are shown in Figures 4.21 and 4.22 respectively. From Figure 4.21 it can be observed that the pressure drop is constant during the NO_x reduction test condition which indicates that the PM in the SCRF® is constant. The pressure drop across the Test Point 8 is plotted in Figure 4.22. It can be observed that during Test Point 8-W/PM-I, Test Point 8-W/PM-II and Test Point 8-W/PM-III, the pressure drop curves across the SCRF® is steep, which is due to the high PM oxidation rate. Hence, the loading condition was repeated during the test to redeposit PM in the SCRF® to maintain PM loading close to 2 g/L. These stages are indicated as Repeat Loading-I and Repeat Loading-II.

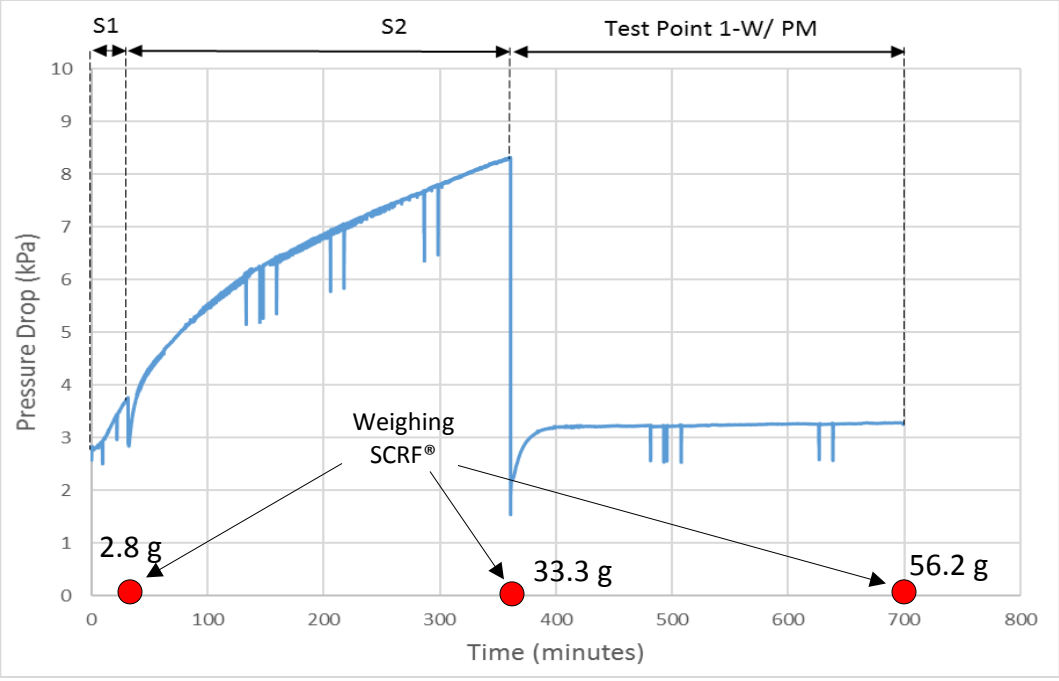

Figure 4.21: Pressure drop across the SCRF® for the Test Point 1, with PM loading 2 g/L

Figure 4.22: Pressure drop across the SCRF® for the Test Point 6, with PM loading 2 g/L

SCRF® Temperature Distribution

In this section, the gas temperature distribution in the SCRF® for the NO_x experimental tests, with and without PM loading is discussed. The study of the gas temperature distribution obtained from experimental data is critical since the experimental data will be used to calibrate the SCR-F model being developed at MTU. Twenty thermocouples were used in the axial and radial direction of the SCRF® labeled from S1 to S20 to obtain the temperature distribution in the SCRF®. The layout of the thermocouples arrangement is as shown in Figure 3.7. The thermocouples S1 to S10 were inserted into the SCRF® through the inlet channels of the SCRF® and the thermocouples S11 to S20 were inserted through the outlet channels of the SCRF®.

The temperature distribution in the SCRF® for Test Point 6 with and without PM loading is shown in Figures 4.23, 4.24, 4.25 and 4.26. Figure 4.23 shows the temperature distribution for Test Point 6, without PM loading in the SCRF®, without urea injection at 4.55 hours (5 minutes before the start of the urea dosing cycle). The isothermal lines are almost straight indicating uniform temperature distribution in the substrate, as there is no

PM in the substrate and no urea injection to cause exotherm via oxidation of PM or occurrence of SCR reactions. Figure 4.24 shows temperature distribution for Test Point 6, without PM loading, with urea injection at ANR 1.0 at 5.42 hours (15 minutes after the start of ANR 1.0). A drop in the gas temperature is observed in the axial direction before 125 mm, as the temperatures are lower than 350 °C (in comparison to Figure 4.23). This endotherm could be due to evaporative cooling caused by the evaporation of the urea solution (DEF) injected into the exhaust stream.

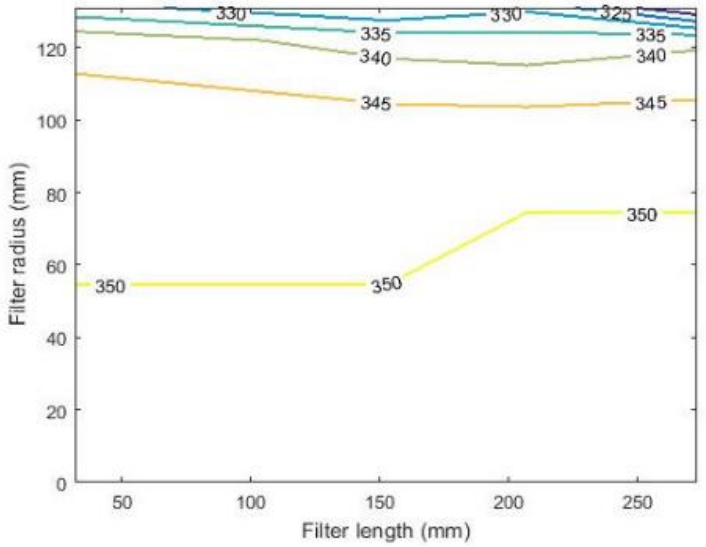

Figure 4.23: Temperature distribution in the SCRF® during NO_x reduction stage for Test Point 6 without PM loading, without urea injection

To study the temperature distribution, further analysis was performed by comparing the SCRF® inlet temperature and temperature distribution in the axial direction at the SCRF® radius 0 mm (S1, S6, S11 and S16 from Figure 3.7) relative to ANR as shown in Figure 4.25. It is observed that the SCRF® inlet temperature and the temperature measured by S1 (first thermocouple in the axial direction at radius 0 mm) decrease as the urea injection is performed at ANR of 0.8. However, the temperatures measured by S6, S11 and S16 increase as the urea injection is performed at ANR of 0.8. The change in temperature with further increase in ANR is negligible. Further investigation will be performed to study the cause of the trend in the temperature distribution.

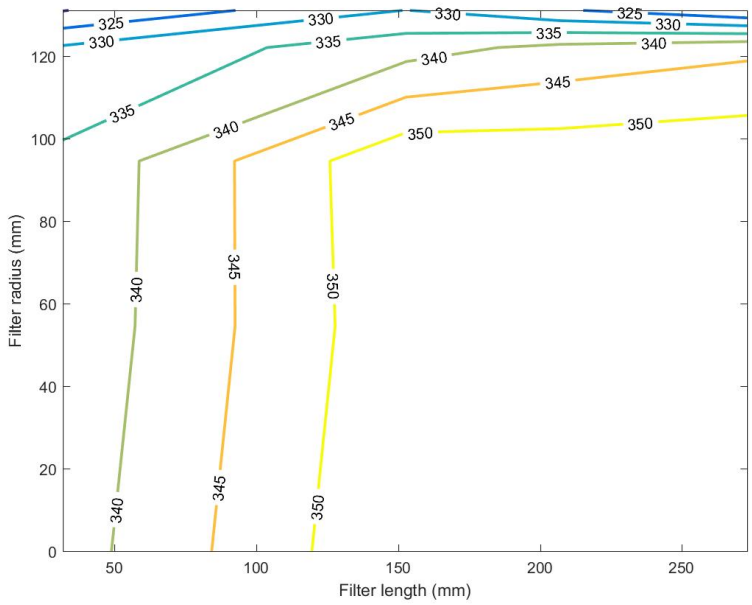

Figure 4.24: Temperature distribution in the SCRF® during NO_x reduction stage for Test Point 6 without PM loading, at ANR 1.0

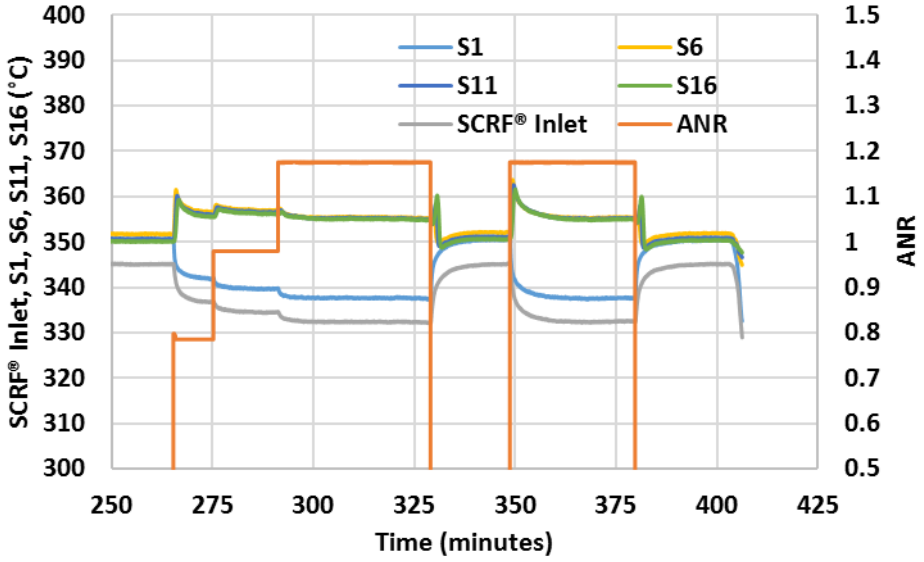

Figure 4.25: SCRF® inlet and axial temperatures relative to ANR for Test Point 6 without PM loading

Figure 4.26 shows temperature distribution for Test Point 6, with 2 g/L PM loading, with urea injection at ANR 1.0 at 13.13 hours (8 minutes after the start of ANR 1.0). A drop in temperature is observed in the axial direction between 0 – 75 mm which could be due to the endotherm caused by the evaporative cooling caused by the evaporation of the urea solution (DEF). However, a 10 – 12 °C increase in temperature is observed in the axial direction between 100 – 200 mm which could be due to exotherm caused via oxidation of PM and occurrence of SCR reactions.

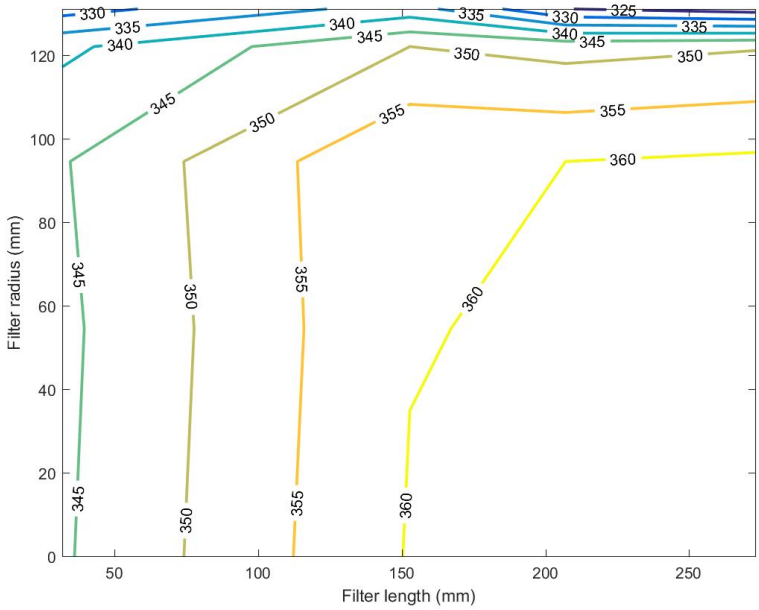

Figure 4.26: Temperature distribution in the SCRF® during NO_x reduction stage for Test Point 6 with 2 g/L PM loading, at ANR 1.0

Figure 4.27 shows temperature distribution for Test Point 6, with 4 g/L PM loading, with urea injection at ANR 1.0 at 15.92 hours (6 minutes after the start of ANR 1.0). A drop in temperature is observed in the axial direction between 0 – 50 mm which could be due to the endotherm caused by the evaporative cooling caused by the evaporation of the urea solution (DEF). However, a 8 – 12 °C increase in temperature is observed in the axial direction between 75 – 200 mm which could be due to exotherm caused via oxidation of PM and occurrence of SCR reactions.

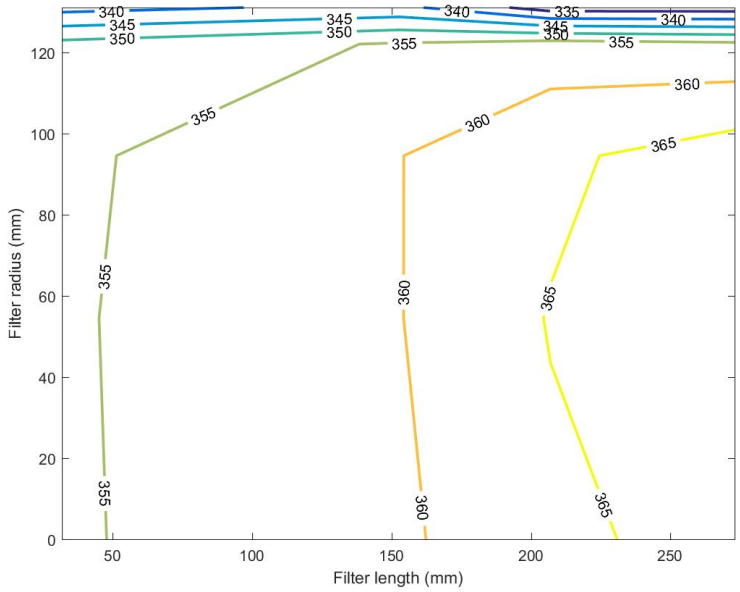

Figure 4.27: Temperature distribution in the SCRF® during NO_x reduction stage for Test Point 6 with 4 g/L PM loading at ANR 1.0

4.5 Comparison of NO_x Reduction: SCRF® to Production-2013-SCR

In this section, the NO_x reduction performance and the NH slip out of the production-2013-SCR/SCRF®, obtained from the configurations 1 and 2 is compared to the NO_x reduction performance of the production-2013-SCR (Baseline).

4.5.1 NO_x Reduction Performance

The NO_x conversion efficiency of the production-2013-SCR and the SCRF® are shown in the Figure 4.27. It can be observed that the production-2013-SCR could achieve NO_x conversion efficiency of $\leq$ 85 % in comparison to the $\geq$ 90 % for the SCRF®, at inlet temperatures below 250 °C and above 450 °C. The NO_x conversion efficiency for the SCRF®, with and without PM in the SCRF®, was $\geq$ 95 % at the inlet temperature range of 300 – 400 °C, which is comparable to the production-2013-SCR.

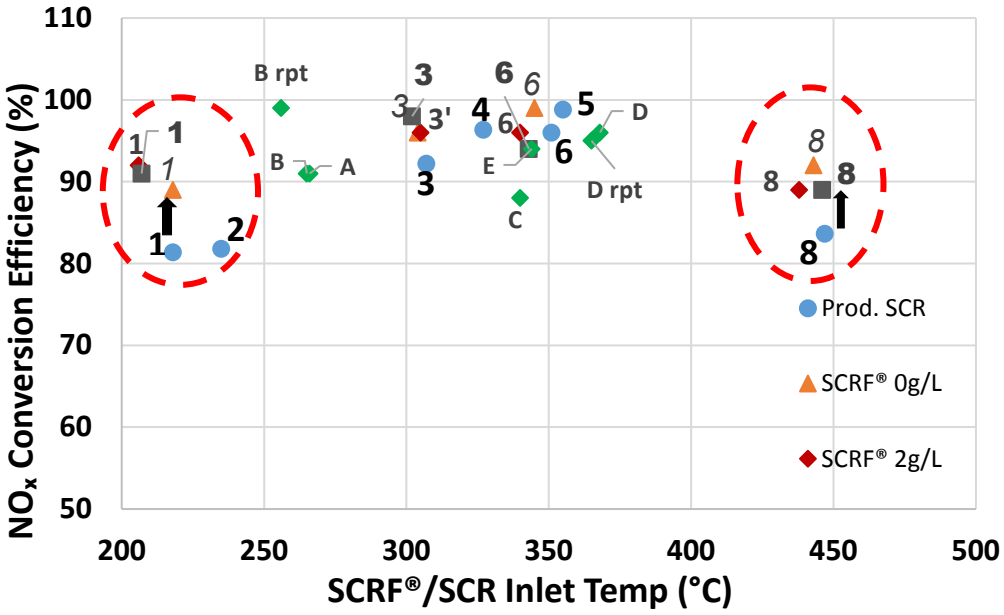

Figure 4.28: NO_x conversion efficiency of the production-2013-SCR and the SCRF® at various inlet temperatures

The combination of NO_x conversion efficiency, ANR and NH_3 slip out of the production-2013-SCR and the SCRF® during the NO_x reduction and passive oxidation tests with urea injection (baseline, configuration 2 and configuration 1), at ANR 1.0, are shown in Figure 4.28. The NH_3 slip >50 ppm for the production-2013-SCR and >20 ppm for the SCRF®, was observed for all the test conditions except Test Point 8, which is high temperature and high space velocity test condition (refer Table 4.10). The low NH_3 slip offers an opportunity to increase the ANR from 1.00 to 1.05 to obtain further improvement in the NO_x reduction in the SCRF®, below SCRF® inlet temperatures of 400°C. Above 400°C, the oxidation of NH_3 is a dominant phenomenon and improvement in NO_x reduction will be insignificant. The study of the improvement in NO_x conversion efficiency at ANR >1.0 with the SCRF® and a downstream SCR-A brick will be performed in the configuration-3, at a later stage of this research.

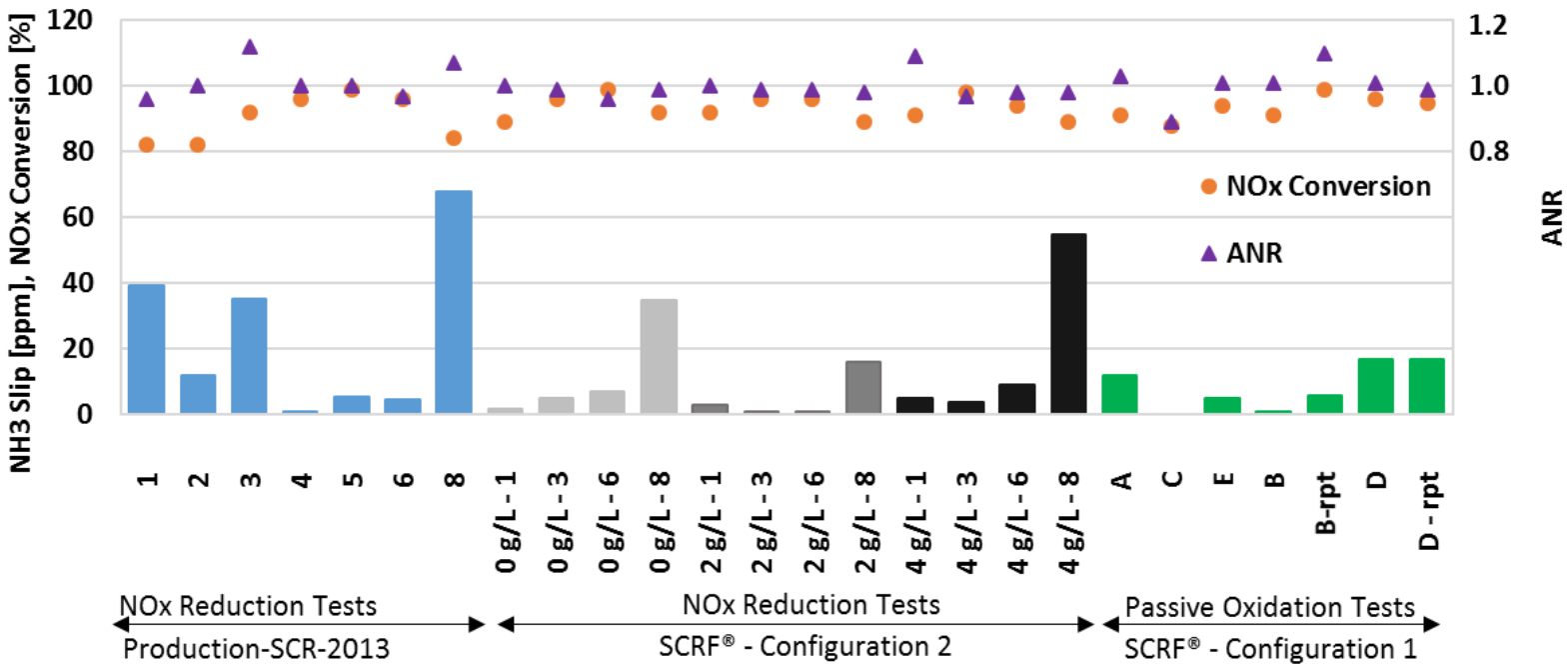

Figure 4.29: NH_3 slip out of the production-2013-SCR/SCRF® during NO_x reduction and passive oxidation with urea injection tests at ANR 1.0

4.5.2 NH_3 Storage

The NH_3 storage at various inlet temperatures for the production-SCR and the SCRF® (with and without PM loading) were estimated using the NO_x concentrations at the inlet and the outlet of the production-2013-SCR/SCRF® and NH_3 concentration at the inlet of the production-2013-SCR/SCRF® at 1.2 ANR, estimated using equation 3.8.

The NO_x converted and the NH_3 slip out of the SCRF® were subtracted from the inlet NH_3 to estimate the NH_3 consumed in the production-2013-SCR/SCRF® as described in equation 4.6. The NH_3 consumed values were subtracted from the inlet NH_3 to obtain the NH_3 stored on the catalyst as indicated in Figure 4.29. The NH_3 storage stabilizes as the NO_x conversion and NH_3 slip out of the production-2013-SCR/SCRF® stabilize. The NH_3 storage was calculated until the curve stabilized. The NH_3 storage on the catalyst was estimated using equation 4.7.

$$NH_3\ \text{Consumed} = \text{Inlet}\ NH_3 - (\text{Inlet}\ NO_x - \text{Outlet}\ NO_x) - NH_3\ \text{Slip} \quad \text{Eqn. 4.6}$$

Where, NH_3 consumed, inlet NH_3, inlet NO_x, outlet NO_x and NH_3 slip are in ppm.

$$NH_3\ \text{Storage} = \frac{\int_{t1}^{t2} \text{Yi} * \text{exhaust flow rate} * dt}{\text{molecular wt. of air} * \text{total volume of the SCR/SCRF®}} \quad \text{Eqn. 4.7}$$

Where NH_3 storage is in (gmol/m^3 of substrate), Y_i is the NH_3 concentration stored on the catalyst (ppm) (Inlet NH_3 – NH_3 consumed), t1 is the start of urea injection (minutes), t2 is the time at which NH_3 stored curve stabilizes (minutes), as shown in Figure 4.29, exhaust flow rate is in (kg/minute), molecular weight of air is 28.96 (g/gmol) and total volume of the production-2013-SCR/SCRF® 17.04 (L). It is also assumed that the

production-2013-SCR and the SCRF® catalyst loading is represented by the total volume of the substrates i.e 17.04 L.

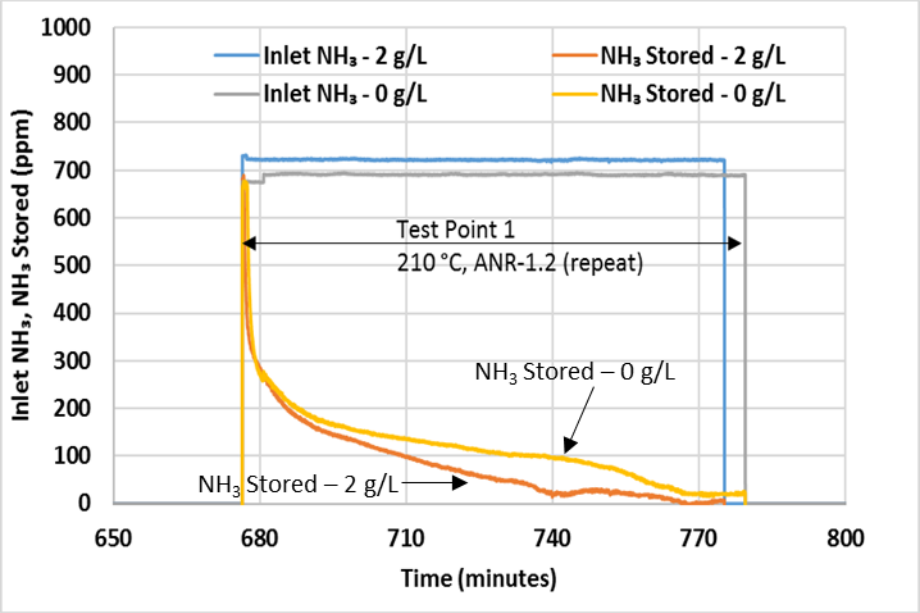

Figure 4.30: Inlet NH_3 and NH_3 stored in the SCRF® at Test Point 1 at ANR 1.2 repeat, without and with PM loading in the SCRF® (0 and 2 g/L), SV = 13.7 k/hr, SCRF® inlet temperature = 210°C

Equation 3.8, for estimation of inlet NH_3 assumes that all the DEF injected into the system is converted to NH_3. However, the DEF to NH_3 conversion reactions are dependent on temperature. The results from reference [85] as shown in Figure 4.30 were used to obtain the fraction of DEF converted into NH_3 at various temperatures. The NH_3 storage ($gmol/m^{3)}$ values were multiplied by the temperature based fraction, to obtain the actual NH_3 stored on the production-SCR/SCRF®.

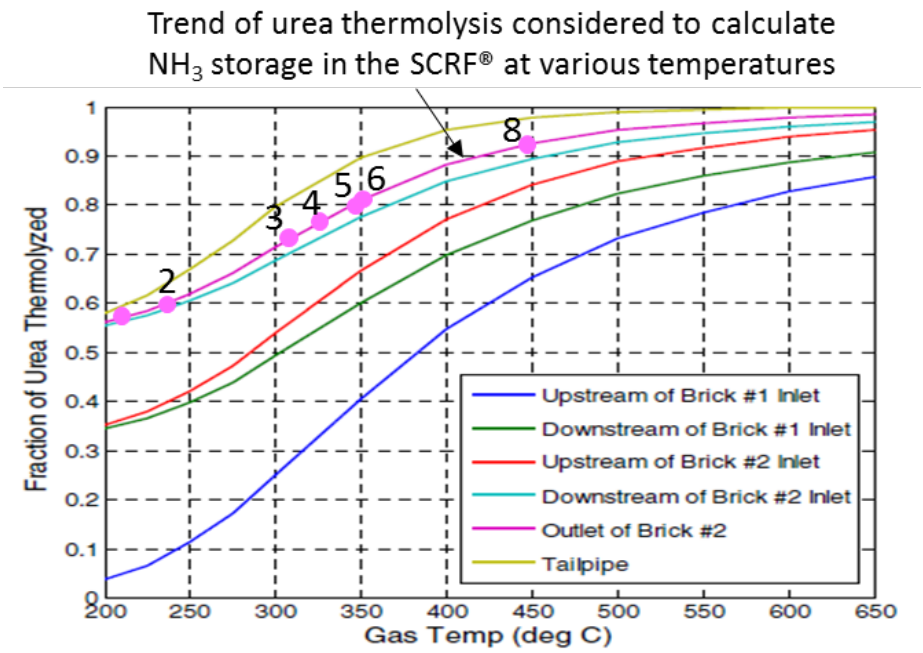

Figure 4.31: Fraction of Urea thermolyzed at various locations, SV = 30 k/hr [85]

From Figure 4.31 it can be observed that the SCR-2010, the production-2013-SCR and the SCRF® (without PM) have approximately same ammonia storage capability at lower and higher temperatures. However, the SCRF® (without PM) demonstrated lower ammonia storage at temperatures around 300°C, when compared to the production-2013-SCR and the SCR-2010 from reference [9]. Also, the ammonia storage capability of the SCRF® with the PM loading of 2g/L, decreases by approximately 30% at lower temperatures (200-250°C), when compared to the ammonia storage in the SCRF® without PM. The reduced NH_3 storage in the SCRF® with PM loading in the SCRF® is also evident from Figure 4.29. The difference reduces as the substrate temperature increases. Further PM loading on the SCRF® to 4 g/L had negligible effect on ammonia storage. Similar results related to the ammonia storage were observed by Tan et al. [70].

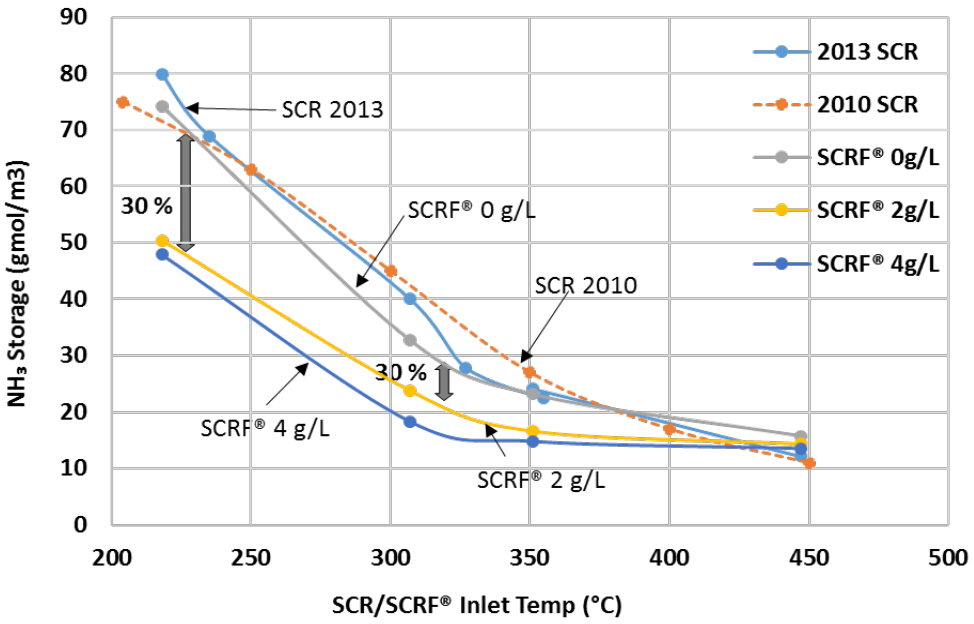

Figure 4.32: NH_3 storage in the production-SCR and the SCRF® at various temperatures

4.6 Calculation of ANR's for Configuration 3: SCRF® + SCR

The experimental data for the SCRF® were studied and analyzed to calculate the targeted ANR to be maintained during the passive oxidation stage of Test Points A, B, C, D and E and NO_x reduction stage of Test Point 1. The data for Test Points A and E obtained from passive oxidation tests with urea injection as a part of configuration 1 are shown in Table 4.23. The NO_x and NH_3 concentrations at the inlet and outlet of the SCRF®, NO_x conversion efficiency and ANR were used to calculate the targeted ANR for configuration 3 such that maximum NO_x reduction and minimum NH_3 slip could be achieved at the outlet of the SCRF® and SCRF® and SCR-A substrate together.

Table 4.23: Performance of the SCRF® during the passive oxidation tests with urea injection in configuration 1 [1]

Test Points	SCRF® Inlet NO_x	SCRF® Inlet NH_3	ANR	SCRF® Outlet NO_x	NH_3 Slip	NO_x Conv. Eff.	Nitrogen Balance
[-]	[ppm]	[ppm]	[-]	[ppm]	[ppm]	[%]	[%]
A	590	607	1.03	55	12	91	90
E	1450	1465	1.01	80	5	94	94

From Table 4.23 it is observed that for Test Point A, NO_x concentration of 55 ppm and NH_3 slip of 12 ppm were measured at the outlet of the SCRF®. The NO_x concentration of 55 ppm could be reduced in the SCRF® if additional SCRF® inlet NH_3 concentration of 67 ppm were available (considering 90% nitrogen balance) during the test. Hence, the targeted ANR to be performed for Test Point A in configuration 3 (SCRF® with a downstream SCR) would be 1.13. The calculations for Test Point A are shown in Figure 4.32.

SCRF® outlet NO_x / Nitrogen balance = Additional SCRF® inlet NH_3

55 / 0.90 = 61

(SCRF® inlet NH_3 + Additional SCRF® inlet NH_3) / SCRF® inlet NO_x = Targeted ANR

(607 + 61) / 590 = 1.13

Figure 4.33: Sample calculations to estimate the targeted ANR for Test Point A

Similarly, for Test Point E, NO_x concentration of 80 ppm could be reduced in the SCRF® if additional SCRF® inlet NH_3 concentration of 85 ppm were available (considering 94% nitrogen balance) during the test. Hence, the targeted ANR to be performed for Test Point E in configuration 3 would be 1.07. The calculations for Test Point E are shown in Figure 4.33.

SCRF® outlet NO_x (ppm)/ Nitrogen balance = Additional SCRF® inlet NH_3 (ppm)

80 / 0.94 = 85

(SCRF® inlet NH_3 + Additional SCRF® inlet NH_3) / SCRF® inlet NO_x = Targeted ANR

(1465 + 85) / 1450 = 1.07

Figure 4.34: Sample calculations to estimate the targeted ANR for Test Point E

Chapter 5. Summary and Conclusions

One of the goals of this research was to investigate the effect of temperature and space velocity on the NO_x reduction performance of the SCRF®, with and without PM loading in the SCRF® and compare it with the performance of the production-2013-SCR. Also, there was a goal to determine the effects of PM loading at 0, 2 and 4 g/L as a function of ANR on the outlet NO, NO_2 and NH_3 and the NOx reduction as affected by the temperature and space velocity. Another goal of this research was to determine the NH_3 storage for the production-2013-SCR and the SCRF®, to study the effect of PM loading on the NH_3 storage. The goals have been met through experimental studies on the production-2013-SCR and the SCRF® coupled with the 1-D SCR model calibration. The important findings and accomplishments from the study and the recommendation for the future work are discussed in this chapter.

5.1 Summary

The test procedures were developed and the test conditions were determined to evaluate the performance of the production-2013-SCR and the SCRF®. Seven NO_x reduction tests were completed to evaluate the NO_x reduction and NH_3 slip performance for production-2013-SCR. Seven passive oxidation and twelve NO_x reduction tests were completed in configurations 1 and 2 respectively, to evaluate the NO_x reduction and NH_3 slip performance of the SCRF®, with 0, 2 and 4 g/L PM loading in the SCRF® as a function of temperature and space velocities for ANR 0.8, 1.0 and 1.2.

NO_x Reduction in Production-2013-SCR and 1-D SCR Model Calibration

The NO_x reduction and NH_3 slip characteristics of the Cu-zeolite based production-2013-SCR were determined at steady state engine operating conditions. During the seven different test conditions, SCR inlet temperatures varied from 208 to 447 °C, space velocity varied from 12.0 to 44.7 k/hr, NO_x varied from 280 to 1730 ppm and NO_2/NO_x varied from 0.2 to 0.5. The NO_x conversion efficiency and NH_3 slip performance of the

production-2013-SCR was considered as the baseline performance and was compared with the NO_x reduction in the SCRF®. Nitrogen balance was performed using the NO_x and NH_3 concentrations at the inlet and outlet of the production-2013-SCR, to validate the consistency of the experimental data. The nitrogen balance of 100 ± 10 % was observed for the seven tests, indicating a good agreement between the concentrations at the inlet and outlet of the production-2013-SCR. NH_3 storage on the production-2013-SCR was calculated using the experimental data.

The 1-D SCR model was calibrated to the engine experimental data obtained from the production-2013-SCR. A unique set of model calibration parameters were determined for Test Points with SCR inlet temperatures in the range of 250 to 450°C. However, a different set of parameters were used for Test Point 1, which has the SCR inlet temperature ~205°C. The calibrated model was validated by comparing the experimental and simulated data using NO, NO_2 and NH_3 concentrations at the SCR outlet.

NO_x Reduction in SCRF® – with and without PM – Configurations 1 and 2

Seven passive oxidation tests with urea injection were conducted in configuration 1 to study the effect of NO_x reduction reactions on the NO_2 assisted PM oxidation. The SCRF® was loaded to 1.8 ± 0.4 g/L before start of the passive oxidation stage. The urea injection was performed to achieve a constant ANR of 1.0 during the passive oxidation stage. The NO_x reduction and NH_3 slip data for the SCRF® were analyzed and the nitrogen balance was performed to validate the consistency of the experimental data.

The Test Points 1, 3, 6 and 8 from Table 3.15 were run in configuration 2, to collect the experimental data to determine the NO_x reduction and NH_3 slip performance of the SCRF®, with and without PM loading in the SCRF® (total twelve tests). The four Test Points cover the SCRF® inlet temperatures in the range of 200 to 450°C, space velocities from 13 to 48 k/hr, SCRF® inlet NO_x from 280 to 1600 ppm. During NO_x reduction tests for the SCRF® without PM loading, the CPF was placed upstream of the SCRF® to filter the PM entering into the SCRF®. Hence, using the data from four tests without PM

loading in the SCRF®, NO_x reduction performance of the clean SCRF® was determined. During NO_x reduction tests for the SCRF® with PM loading, the CPF was replaced with a spacer, so that the engine-out PM was filtered and deposited on the SCRF® to achieve the target PM loading of 2 and 4 g/L. The urea dosing cycle was performed to achieve the ANR of 0.8, 1.0, 1.2 and 1.2 repeat to study the NO_x reduction and NO, NO_2 and NH_3 slip from the SCRF®, with 0, 2 and 4 g/L PM loading. NH_3 storage on the SCRF®, with and without PM loading on the SCRF® was calculated using the experimental data from the twelve NO_x reduction tests in the configuration 2.

NO_x reduction, NH_3 slip and NH_3 storage data for the SCRF®, obtained from configurations 1 and 2 were compared to the baseline data for the production-2013-SCR.

5.2 Conclusions

The experimental data obtained from the tests conducted with the production-2013-SCR and the SCRF® (configurations 1 and 2, with and without PM loading) were analyzed to determine the NO_x conversion efficiency, NH_3 storage and NH_3 slip characteristics of the production-2013-SCR and the SCRF®. The 1-D SCR model was calibrated using the experimental data obtained from the seven tests with the production-2013-SCR. The conclusions with respect to the goals and objectives of this study are discussed in the following sections.

NO_x Reduction, NH_3 storage and 1-D SCR Model Calibration – Production-2013-SCR

1. The production-2013-SCR can achieve 90 – 95 % NO_x reduction with NH_3 slip <40 ppm at ANR 1.0, for the inlet temperature range of 300 – 350°C. However, the NO_x reduction performance decreases to 80 – 85 % at ANR 1.0, with NH_3 slip <20
   and <70 ppm for inlet temperatures below 250°C and above 450°C respectively.
2. Maximum NH_3 storage of 75 gmol/m3 of substrate at 200 °C was observed on the production-2013-SCR. The NH_3 storage values for the production-2013-SCR

were within ±5 gmol/m3 when compared to the production-SCR-2010, for the inlet temperature range of 200 – 450°C.

3. The 1-D SCR model was calibrated to ±20 ppm of the experimental data, for NO and NO_2 gaseous concentrations at the outlet of the production-2013-SCR. The model was also calibrated to ±30 ppm of the experimental data, for NH_3 slip out of the production-2013-SCR.

NO_x Reduction – SCRF®: Configuration 1

1. The NO_x reduction >90 % and NH_3 slip <20 ppm at ANR 1.0, can be achieved with the SCRF®, with PM loading of 2 g/L in the SCRF®, for the inlet temperature range of 260 to 370 °C.
2. The SCRF® exhibits potential for the NO_x reduction >95% at ANR between 1.05 – 1.10, since the NH_3 slip values for the seven passive oxidation tests with urea injection were <20 ppm at ANR 1.0.

NO_x Reduction and NH_3 storage – SCRF®: Configuration 2

1. The NO_x reduction >90 % and NH_3 slip <50 ppm at ANR 1.0, can be achieved with the SCRF®, with and without PM loading in the SCRF®, for the inlet temperature range of 200 to 450 °C and inlet NO_2/NO_x ratio in the range of 0.2 to 0.5. Maximum NO_x reduction of 95% at ANR 1.0 was observed, for the inlet temperature range of 300 to 400 °C.
2. The SCRF® (with and without PM loading) provides 5 – 7 % improvement in the NO_x reduction when compared to the production-2013-SCR at the inlet temperatures below 250 °C and above 400 °C
3. The SCRF® outlet NO_2/NO_x ratio decreases above 300 °C with increase in PM loading on the SCRF® from 0 to 2 g/L and from 2 to 4 g/L. This decrement in NO_2/NO_x ratio is due to the consumption of NO_2 via passive oxidation of PM. Hence, the effective NO_2/NO_x ratio on the SCR catalyst in the SCRF® could be

significantly lower than the inlet NO_2/NO_x ratio, having effects on the NO_x reduction in the SCRF®.

4. The impact of PM loading on the NO_x reduction in the SCRF® was insignificant below 300 °C. The NO_x reduction decreased by 3 – 5 % above 350 °C with the increase in PM loading from 0 to 2 and 4 g/L, due to consumption of NO_2 via passive oxidation of PM.
5. NH_3 storage on the SCRF® without PM loading is similar to the production-2013-SCR. Maximum storage of 75 gmol/m3 of substrate was observed at 200 °C for the SCRF®.
6. The SCRF® showed 20 - 30 % reduction in NH_3 storage when comparing 0 g/L loading to 2 and 4 g/L PM loading for the temperature range of 200 to 350 °C. The decrease in the NH_3 storage with PM loading was insignificant for the SCRF® inlet temperatures above 350 °C. The increase in PM loading from 2 to 4 g/L has minimal impact on the NH_3 storage.

References

[1] E. Gustafson, "An Experimental Investigation into NO_2 Assisted Passive Oxidation with and without Urea Dosing and Active Regeneration of Particulate Matter for a SCR Catalyst on a DPF," *MS Thesis, Michigan Technological University, 2016.*

[2] "DieselNet, www.dieselnet.com," [Online].

[3] K. Raghavan, "An Experimental Investigation into the Effect of NO_2 and Temperature on the Passive Oxidation and Active Regeneration of Particulate Matter in a Diesel Particulate Filter," MS Thesis, Michigan Technological University, 2015.

[4] M. Colombo, I. Nova and E. Tronconi, "A comparative study of the NH_3-SCR reactions over a Cu-zeolite and a Fe-zeolite catalyst," *Catalysis Today 2010;151:223-230, 2010.*

[5] H. Surenahalli, "Dynamic Model Based State Estimation In a Heavy Duty Diesel Aftertreatment System For Onboard Diagnostics And Controls," PhD Dissertation, Michigan Technological University, 2013.

[6] J. Pidgeon, "An Experimental Investigation into the Effects of Biodiesel Blends on Particulate Matter Oxidation in a Catalyzed Particulate Filter during Active Regeneration," *MS Thesis, Michigan Technological University, 2013.*

[7] C. Hutton, "An Experimental Investigation into the Passive Oxidation of Particulate Matter in a Catalyzed Particulate Filter," *MS Thesis, Michigan Technological University, 2010.*

[8] X. Song, J. Naber, J. Johnson and G. Parker, "An Experimental and Modeling Study of Reaction Kinetics for a Cu-Zeolite SCR Catalyst Based on Engine Experiments," *SAE Technical Paper 2013-01-1054, doi:10.4271/2013-01-1054, 2013.*

[9] X. Song, "A SCR Model based on Reactor and Engine Experimental Studies for a Cu-zeolite Catalyst," PhD Dissertation, Michigan Technological University, 2013.

[10] T. Ballinger, . J. Cox, M. Konduru and D. De, "Evaluation of SCR Catalyst Technology on Diesel Particulate Filters," *SAE Int. J. Fuels Lubr. 2(1):369-374, doi:10.4271/2009-01-0910, 2009.*

[11] Y. He, D. Brown, S. Lu, M. Paratore and J. Li, "Opportunities and Challenges for Blended 2-Way SCR/DPF Aftertreatment Technologies," *SAE Technical Paper 2009-01-0274, 2009.*

[12] X. Song, J. Johnson and J. Naber, "A review of the literature of selective catalytic reduction catalysts integrated into diesel particulate filters," *International Journal of Engine Research, doi:10.1177/1468087414545094, 2014.*

[13] B. Mahadevan, J. Johnson and M. Shahbakhti, "Development of a Catalyzed Diesel Particulate Filter Multi-zone Model for Simulation of Axial and Radial Substrate Temperature and Particulate Matter Distribution," *Emission Control Science and Technology, DOI 10.1007/s40825-015-0015-x, 2015.*

[14] J. Chowng, I. Nam and S. Ham, "Effect of promoters including tungsten and barium on the thermal stability of V2O5/sulfated TiO_2 catalyst for NO reduction by NH_3," *Catal. Today 111, 242-247, 2009.*

[15] M. Vargas, M. Casanova, A. Trovarelli and G. Busca, "An IR study of thermally stable V2O5-WO_3-TiO_2 SCR catalysts modified with silica and rare-earths (Ce, Tb, Er)," *Appl. Catal. B: Environ. 75, 303-311, 2007.*

[16] J. Spengler, D. Trandal and S. Iretskaya, "Development of Vanadia-Based SCR for High-Temperature Application," *IAV MinNO$_x$ Conference, Berlin, June 2014.*

[17] I. Nova and E. Tronconi, "Urea-SCR technology for deNO_x after treatment of diesel exhausts," *Fundamental and Applied Catalysis 2014.*

[18] M. Castagnola, J. Caserta, S. Chatterjee and H. Chen, "Engine Performance of Cu- and Fe-Based SCR Emission Control Systems for Heavy Duty Diesel Applications," *SAE Technical Paper 2011-01-1329, doi:10.4271/2011-01-1329, 2011.*

[19] G. Cavataio, J. Girard, G. Cabaralo and C. Lambert, "Laboratory Testing of Urea-SCR Formulations to Meet Tier 2 Bin 5 Emissions," *SAE Technical Paper 2007-01-1575, 2007.*

[20] J. Girard, R. Snow, G. Cabaralo and C. Lambert, "The Influence of Ammonia to NO_x Ratio on SCR Performance," *SAE Technical Paper 2007-01-1581, 2007.*

[21] S. Schmieg and J. Lee, "Evaluation of Supplier Catalyst Formulations for the Selective Catalytic Reduction of NO_x with Ammonia," *SAE Technical Paper 2005-01-3881, 2005.*

[22] H. Nishiyama, Y. Tanaka, T. Adachi and S. Kawamura, "A Study on the Improvement of NO_x Reduction Efficiency for a Urea SCR System," *SAE Technical Paper 2015-01-2014, 2015.*

[23] K. Kamasamudram, N. Currier, T. Szailer and A. Yezerets, "Why Cu- and Fe-Zeolite SCR Catalysts Behave Differently at Low Temperatures," *SAE Technical Paper 2010-01-1182, 2010.*

[24] B. Shakya, M. Harold and V. Balakotaiah, "Simulations and optimization of combined Fe- and Cu-zeolite SCR monolith catalysts," *Chemical Engineering Journal, Volume 278, 2015.*

[25] S. Hirose, H. Yamamoto, H. Suenobu and H. Sakamoto, "Development of High Porosity Cordierite Honeycomb Substrate for SCR Application to Realize High NO_x Conversion Efficiency and System Compactness," *SAE Int. J. Mater. Manf. 7(3):682-687, doi:10.4271/2014-01-1528, 2014.*

[26] J. Pless, M. Naseri, W. Klink and G. Spreitzer, "Development of SCR on High Porosity Substrates for Heavy Duty and Off-Road Applications," *SAE Int. J. Commer. Veh. 7(1):177-185, doi:10.4271/2014-01-1521, 2014.*

[27] T. Zhang, R. Qu, W. Su and J. Li, "A novel Ce-Te mixed oxide catalyst for the selective catalytic reduction of NO_x with NH_3," *Applied Catalysis B: Environmental 2015.*

[28] P. Li, Y. Xin, Q. Li, Z. Wang, Z. Zhang and L. Zheng, "Ce–Ti Amorphous Oxides for Selective Catalytic Reduction of NO with NH3: Confirmation of Ce–O–Ti Active Sites," *Environ. Sci. Technol. 46, 9600–9605, 2012.*

[29] Y. Peng, R. Qu, X. Zhang and J. Li, "The relationship between structure and activity of MoO_3–CeO_2 catalysts for NO removal: influences of acidity and reducibility," *Chem. Commun. 49, 6215–6217, DOI: 10.1039/C3CC42693A, 2013.*

[30] Z. Liu, Y. Yi, J. Li, S. Woo, B. Wang, X. Cao and Z. Li, "A superior catalyst with dual redox cycles for the selective reduction of NO_x by ammonia," *Chem. Commun. 49, 7726–7728, DOI: 10.1039/C3CC43041C, 2013.*

[31] G. Busca, L. Lietti, G. Ramis and F. Berti, "Chemical and mechanistic aspects of the selective catalytic reduction of NO_x by ammonia over oxide catalysts," *Appl. Catal. B 18, 1–36, doi:10.1016/S0926-3373(98)00040-X, 1998.*

[32] F. Liu, A. He, W. Shan, X. Shi and C. Zhang, "Influence of sulfation on iron titanate catalyst for the selective catalytic reduction of NO_x with NH_3," *Appl. Catal. B 103,*

369–377, doi:10.1016/j.apcatb.2011.01.044, 2011.

[33] D. Pappas, T. Boningari, P. Boolchand and P. Smirniotis, "Novel manganese oxide confined interweaved titania nanotubes for the low-temperaature Selective Catalytic reduction of NO_x by NH_3," *Journal of Catalysis, Volume 334, doi:10.1016/j.jcat.2015.11.013, 2016.*

[34] T. Boningari and P. Smirinotis, "Nickel-doped Mn/TiO_2 as an efficient catalyst for the low-temperature SCR of NO with NH_3: Catalytic evaluation and characterizations," *Journal of Catalysis, volume 288, doi:10.1016/j.jcat.2012.01.003, 2012.*

[35] K. Zhuang, J. Qiu, F. Tang, B. Xu and Y. Fan, "The structure and catalytic activity of anatase and rutile titania supported manganese oxide catalysts for selective catalytic reduction of NO by NH3," *Phys. Chem. Chem. Phys 13, 4463, 2011.*

[36] A. Schuler, M. Votsmeier, P. Kiwic, J. Giwshoff, W. Hautpmann, A. Drochner and H. Vogel, "NH_3-SCR on Fe zeolite catalysts – From model setup to NH_3 dosing," *Chemical Engineering Journal, volume 154, 2009.*

[37] J. Chi, "Control Challenges for Optimal NO_x Conversion Efficiency from SCR Aftertreatment Systems," *SAE Technical Paper 2009-01-0905, doi:10.4271/2009-01-0905, 2009.*

[38] E. Faghihi and A. Shamekhi, "Development of a neural network model for selective catalytic reduction (SCR) catalytic converter and ammonia dosing optimization using multi objective genetic algorithm," *Chemical Engineering Journal, vol. 165, 2010.*

[39] P. Gaynor, B. Reid, G. Hargrave and T. Lockyer, "An Experimental Investigation into DEF Dosing Strategies for Heavy Duty Vehicle Applications," *SAE Int. J. Engines 8(3):1196-1206, doi:10.4271/2015-01-1028, 2015.*

[40] H. Dong, S. Shuai and J. Wang, "Effect of Urea Thermal Decomposition on Diesel NO_x-SCR Aftertreatment Systems," *SAE Technical Paper 2008-01-1544, doi:10.4271/2008-01-1544, 2008.*

[41] B. Guan, "Southwest Research Institute, “Review of state of the art technologies of selective catalytic reduction of NO_x from diesel engine exhaust," *Applied Thermal Engineering, volume 66, 1359-4311, 2014.*

[42] G. Bartley, C. Chadwell, T. Kostek and R. Zhan, "SCR Deactivation Kinetics for Model-Based Control and Accelerated Aging Applications," *SAE Technical Paper*

2012-01-1077, doi:10.4271/2012-01-1077, 2012.

[43] J. Theis, J. Ura and R. McCabe, "The Effects of Sulfur Poisoning and Desulfation Temperature on the NO_x Conversion of LNT+SCR Systems for Diesel Applications," *SAE Int. J. Fuels Lubr. 3(1):1-15, doi:10.4271/2010-01-0300, 2010.*

[44] M. Pereira, A. Nicolle and D. Berthout, "Hydrothermal aging effects on Cu-zeolite NH_3-SCR catalyst," *Catalysis Today, Volume 258, 2015.*

[45] J. Kwak, D. Tran, S. Burton, J. Szanyi, J. Lee and C. Peden, "Effects of hydrothermal aging on NH_3-SCR reaction over Cu/zeolites," *Journal of Catalysis, Volume 284, 2012.*

[46] J. Luo, H. An, K. Kamasamudram and N. Currier, "Impact of Accelerated Hydrothermal Aging on Structure and Performance of Cu-SSZ-13 SCR Catalysts," *SAE Int. J. Engines 8(3):1181-1186, doi:10.4271/2015-01-1022, 2015.*

[47] Y. Huang, Y. Cheng and C. Lambert, "Deactivation of Cu/Zeolite SCR Catalyst Due to Reductive Hydrothermal Aging," *SAE Int. J. Fuels Lubr. 1(1):466-470, doi:10.4271/2008-01-1021, 2009.*

[48] G. Cavataio, H. Jen, J. Warner and J. Girard, "Enhanced Durability of a Cu/Zeolite Based SCR Catalyst," *SAE Int. J. Fuels Lubr. 1(1):477-487, 2009, doi:10.4271/2008-01-1025, 2009.*

[49] J. Fedeyko, H. Chen, T. Ballinger and E. Weigert, "Development of Thermally Durable Cu/SCR Catalysts," *SAE Technical Paper 2009-01-0899, doi:10.4271/2009-01-0899, 2009.*

[50] G. Cruciani, "Zeolites upon heating: Factors governing their thermal stability and structural changes," *Journal of Physics and Chemistry of Solids, Volume 67:1973–1994, 2006.*

[51] J. Luo, A. Yezerets, C. Henry and H. Hess, "Hydrocarbon Poisoning of Cu-Zeolite SCR Catalysts," *SAE Technical Paper 2012-01-1096, doi:10.4271/2012-01-1096, 2012.*

[52] C. Montreuil and C. Lambert, "The effect of hydrocarbons on the selective catalyzed reduction of NO_x over low and high temperature catalyst formulations," *SAE Technical Paper 2008–01–1030, 2008.*

[53] J. Girard, R. Snow and G. Cavataio, "Influence of hydrocarbon storage on the

durability of SCR catalysts," *SAE Technical Paper 2008–01–0767, 2008.*

[54] E. Japkea, M. Casapua, M. Truoilletb, O. Deutschmanna and J. Grunwaldta, "Soot and hydrocarbon oxidation over vanadia based SCR catalysts," *Catalysis Today, Volume 258, doi:10.1016/j.cattod.2015.04.020, 2015.*

[55] N. Ottinger, B. Foley, Y. Xi and Z. Liu, "Impact of Hydrocarbons on the Dual (Oxidation and SCR) Functions of Ammonia Oxidation Catalysts," *SAE Int. J. Engines 7(3):1262-1268, doi:10.4271/2014-01-1536, 2014.*

[56] S. Shwan, J. Jansson, L. Olsson and M. Skoglundh, "Chemical deactivation of Fe-BEA as NH_3-SCR catalyst—Effect of phosphorous," *Applied Catalyst B: Environmental 147, 2014.*

[57] G. Cavataio, H. Jen, D. Dobson and J. Warner, "Laboratory Study to Determine Impact of Na and K Exposure on the Durability of DOC and SCR Catalyst Formulations," *SAE Technical Paper 2009-01-2823, doi:10.4271/2009-01-2823, 2009.*

[58] J. Chi and H. DaCosta, "Modeling and Control of a Urea-SCR Aftertreatment System," *SAE Technical Paper 2005-01-0966, doi:10.4271/2005-01-0966, 2005.*

[59] E. Abu-Ramadan, K. Saha and X. Li, "Numerical Modeling of the Impingement Process of Urea-Water Solution Spray on the Heated Walls of SCR Systems," *SAE Technical Paper 2012-01-1301, 2012.*

[60] M. Koebel, M. Elsener and M. Kleemmann, "Urea-SCR: a promising technique to reduce NO_x emissions from automotive diesel engines," *Catal. Today 56 (2000) 335-345, 2000.*

[61] H. Fang and H. DaCosta, "Urea thermolysis and NO_x reduction with and without SCR catalysts," *Appl. Catal. B: Environ. 46, 14-34, 2003.*

[62] J. Lee, M. Paratore and D. Brown, "Evaluation of Cu-Based SCR/DPF Technology for Diesel Exhaust Emission Control," *SAE Int. J. Fuels Lubr. 1(1):96-101, doi:10.4271/2008-01-0072, 2009.*

[63] Y. Yang, G. Cho and C. Rutland, "Model Based Study of $DeNO_x$ Characteristics for Integrated DPF/SCR System over Cu-Zeolite," *SAE Technical Paper 2015-01-1060, doi:10.4271/2015-01-1060, 2015.*

[64] E. Tronconi, "Interaction of NO_x Reduction and Soot Oxidation in a DPF with Cu-Zeolite SCR Coating," *Emission Control Science and Technology, DOI 10.1007/s40825-015-0014-y, 2015.*

[65] M. Naseri, S. Chatterjee, M. Castagnola and H. Chen, "Development of SCR on Diesel Particulate Filter System for Heavy Duty Applications," *SAE Int. J. Engines 4(1):1798-1809, doi:10.4271/2011-01-1312, 2011.*

[66] J. Czerwinski, Y. Zimmerli, A. Mayer and J. Lemaire, "Investigations of SDPF - Diesel Particle Filter with SCR Coating for HD-Applications," *SAE Technical Paper 2015-01-1023, doi:10.4271/2015-01-1023, 2015.*

[67] T. Watling, "Development, validation and application of a model for an SCR catalyst coated diesel particulate filter," *Catal. Today, doi:10.1016/j.cattod. 2012.02.007, 2012.*

[68] S. Park, K. Narayanaswamy, S. Schmieg and C. Rutland, "A Model Development for Evaluating Soot-NOx Interactions in a Blended 2-Way Diesel Particulate Filter/Selective Catalytic Reduction," *Ind. Eng. Chem. Res., 2012..*

[69] W. Tang, D. Youndren, M. SantaMaria and S. Kumar, "On-Engine Investigation of SCR on Filters (SCRoF) for HDD Passive Applications," *SAE Int. J. Engines 6(2):862-872, doi:10.4271/2013-01-1066, 2013.*

[70] J. Tan, C. Solbrig and S. Schmieg, "The Development of Advanced 2-Way SCR/DPF Systems to Meet Future Heavy-Duty Diesel Emissions," *SAE Technical Paper 2011-01-1140, doi:10.4271/2011-01-1140, 2011.*

[71] F. Schrade, M. Brammer, J. Schaeffner and K. Langeheinecke, "Physico-Chemical Modeling of an Integrated SCR on DPF (SCR/DPF) System," *SAE Int. J. Engines 5(3):958-974, doi:10.4271/2012-01-1083, 2012.*

[72] J. Czerwinski, Y. Zimmerli, A. Mayer, G. D'Urbano and D. Zurcher, "Emission Reduction with Diesel Particle Filter with SCR Coating (SDPF)," *Emission Control Science and Technology, Volume 1, 2015.*

[73] G. Cavataio, J. Girard and C. Lambert, "Cu/Zeolite SCR on High Porosity Filters: Laboratory and Engine Performance Evaluations," *SAE Technical Paper 2009-01-0897, doi:10.4271/2009-01-0897, 2009.*

[74] K. Johansen, H. Bentzer, A. Kustov and K. Larsen, "Integration of Vanadium and Zeolite Type SCR Functionality into DPF in Exhaust Aftertreatment Systems - Advantages and Challenges," *SAE Technical Paper 2014-01-1523, doi:10.4271/2014-01-1523, 2014.*

[75] R. Conway, S. Chatterjee, M. Naseri and C. Aydin, "Demonstration of SCR on a Diesel Particulate Filter System on a Heavy Duty Application," *SAE Technical Paper, doi:10.4271/2015-01-1033, 2015.*

[76] H. Kojima, M. Fischer, H. Haga and N. Ohya, "Next Generation All in One Close-Coupled Urea-SCR System," *SAE Technical Paper 2015-01-0994, doi:10.4271/2015-01-0994, 2015.*

[77] K. Rappe, "Integrated Selective Catalytic Reduction−Diesel Particulate Filter Aftertreatment: Insights into Pressure Drop, NO_x Conversion, and Passive Soot Oxidation Behavior," *Industrial and Engineering Chemistry Research, 2014.*

[78] M. Naseri, R. Conway, H. Hess and C. Aydin, "Development of Emission Control Systems to Enable High NO_x Conversion on Heavy Duty Diesel Engines," *SAE Technical Paper 2014-01-1525, doi:10.4271/2014-01-1525, 2014.*

[79] V. Strots, A. Kishi, S. Adelberg and L. Kramer, "Application of Integrated SCR/DPF Systems in Commercial Vehicles," *JSAE Annual Congress, 454-20145174, 2014.*

[80] K. Premchand, "Development of a 1-D Catalyzed Diesel Particulate Filter Model for Simulation of the Performance and the Oxidation of Particulate Matter and Nitrogen Oxides using Passive Oxidation and Active Regeneration Engine Experimental Data," *PhD Dissertation, Michigan Technological University, 2013.*

[81] R. Foley, "Experimental Investigation into Particulate Matter Distribution in Catalyzed Particulate Filters using a 3D Terahertz Wave Scanner," *MS Thesis, Michigan Technological University, 2013.*

[82] K. Shiel, "A Study of the Effect of Biodiesel Fuel on Passive Oxidation in a Catalyzed Particulate Filter," *MS Thesis, Michigan Technological University, 2012.*

[83] J. Pidgeon, "An Experimental Investigation into the Effects of Biodiesel Blends on Particulate Matter Oxidation in a Catalyzed Particulate Filter during Active Regeneration," *MS Thesis, Michigan Technological University, 2013.*

[84] K. Chilumukuru, R. Arasappa, J. Johnson and J. Naber, "An Experimental Study of Particulate Thermal Oxidation in a Catalyzed Filter During Active Regeneration," *SAE Technical Paper 2009-01-1474, doi:10.4271/2009-01-1474, 2009.*

[85] T. McKinley and A. Alleyne, "A Urea Decomposition Modeling Framework for SCR Systems," *SAE Int. J. Fuels Lubr. 2(1):612-626, doi:10.4271/2009-01-1269, 2009.*

[86] S. Gupta, "An Experimental Investigation into the Effect of Particulate Matter on NO_x Reduction in a SCR Catalyst on a DPF," *MS Report, Michigan Technological University, 2016.*

Appendix A. MS Start up, Shut down and Calibration Procedures

The MS is ON and in STANDBY mode during the daily operation. In case the MS is turned OFF for the repair or any other purpose for more than 4 hours, the MS is to be switched ON at least 5 hours before its use for emission measurement. During the warm-up period, the system is stabilized for the data collection, since the sensitivity of the cold analyzer is unstable and the measurements may not be reliable due to inaccurate calibration. It also can cause the MS to drift while measuring emission concentrations during the test. The emission data and the system operation parameters can be monitored, recorded and controlled through the V&F Viewer software installed in a desktop computer. Ensure that the computer is turned ON and the analyzer is connected to the computer via a LAN cable. To initiate the start-up process, open the valve on the xenon gas bottle located inside the MS. Purging the analyzer with xenon removes the oxygen that may have leaked into the analyzer. The oxygen in the gas lines and analyzer may cause damage to the filament which generates electrons. Now switch ON the MS and confirm that the red LEDs are displayed on the RF generator, indicating the status of the MS. The LEDs will turn orange and green in color as the MS has warmed up and stabilized. Open the V&F Viewer and connect to the MS. Select the measurement method "SCR" from the drop-down list in the software. Put the MS in the STANDBY mode when not in use. Refrain from moving the MS when it is turned ON, to avoid any possible damage to the turbo-pump.

In this study, the MS was used to measure the concentration of NO, NO_2, NH_3 and O_2 in the exhaust flow. The MS needs to be calibrated before each test, using the gas bottles for each species of known concentration. The N_2 gas with purity of 99.999% was used as the zero gas. The details of calibration gases are given in Table 3.10. The calibration can be performed either automatically, using the calibration option in the software, or manually, by adjusting the concentration measurement to that of the calibration gas. For the automatic calibration, open the valves on all the calibration gas bottles and N_2. Click on

“Calibrate” option in the side menu and select all the species to be calibrated. Press “Start” to initiate the calibration process. It takes about 8 – 10 minutes to complete the procedure. After the calibration procedure, put the MS in the “Measure” mode till the end of the test.

To perform the manual calibration, plug the calibration gas bottle of the species to be calibrated into the quick connect valve on the front panel of the MS. Unplug the other gases and release the pressure in the line, to prevent their interference during the calibration, due to leakage of the gas through the quick connect valve or the gas lines of the analyzer. Put the MS in the “Measure” mode. Select the quick connect valve from the “Sample inlet” function (the top right section of the software) and the MS starts measuring the calibration gas. Now zero the MS by selecting “inert gas” from the list. Perform zeroing of MS in automatic mode by selecting only “inert gas” in the list. After completion of zeroing step, select other gases of interest. After the measurement has stabilized, select the gas type from the “molecule list” displayed on the right side of the software. Then select channel calibration and enter the concentration mentioned on the gas bottle in the open window. Observe the change in the measurement. If the updated concentration measurement is not correct, re-enter the concentration value, else click OK to accept the calibration. Then repeat the procedure for each species to be calibrated. The calibration procedure was also performed during the test to confirm the accuracy of the data.

To turn OFF the analyzer, select “turn off analyzer” from tools menu of the V&F software. This prevents loss of data and ensures proper shut down of the analyzer. Then turn OFF the power switch located on the rear panel of the analyzer. Then close the valves on the source gas and calibration gas bottles to prevent any possible leakage. Wait for 30 mins if the system is to be accessed for replacement/repair of components. This provides time for the turbofan to stop completely and the system to cool down.

Appendix B. Calibration of NH_3 Sensor using the MS

NH_3 slip from the SCR/SCRF® was measured using the MS and the NH_3 sensor as described in the Chapter 3. It was observed from the experimental results that the NH_3 slip measured by the MS were lower than the values measured by the NH_3 sensor. In order to compare the NH_3 slip measurements from the NH_3 sensor and the MS, it is important to know the empirical relation between the two values. The IMR-MS is calibrated before each test using the calibration gas of known concentration as explained in Appendix A.

To determine the empirical relation between the NH_3 sensor and the IMR-MS, a test was conducted. The test condition and results of the NH_3 sensor calibration are given in Table B.1. The engine was stabilized at the baseline condition as explained in the Chapter 3. During the test, the DEF injection rate was varied to achieve the ANR of 1.2, 1.5, 1.8 and 2.0. At each ANR the NH_3 slip was measured by the MS and the NH_3 sensor at the same time, until the NH_3 measurements from both the instruments reached the steady state for 5 minutes. Then the steady state NH_3 slip measurements from both the instruments were compared to estimate the ratio of NH_3 slip from the sensor to the NH_3 slip from the MS. The average of the ratios can be used as the NH_3 sensor calibration factor during calibration of the SCR-F model.

Table B.1: Results of NH_3 sensor calibration

Speed	**Load**	**Exhaust Flow Rate**	**SCRF® Inlet Temp.**	**ANR**	**NH_3 Sensor**	**NH_3 MS**	**Ratio**
[RPM]	**[N.m]**	**[kg/min]**	**[°C]**	**[-]**	**[ppm]**	**[ppm]**	**[-]**
1661	478	8.1	325	0.0	0	0	-
1662	477	8.1	323	1.2	81	71	1.15
1661	479	8.1	323	1.5	252	220	1.15
1662	479	8.1	321	1.8	420	360	1.17
1662	478	8.1	320	2.0	556	469	1.19
1662	477	8.1	321	0.0	0	6	-
						Average	1.16

Appendix C. Calibration of the DEF Injector

The ANR and the NH_3 concentration at the SCR/SCRF® inlet is estimated from the DEF injection rate, exhaust flow rate and urea properties. Hence, it is important to accurately control the DEF injection rate. The DEF injection rate is controlled by entering the targeted DEF injection rate into the Cummins proprietary software "Calterm", which communicates the command to the engine ECM. The DEF injector calibration procedure is described below.

1) Remove the DEF injector mounted on the decomposition tube.
2) Position a 500 ml measuring cylinder under the DEF injector.
3) Start the DEF injection and continue injecting for 10 minutes. For flow rates below 0.1 ml/s, perform DEF injection for 20 minutes or higher to reduce the error.
4) Stop the DEF injection and remove the measuring cylinder. Place it on a flat surface and wait until no bubbles can be seen in the DEF collected.
5) Record the volume of the DEF collected in the measuring cylinder. Pour the DEF back into the DEF tank.

The relationship between the targeted DEF flow rate (command sent to the ECM) and the actual DEF flow rate (obtained from Calterm) are plotted in Figure C.1. The linear trend line characterizes the relationship between the targeted and the actual DEF flow rate. The actual DEF flow rate was obtained from the Calterm parameter "V_UIM_flm_EstUreaInjRate" and was used to calculate the NH_3 concentrations and ANR at the inlet of the SCRF®.

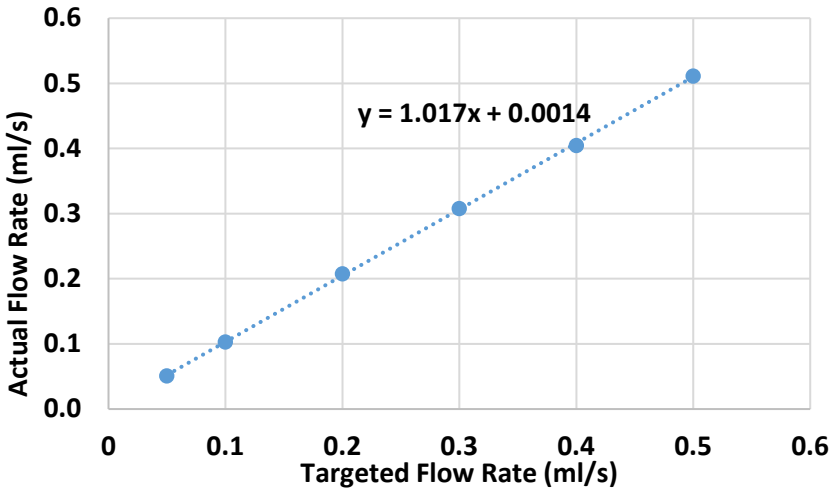

Figure C.1: Calibration curve for the DEF injection

Appendix D. Production-2013-SCR Experimental Results, 1-D SCR Model Calibration Procedure and Simulation Results

The NO, NO_2 and NH_3 concentrations and the NO_x reduction performance of the production-2013-SCR at ANR of 0.3, 0.5, 0.8, 1.0 (repeat) and 0.8 (repeat) are given in Tables D.1 through D.5.

Table D.1: NO_x reduction performance of the production-2013-SCR at target ANR of 0.3

Test Points	**SCR Inlet Temp.**	**NO [ppm]**		**NO_2 [ppm]**		**NH_3 [ppm]**		**ANR**	**NO_x Conv. Efficiency**	**Nitrogen Balance**
[-]	**[°C]**	**In**	**Out**	**In**	**Out**	**In**	**Out**	**[-]**	**[%]**	**[%]**
1	219	470	347	178	125	177	0	0.27	25	99
2	238	177	142	102	78	72	1	0.26	22	83
3	307	199	139	91	67	87	0	0.30	30	97
4	327	185	122	158	127	93	0	0.27	28	101
5	354	325	203	227	179	165	0	0.30	29	103
6	352	1045	647	685	578	476	32	0.28	31	113
8	447	443	336	99	53	163	0	0.30	27	94

Table D.2: NO_x reduction performance of the production-2013-SCR at target ANR of 0.5

Test Points	**SCR Inlet Temp.**	**NO [ppm]**		**NO_2 [ppm]**		**NH_3 [ppm]**		**ANR**	**NO_x Conv. Efficiency**	**Nitrogen Balance**
[-]	**[°C]**	**In**	**Out**	**In**	**Out**	**In**	**Out**	**[-]**	**[%]**	**[%]**
1	219	470	289	178	78	301	1	0.46	42	94
2	238	177	113	102	34	126	1	0.45	41	106
3	307	199	105	91	38	148	1	0.51	51	100
4	327	185	86	158	92	156	0	0.45	48	106
5	354	325	142	227	122	271	0	0.49	51	106
6	352	1045	474	685	405	802	0	0.46	50	106
8	447	443	252	99	12	276	0	0.51	50	101

Table D.3: NO_x reduction performance of the production-2013-SCR at target ANR of 0.8

Test Points	SCR Inlet Temp.	NO [ppm]		NO_2 [ppm]		NH_3 [ppm]		ANR	NO_x Conv. Efficiency	Nitrogen Balance
[-]	[°C]	In	Out	In	Out	In	Out	[-]	[%]	[%]
1	219	470	217	178	27	481	1	0.74	61	84
2	238	177	82	102	23	205	1	0.73	63	85
3	307	199	50	91	3	238	0	0.82	82	100
4	327	185	40	158	41	254	0	0.74	76	103
5	354	325	61	227	38	435	0	0.79	82	104
6	352	1045	244	685	139	1291	0	0.75	78	104
8	447	443	124	99	1	442	15	0.82	77	98

Table D.4: NO_x reduction performance of the production-2013-SCR at target ANR of 1.0 (Repeat)

Test Points	SCR Inlet Temp.	NO [ppm]		NO_2 [ppm]		NH_3 [ppm]		ANR	NO_x Conv. Efficiency	Nitrogen Balance
[-]	[°C]	In	Out	In	Out	In	Out	[-]	[%]	[%]
1	219	470	110	178	0	606	39	0.94	2	95
2	238	177	30	102	0	260	12	0.93	89	100
3	307	199	24	91	0	293	35	1.01	92	103
4	327	185	6	158	4	316	1	0.92	97	106
5	354	325	3	227	0	539	6	0.98	100	103
6	352	1045	85	685	1	1713	5	0.99	95	96
8	447	443	89	99	0	554	68	1.02	83	94

Table D.5: NO_x reduction performance of the production-2013-SCR at target ANR of 0.8 (repeat)

Test Points	SCR Inlet Temp.	NO [ppm]		NO_2 [ppm]		NH_3 [ppm]		ANR	NO_x Conv. Efficiency	Nitrogen Balance
[-]	[°C]	In	Out	In	Out	In	Out	[-]	[%]	[%]
1	219	470	144	178	0	483	6	0.75	77	106
2	238	177	67	102	2	206	3	0.74	75	103
3	307	199	49	91	1	232	1	0.80	83	104
4	327	185	40	158	33	253	0	0.74	79	107
5	354	325	70	227	33	437	0	0.79	81	103
6	352	1045	274	685	124	1300	0	0.75	78	102
8	447	443	131	99	0	443	13	0.82	75	96

The experimental data acquired from the seven NO_x reduction Test Points that cover a range of SCR inlet temperatures, space velocities and inlet NO_x concentrations were used

to prepare the time varying inputs and calibrate the model. The time varying inputs required for the model are:

I. Exhaust mass flow rate
II. Concentration of chemical species (NO, NO_2, NH_3, H_2O, CO_2 at the inlet of the SCR)
III. SCR inlet temperature and pressure

The primary objective of the calibration procedure was to determine a single set of parameters that could simulate the NO_x reduction performance of the production-2013-SCR for the seven Test Points. The SCR model parameters used for calibrating the model to the engine experimental data from the Cummins ISB 2010 engine, were used as the starting values. The simulation data from the model were compared with the experimental data, to determine the difference and evaluate the performance of the 1-D SCR model. The model parameters were changed manually to reduce the cost function. The cost function value for each species is defined as the accumulative absolute error between the model prediction and the experimental measurement divided by the simulation time. The equation calculating the cost function value for each species is given in Equation D.1. The Equation D.1 is from reference [9].

$$Cost_i = \frac{\sum_{t_0}^{t_{end}} | C_{i,Sim} - C_{i,Exp} |}{t_{end}} \qquad \text{D.1}$$

Where $Cost_i$ is the cost function for gas species i (i =NO, NO_2, NH_3). t_o and t_{end} are the start and stop time in seconds for the simulation. $C_{i,Sim}$ and $C_{i,Exp}$ are the model simulated and experimentally measured gas concentrations for the gas species i respectively [9].

Manual Optimization

The manual optimization procedure illustrated in Figure D.1 is explained in the following steps:

I. Run the model with the input file and the initial set of parameters. Initial parameters for engine data were taken from Table 5.1 in reference [9].
II. The model simulated data and the experimental data were plotted to determine the difference in concentrations of NO, NO_2 and NH_3 at the production-2013-SCR outlet location. The difference in concentration during steady state operation was used to estimate the parameter to be optimized.
III. The parameter is changed to reduce the difference.
IV. The parameters were changed based on the cost function. The parameters were also tuned to reduce the difference between the experimental and simulated data during transient and steady state conditions. Then step 2 was repeated.
V. The step III and IV were repeated till the model was calibrated to within ± 20 ppm for NO and NO_2, and ± 30 ppm for NH_3 concentrations.

The activation energy for the twelve reactions in the MY2013 production-2013-SCR were assumed to be same as that of MY2010 production. The pre-exponential factor for R1, R2, R7 and R9 described in Chapter 2, which are labelled as "A_ads1", "A_des1", " A_std" and "A_fst" respectively, were calibrated based on trial-and-error method since only these factors affected the simulation results significantly. The modified pre-exponential values are highlighted in Table 4.5. The plot of reaction rate constant vs 1000/T is shown in Figure D.2. It is observed from Figure D.2 that the reaction rate constant for each reaction followed a linear trend in the Arrhenius form, meaning that the effect of the temperature on the reaction rates was well captured by the model. The slope m and the interception c of each fit trend line were used to calculate the pre-exponential constant and the activation energy of each reaction. Comparison of the simulation of SCR outlet concentrations of NO, NO_2 and NH_3 data to the experimental data for Test Points 2, 3, 4, 6 and 8 are shown in Figures D.3 to D.7.

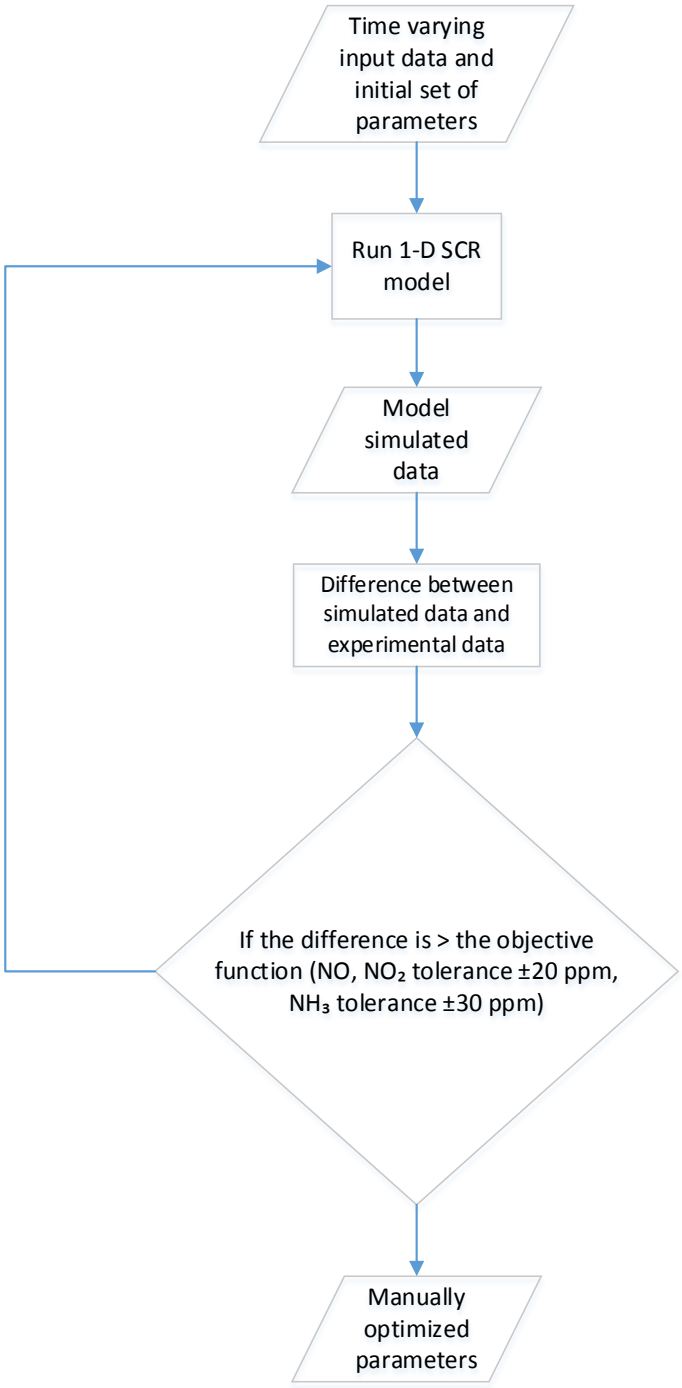

Figure D.1: Flow chart of manual optimization procedure to calibrate 1-D SCR model

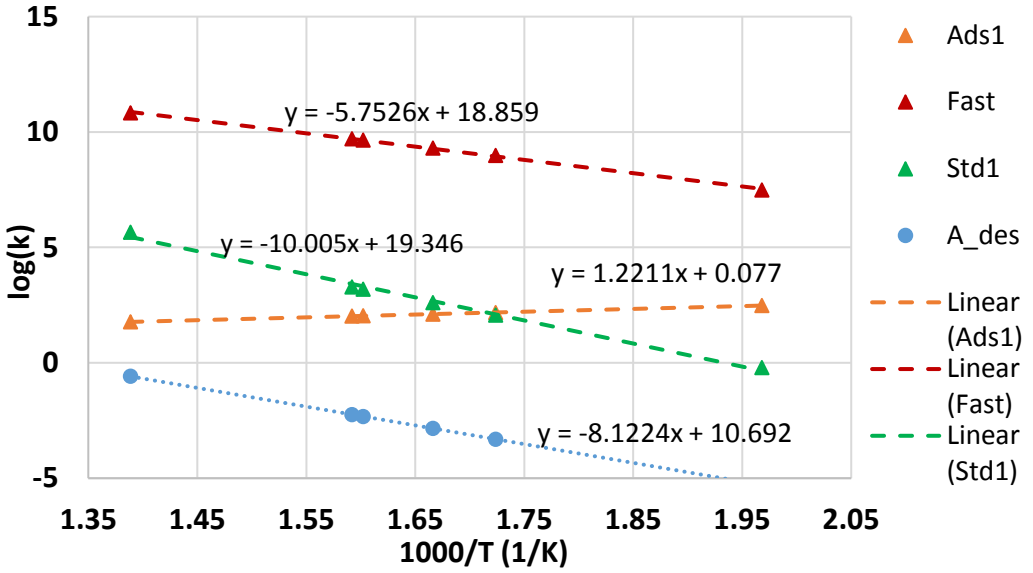

Figure D.2: Arrhenius plots of reaction rate constants for reactions R1, R2, R7 and R9

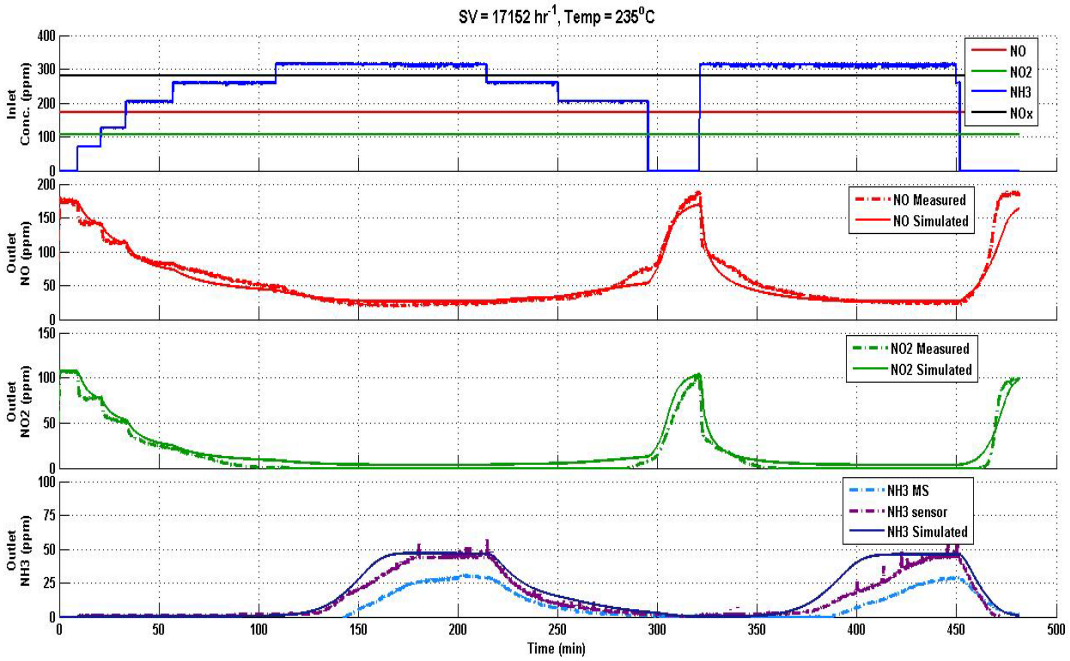

Figure D.3: Comparison of the SCR outlet gaseous concentrations between simulation results and experimental measurements for Test Point 2 (SCR inlet temperature 235°C, SV 17.2 k/hr

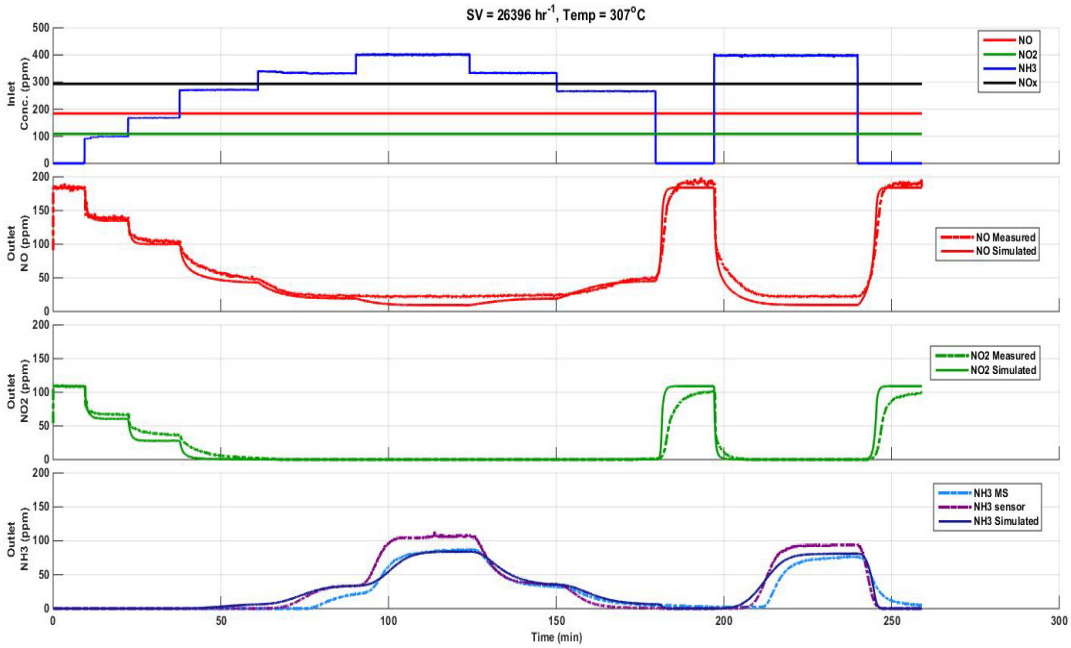

Figure D.4: Comparison of the SCR outlet gaseous concentrations between simulation results and experimental measurements for Test Point 3 (SCR inlet temperature 307°C, SV 26.4 k/hr

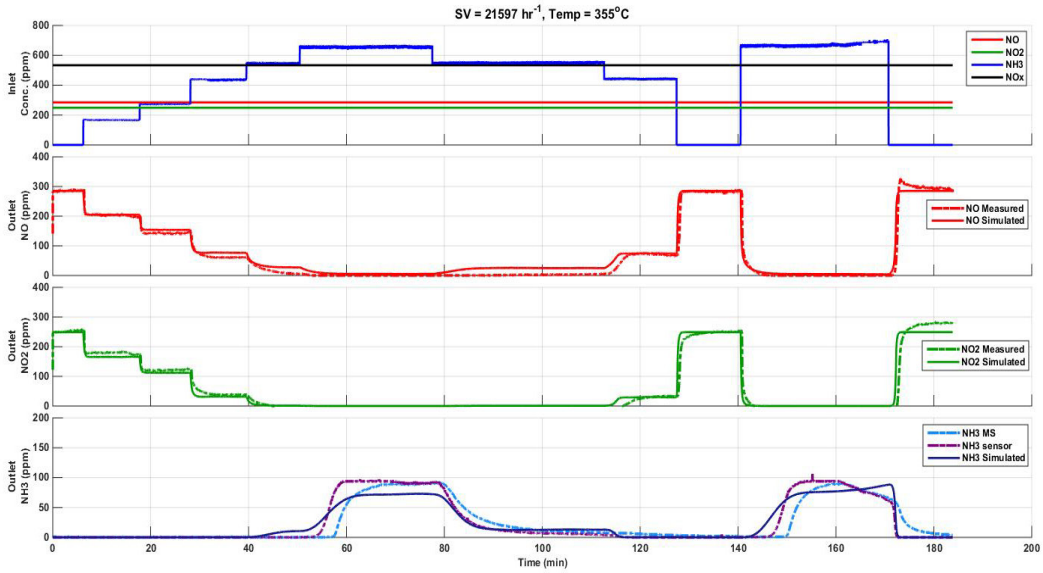

Figure D.5: Comparison of the SCR outlet gaseous concentrations between simulation results and experimental measurements for Test Point 5 (SCR inlet temperature 355°C, SV 21.6 k/hr

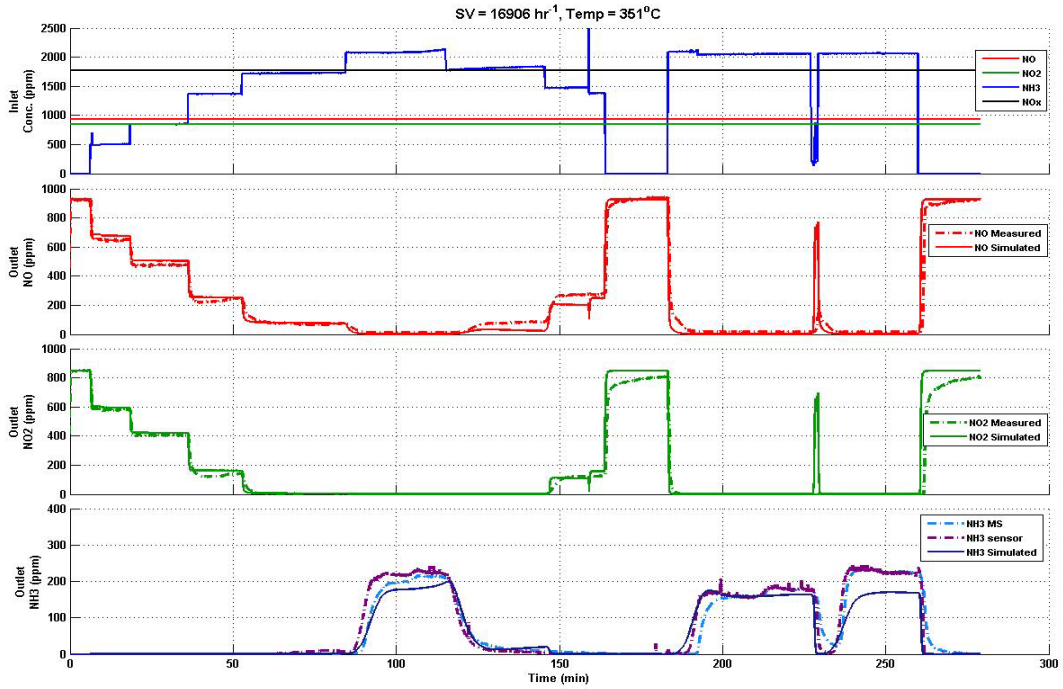

Figure D.6: Comparison of the SCR outlet gaseous concentrations between simulation results and experimental measurements for Test Point 6 (SCR inlet temperature 351°C, SV 16.9 k/hr

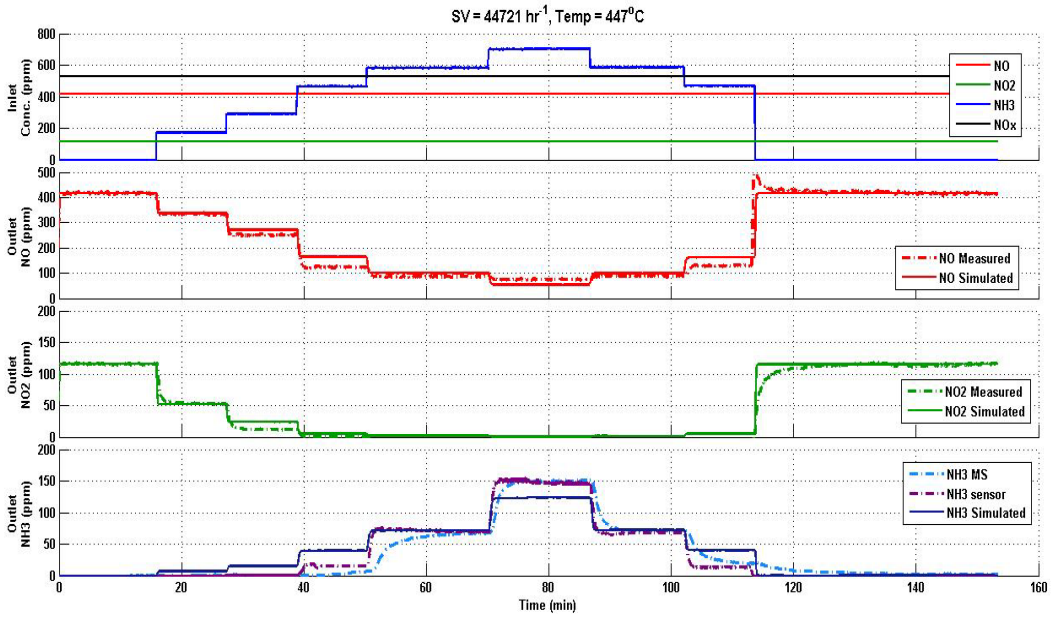

Figure D.7: Comparison of the SCR outlet gaseous concentrations between simulation results and experimental measurements for Test Point 8 (SCR inlet temperature 447°C, SV 44.7 k/hr

Appendix E. Engine, Exhaust conditions and PM Mass Balance for each Stage – Configuration 2 (with PM loading)

The engine conditions, exhaust conditions at the inlet of the SCRF® and PM mass balance across the SCRF® for stages 1 and 2 and NO_x reduction stages are presented in this appendix. The engine speed, load, the engine out and SCRF® inlet (temperature, $NO/NO_2/NO_x$ concentration, PM concentration) conditions are analyzed and compared for deviation in Table E.1, E.2, E.5, and E.6. The filtration efficiency of the SCRF® and PM oxidation in the SCRF® is summarized in Table E.3, E.4, E.7, and E.8.

Stage 1 and Stage 2 for PM Loading 2 g/L

It is seen from Table E.1 and E.2 that the species concentration (NO, NO_2 and NO_x) and engine out PM are consistent for all Test Points. The speed and load values were kept at constant values of 2400 RPM and 200 Nm and have very small deviation. The average engine-out particulate matter is 11.4 mg/scm (milligrams /standard cubic meter) and is consistent for all tests with a standard deviation of 0.5 mg/scm and 0.3 mg/scm for stage 1 and stage 2 respectively.

The parameters such as PM concentration into SCRF®, NO_2/PM ratio, temperature into SCRF® and loading duration which affected the PM deposition and oxidation in the SCRF® are given in Table E.3 and E.4. The Test Point 3 (2401 rpm engine speed, 203 Nm load) has least $PM_{Retained}$ of 27.9 grams in the SCRF® for the high PM concentration coming into the SCRF® and hence high $PM_{Available}$ for oxidation. Another reason was that the Test Point 3 was run for least time period of approximately 300 minutes.

PM oxidized (percentage) in stage 1 as shown in Table E.3 has the similar trend to that of PM oxidized (percentage) in stage 2 as shown in Table E.4. This is because mass loaded in stage 1 is estimated assuming the same rate of loading as in stage 2. The filtration

efficiency for stage 2 is obtained using the upstream and downstream SCRF® PM samples collected during stage 2.

Table E.1: Engine and exhaust conditions for the SCRF® during stage 1 – Configuration 2 (PM loading 2 g/L)

Test Point	Speed	Load	Temp. into SCRF ®	Exhaust Flowrate	SCRF® Std. Space Vel.	SCRF® Act. Space Vel.	NO into SCRF ®	NO_2 into SCRF ®	NO_x into SCRF ®	NO out of SCRF ®	NO_2 out of SCRF ®	NO_x out of SCRF ®	Engine Out PM Conc.
[-]	[RPM]	[N-m]	[°C]	[kg/min]	[k/hr]	[k/hr]	[ppm]	[ppm]	[ppm]	[ppm]	[ppm]	[ppm]	[mg/scm]
1	2383	205	276	11.2	30.5	57.6	118	62	180	127	50	177	11.0
3	2395	205	274	11.2	33.3	57.3	138	38	176	132	39	171	12.2
6	2400	203	274	11.2	33.5	57.6	118	72	190	130	58	18	11.4
8	2397	201	284	11.3	33.7	59.1	124	66	190	129	55	184	11.0
Mean	2394	204	277	11.2	32.7	57.9	124	59	184	130	50	180	11.4
Std. Dev.	7	2	5	0.1	1.5	0.8	9	15	7	2	8	8	0.5
ULIM 95%	2401	205	282	11.3	34.2	58.7	134	74	191	132	58	187	11.9
LLIM 95%	2387	202	272	11.2	31.3	57.1	115	45	177	127	42	172	10.9
95% CI	14	3	9	0.1	2.9	1.6	18	29	14	4	16	15	1.1

Table E.2: Engine and exhaust conditions for the SCRF® during stage 2 – Configuration 2 (PM loading 2 g/L)

Test Point	Speed	Load	Temp. into SCRF®	Exhaust Flowrate	SCRF® Std. Space Vel.	SCRF® Act. Space Vel.	NO into SCRF®	NO_2 into SCRF®	NO_x into SCRF®	NO out of SCRF®	NO_2 out of SCRF®	NO_x out of SCRF®	Engine Out PM Conc.	SCRF® delta P at the end of S2
[-]	[RPM]	[N-m]	[°C]	[kg/min]	[k/hr]	[k/hr]	[ppm]	[ppm]	[ppm]	[ppm]	[ppm]	[ppm]	[mg/scm]	[kPa]
1	2401	203	279	11.3	30.7	58.3	114	82	196	136	51	187	11.0	6.6
3	2401	203	274	11.2	30.5	57.3	131	56	187	146	44	190	11.8	6.4
6	2399	200	269	11.3	30.8	57.5	122	65	186	145	37	182	11.4	6.3
8	2399	202	274	11.2	30.6	57.7	127	69	197	133	51	184	11.2	6.2
Mean	2400	202	274	11.2	30.7	57.7	123	68	191	140	46	186	11.4	6.4
Std. Dev.	1	1	4	0.1	0.1	0.4	7	11	6	7	7	4	0.3	0.2
ULIM 95%	2401	203	278	11.3	30.8	58.1	131	79	197	146	52	189	11.7	6.5
LLIM 95%	2399	201	270	11.2	30.5	57.3	116	57	186	133	39	182	11.0	6.2
95% CI	2	2	8	0.1	0.3	0.8	15	21	11	13	13	7	0.7	0.3

Table E.3: Particulate matter mass balance during stage 1 – Configuration 2 (PM loading 2 g/L)

Test Point	PM Conc. Into SCRF®	NO_2/PM Ratio	NO_x/PM Ratio	Filtration Efficiency of SCRF®	PM_{In}	PM_{Out}	$PM_{Available}$	$PM_{Oxidized}$	$PM_{Retained}$	Duration	PM Oxidized
[-]	[mg/scm]	[mg NO_2: mg PM]	[mg NO_x: mg PM]	[%]	[g]	[g]	[g]	[g]	[g]	[min]	[%]
1	11.0	10.6	30.8	96.9	3.1	0.1	3.1	0.2	2.8	30	7%
3	12.2	5.8	27.1	97.7	3.5	0.1	3.5	0.9	2.6	31	25%
6	11.4	11.8	31.2	97.4	3.3	0.1	3.3	0.7	2.5	31	20%
8	11.0	11.3	32.4	97.8	3.3	0.1	3.3	0.4	2.8	32	13%
Mean	11.4	9.9	30.4	97.4	3.3	0.1	3.3	0.5	2.7	31	16%
Std. Dev.	0.5	2.7	2.3	0.4	0.2	0.0	0.2	0.3	0.2	0	8%
ULIM 95%	11.9	12.6	32.6	97.8	3.5	0.1	3.5	0.8	2.8	31	24%
LLIM 95%	10.9	7.2	28.2	97.1	3.2	0.1	3.2	0.3	2.5	30	8%
95% CI	1.1	5.4	4.4	0.7	0.3	0.0	0.3	0.6	0.3	1	15%

Table E.4: Particulate matter mass balance during stage 2 – Configuration 2 (PM loading 2 g/L)

Test Point	PM Conc. Into SCRF®	NO_2/PM Ratio	NO_x/PM Ratio	Filtration Efficiency of SCRF®	PM_{In}	PM_{Out}	$PM_{Available}$	$PM_{Oxidized}$	$PM_{Retained}$	Duration	%Oxidized	PM Loading at the end of S2
[-]	[mg/scm]	[mg NO_2: mg PM]	[mg NO_x: mg PM]	[%]	[g]	[g]	[g]	[g]	[g]	[min]	[%]	[g/L]
1	11.0	14.1	33.5	96.9	34.6	1.1	37.4	3.0	33.3	330	8%	2.0
3	11.8	9.0	29.8	97.7	33.5	0.8	36.1	7.4	27.9	300[1]	21%	1.6[1]
6	11.4	10.6	30.6	97.4	36.6	1.0	39.1	8.0	30.1	334	20%	1.8
8	11.2	11.6	32.9	97.8	35.3	0.8	38.1	4.8	32.5	330	13%	1.9
Mean	11.4	11.3	31.7	97.4	35.0	0.9	37.7	5.8	31.0	323	15%	1.8
Std. Dev.	0.3	2.1	1.8	0.4	1.3	0.1	1.3	2.4	2.5	16	6%	0.1
ULIM 95%	11.7	13.4	33.5	97.8	36.2	1.0	38.9	8.1	33.4	339	22%	2.0
LLIM 95%	11.0	9.2	30.0	97.1	33.7	0.8	36.4	3.5	28.5	308	9%	1.7
95% CI	0.7	4.2	3.5	0.7	2.5	0.3	2.5	4.6	4.9	31	12%	0.3

[1] – Stage 2 for the Test Point 3 was run for a shorter duration (300 minutes) when compared to the other Test Points (330 minutes)

Stage 1 and Stage 2 at 4 g/L Loading

Table E.5 and E.6 give the consistent values for engine speed, load, SCRF® inlet species concentration and engine out PM concentration for all Test Points. The average engine-out particulate matter is 18.7 mg/scm and 19.4 mg/scm for stage 1 and stage 2 respectively.

Table E.8 shows that the PM oxidized (percentage) for stage 2 is consistent for all Test Points with mean oxidation 24 %. The $PM_{Retained}$ in the SCRF® is 4 g and 69.4 g for stage 1 and stage 2 respectively. The filtration efficiency of 99.1% is obtained using the samples collected during stage 2 which is considered to be same for stage 1.

Table E.5: Engine and exhaust conditions for the SCRF® during stage 1 – Configuration 2 (PM loading 4 g/L)

Test Point	Speed	Load	Temp. into SCRF ®	Exhaust Flowrate	SCRF® Std. Space Vel.	SCRF® Act. Space Vel.	NO into SCRF ®	NO_2 into SCRF ®	NO_x into SCRF ®	NO out of SCRF ®	NO_2 out of SCRF ®	NO_x out of SCRF ®	Engine Out PM Conc.	SCRF ® delta P
[-]	[RPM]	[N-m]	[°C]	[kg/min]	[k/hr]	[k/hr]	[ppm]	[ppm]	[ppm]	[ppm]	[ppm]	[ppm]	[mg/scm]	[kPa]
1	2401	205	285	11.4	31.0	61.1	112	42	154	112	32	144	15.1	3.7
3	2398	205	285	11.4	33.9	61.0	98	46	144	104	35	139	21.2	3.7
6	2396	201	286	11.3	33.8	61.0	101	46	147	117	31	149	18.8	3.7
8	2399	205	294	11.4	34.0	62.2	107	50	157	114	34	148	19.7	3.8
Mean	2399	204	288	11.4	33.2	61.3	105	46	151	112	33	145	18.7	3.7
Std. Dev.	2	2	5	0.0	1.5	0.6	6	3	6	6	2	4	2.6	0.1
ULIM 95%	2400	206	292	11.4	34.6	61.9	111	49	157	117	35	149	21.2	3.8
LLIM 95%	2397	202	283	11.3	31.7	60.8	99	43	145	107	32	141	16.2	3.6
95% CI	4	4	9	0.1	2.9	1.1	12	6	12	11	3	9	5.0	0.1

Table E.6: Engine and exhaust conditions for the SCRF® during stage 2 – Configuration 2 (PM loading 4 g/L)

Test Point	Speed	Load	Temp. into SCRF ®	Exhaust Flowrate	SCRF® Std. Space Vel.	SCRF® Act. Space Vel.	NO into SCRF ®	NO_2 into SCRF ®	NO_x into SCRF ®	NO out of SCRF ®	NO_2 out of SCRF ®	NO_x out of SCRF ®	Engine Out PM Conc.	SCRF ® delta P
[-]	[RPM]	[N-m]	[C]	[kg/min]	[k/hr]	[k/hr]	[ppm]	[ppm]	[ppm]	[ppm]	[ppm]	[ppm]	[mg/scm]	[kPa]
1	2401	205	288	11.4	31.1	58.5	110	53	163	135	17	152	17.7	9.4
3	2387	202	283	11.3	30.9	57.8	100	53	153	118	25	143	21.2	9.1
6	2402	204	297	11.6	31.5	59.8	122	54	175	156	23	179	19.5	10.0
8	2402	204	298	11.5	31.3	59.6	102	48	150	132	18	150	19.2	9.9
Mean	2398	204	291	11.5	31.2	58.9	109	52	161	135	21	156	19.4	9.6
Std. Dev.	8	1	7	0.1	0.2	0.9	10	3	11	16	4	16	1.4	0.4
ULIM 95%	2405	205	298	11.5	31.5	59.8	118	55	172	151	24	172	20.8	10.0
LLIM 95%	2390	203	284	11.4	31.0	58.0	99	49	149	120	17	140	18.0	9.1
95% CI	15	2	14	0.2	0.5	1.9	19	5	22	31	7	31	2.7	0.9

Table E.7: Particulate matter mass balance during stage 1 – Configuration 2 (PM loading 4 g/L)

Test Point	PM Conc. Into SCRF®	NO_2 Ratio	NO_x/PM Ratio	Filtration Efficiency of SCRF®	PM_{In}	PM_{Out}	$PM_{Available}$	$PM_{Oxidized}$	$PM_{Retained}$	Duration	%Oxidized
[-]	[mg/scm]	[mg NO_2: mg PM]	[mg NO_x: mg PM]	[%]	[g]	[g]	[g]	[g]	[g]	[min]	[%]
1	15.1	5.2	19.2	99.0	4.5	0.05	4.5	0.5	4.0	31	11%
3	21.2	4.0	12.8	98.3	6.0	0.10	6.0	2.1	3.8	30	35%
6	18.8	4.6	14.7	99.0	5.3	0.05	5.3	1.4	3.9	30	26%
8	19.7	4.8	15.0	99.0	5.9	-0.01	5.9	1.5	4.3	31	26%
Mean	18.7	4.7	15.4	98.8	5.4	0.05	5.4	1.4	4.0	30	25%
Std. Dev.	2.6	0.5	2.7	0.3	0.7	0.04	0.7	0.6	0.2	1	10%
ULIM 95%	21.2	5.1	18.0	99.2	6.1	0.09	6.1	2.0	4.2	31	34%
LLIM 95%	16.2	4.2	12.8	98.5	4.8	0.00	4.8	0.7	3.8	30	15%
95% CI	5.0	1.0	5.2	0.7	1.3	0.09	1.3	1.3	0.4	1	19%

Table E.8: Particulate matter mass balance during stage 2 – Configuration 2 (PM loading 4 g/L)

Test Point	PM Conc. Into SCRF®	NO_2 Ratio	NO_x/PM Ratio	Filtration Efficiency of SCRF®	PM_{In}	PM_{Out}	$PM_{Available}$	$PM_{Oxidized}$	$PM_{Retained}$	Duration	%Oxidized	PM Loading at the end of S2
[-]	[mg/scm]	[mg NO_2: mg PM]	[mg NO_x: mg PM]	[%]	[g]	[g]	[g]	[g]	[g]	[min]	[%]	[g/L]
1	17.7	5.6	17.3	99.0	87.7	0.9	91.7	21.6	69.2	511	24%	4.1
3	21.2	4.7	13.6	98.3	93.6	1.6	97.4	34.3	61.5	450[2]	21%	3.6[2]
6	19.5	5.2	16.9	99.0	97.5	1.0	101.4	29.3	71.1	510	29%	4.2
8	19.2	4.7	14.7	99.0[3]	95.5	-0.1	99.8	24.2	75.7	510	24%	4.4
Mean	19.4	5.0	15.6	98.8	93.6	0.8	97.6	27.4	69.4	497	24%	4.1
Std. Dev.	1.4	0.4	1.8	0.3	4.2	0.7	4.2	5.6	5.9	25	3%	0.3
ULIM 95%	20.8	5.5	17.3	99.2	97.7	1.5	101.7	32.9	75.2	522	28%	4.4
LLIM 95%	18.0	4.6	13.9	98.5	89.4	0.1	93.4	21.8	63.6	473	21%	3.7
95% CI	2.7	0.9	3.4	0.7	8.3	1.4	8.3	11.1	11.6	49	7%	0.7

[2] – Stage 2 for the Test Point 3 was run for a shorter duration (450 minutes) when compared to the other Test Points (510 minutes)
[3] – The value is taken same as that for the Test Point 6 since the downstream SCRF® PM sample was damaged.

The $PM_{Retained}$ in the SCRF® at the end of the stage 1, stage 2 and NO_x reduction stage are given in Table E.9. The $PM_{Retained}$ are calculated using the equations described in section 3.6.7 of this thesis. From Table E.9 it is observed that for the NO_x experimental tests with target PM loading of 2 and 4 g/L, the $PM_{Retained}$ at the end of stage 1 and stage 2 were consistent and PM loading of 2 ± 0.2 g/L and 4 ± 0.4 g/L were achieved for all the tests except for Test Point 3. The stage 2 duration for Test Point 3 was 30 minutes shorter than the other Test Points. It is also observed that the $PM_{Retained}$ at the end of NO_x reduction stage for Test Point 1 is 23 – 24 grams higher that the $PM_{Retained}$ at the end of stage 2 for PM loading of 2 and 4 g/L. This could be due to higher NH_3 storage in the SCRF® and water adsorption in the SCRF since Test Point 1 is a low temperature test condition (~213 °C). The NH_3 stored in the SCRF® for all Test Points, with PM loading of 2 and 4 g/L are given in Table E.10. It is also observed that the Test Points 6 and 8 indicated significant PM oxidation during NO_x reduction stage with PM loading of 2 g/L, since the $PM_{Retained}$ at the end of NO_x reduction stage is lower than the $PM_{Retained}$ at the end of stage 2. However, the $PM_{Retained}$ at the end of NO_x reduction stage is higher than the $PM_{Retained}$ at the end of stage 2 for Test Points 6 and 8 with PM loading of 4 g/L. This appears to be an error in the mass measurement of the SCRF® substrate at the end of NO_x reduction stage.

Table E.9: $PM_{Retained}$ in the SCRF® at the end of the stage 1, stage 2 and NO_x reduction stage for Test Points in configuration 2

Test Points	SCRF® inlet Temp.	Configuration 2 - $PM_{Retained}$, (grams)					
		Target PM Loading - 2 g/L			Target PM Loading - 4 g/L		
		Stage 1	Stage 2	NO_x Reduction Stage	Stage 1	Stage 2	NO_x Reduction Stage
1	213	2.8	33.3	56.2	4.0	69.2	93.1
3	301	2.6	27.9[1]	24.6	3.8	61.5[1]	59.8
6	345	2.5	30.1	25.9	3.9	71.1	82.7[2]
8	443	2.8	32.5	10.1	4.3	75.7	80.8[2]

[1] – Lower $PM_{Retained}$ since the stage 2 was run for shorter duration

[2] – Appears to be an error in the mass measurement

Table E.10: NH_3 stored (grams) in the SCRF® for various Test Points in configuration 2

Test Point	**[-]**	**1**	**3**	**6**	**8**
SCRF® inlet Temp.	**[°C]**	213	301	345	443
NH_3 stored – PM Loading 2 g/L	**[g]**	14.6	6.9	4.8	4.2
NH_3 stored – PM Loading 4 g/L	**[g]**	13.9	5.3	4.3	3.9

Appendix F. Gaseous Emissions by Stage

This appendix describes the emission concentrations during stage 1 and stage 2 of NO_x reduction tests with PM loading of 2 and 4 g/L in the SCRF® from Tables F.1 through F.4. The emission concentrations for NO_x reduction at ANRs 0.8, 1.0 and 1.2 are discussed in Chapter 4 and the emission concentrations at ANR of 1.2 (repeat) are summarized in this section in Tables F.6. All the measurements presented in the Tables F.1 through F.5 were measured using a mass spectrometer. The positive and negative values of NO conversion efficiency shows reduction and increment in NO concentration across the components (DOC, SCRF®) respectively.

Due to problems with the Mass Spectrometer emission analyzer, the NO_2 concentrations were not available correctly at the upstream DOC location for some the Test Points. After the repair of the MS, the correct concentrations upstream DOC were obtained for NO_x reduction tests with PM loading of 4 g/L. The NO_x is determined as the sum of NO and NO_2 concentrations at the respective locations. The effect of PM loading on NO_x reduction efficiency for the four Tests points at ANR-1.2 (repeat) is shown in Figure F.1.

Stage 1 and Stage 2 Loading at 2 g/L

Table F.1: NO, NO_2, NO_x concentrations at inlet and outlet of the DOC and SCRF® during stage 1 – Configuration 2 (PM loading at 2 g/L)

Test Point	NO			NO_2			NO_x			NO Conv. %	
	UDOC	USCRF®	DSCRF®	UDOC	USCRF®	DSCRF®	UDOC	USCRF®	DSCRF®	DOC	SCRF®
[-]	[ppm]	[ppm]	[ppm]	[ppm]	[ppm]	[ppm]	[ppm]	[ppm]	[ppm]	[%]	[%]
1	182	118	127	1[2]	62	50	183	180	177	35	-8
3	170	138[1]	132[1]	1[2]	38	39	171	176	171	19	4
6	181	118	130	1[2]	72	58	182	190	188	35	-10
8	181	124	129	1[2]	66	55	182	190	184	32	-4
Mean	179	124	130	1	59	50	180	184	180	30	-5
Std. Dev.	6	9	2	0	15	8	6	7	8	8	6
ULIM 95%	184	134	132	1	74	58	185	191	187	38	2
LLIM 95%	173	115	127	1	45	42	174	177	172	23	-11
95% CI	11	18	4	0	29	16	11	14	15	15	12

[1] – The concentration of NO at USCRF® and DSCRF® are flagged because of calibration issues with the mass spectrometer during Test Point 3.

[2] _ Appears to be an error in the NO_2 concentrations due to calibration issues in the MS

Table F.2: NO, NO_2, NO_x concentrations at inlet and outlet of the DOC and SCRF® during Stage 2 – Configuration 2 (PM loading at 2 g/L)

Test Point	NO			NO_2			NO_x			NO Conv. %	
	UDOC	USCRF®	DSCRF®	UDOC	USCRF®	DSCRF®	UDOC	USCRF®	DSCRF®	DOC	SCRF®
[-]	[ppm]	[ppm]	[ppm]	[ppm]	[ppm]	[ppm]	[ppm]	[ppm]	[ppm]	[%]	[%]
1	172	114	136	1[2]	82	51	173	196	187	34	-20
3	180	131	146	1[2]	56	44	181	187	190	27	-12
6	170	122	145	8[2]	65	37	178	186	182	28	-19
8	185	127	133	6[2]	69	51	191	197	184	31	-5
Mean	177	123	140	4	68	46	181	191	186	30	-14
Std. Dev.	7	7	7	4	11	6	7	6	4	3	7
ULIM 95%	183	131	146	7	79	52	188	197	189	33	-7
LLIM 95%	170	116	133	1	57	40	173	186	182	27	-21
95% CI	14	15	13	7	21	13	15	11	7	6	14

[2] _ Appears to be an error in the NO_2 concentrations due to calibration issues in the MS

Table F.3: NO, NO_2, NO_x concentrations at inlet and outlet of the DOC and SCRF® during Stage 1 – Configuration 2 (PM loading at 4 g/L)

Test Point	NO			NO_2			NO_x			NO Conv. %	
	UDOC	USCRF®	DSCRF®	UDOC	USCRF®	DSCRF®	UDOC	USCRF®	DSCRF®	DOC	SCRF®
[-]	[ppm]	[ppm]	[ppm]	[ppm]	[ppm]	[ppm]	[ppm]	[ppm]	[ppm]	[%]	[%]
1	147	112	112	1[2]	42	32	148	154	144	24	0
3	138	98	104	0[2]	46	35	138	144	139	29	-6
6	125	101	117	22	46	31	147	147	149	19	-16
8	130	107	114	18	50	34	148	157	148	18	-7
Mean	135	105	112	10	46	33	145	151	145	22	-7
Std. Dev.	10	6	6	11	3	2	5	6	4	5	7
ULIM 95%	144	111	117	22	49	35	150	157	149	27	-1
LLIM 95%	125	99	107	-1	43	32	140	145	141	17	-14
95% CI	19	12	11	23	6	3	10	12	9	10	13

[2] _ Appears to be an error in the NO_2 concentrations due to calibration issues in the MS

Table F.4: NO, NO_2, NO_x concentrations at inlet and outlet of the DOC and SCRF® during Stage 2 – Configuration 2 (PM loading at 4 g/L)

Test Point	NO			NO_2			NO_x			NO Conv. %	
	UDOC	USCRF®	DSCRF®	UDOC	USCRF®	DSCRF®	UDOC	USCRF®	DSCRF®	DOC	SCRF®
[-]	[ppm]	[ppm]	[ppm]	[ppm]	[ppm]	[ppm]	[ppm]	[ppm]	[ppm]	[%]	[%]
1	133	110	135	18	53	17	152	163	152	17	-22
3	145	100	118	2[2]	53	25	147	153	143	31	-18
6	147	122	156	23	54	23	170	175	179	17	-29
8	135	102	132	17	48	18	152	150	150	24	-29
Mean	140	109	135	15	52	21	155	161	156	23	-24
Std. Dev.	7	10	16	9	3	4	10	11	16	6	6
ULIM 95%	147	118	151	24	55	24	165	172	172	29	-19
LLIM 95%	133	99	120	6	49	17	145	149	140	16	-30
95% CI	14	19	31	18	5	7	20	22	31	12	11

[2] _ Appears to be an error in the NO_2 concentrations due to calibration issues in the MS

NO_x Reduction Stage

Table F.5: NO and NO_2 concentrations at inlet and outlet of the SCRF® for NO_x reduction Test Points, at ANR – 0

Test Point	NO [ppm]						NO_2 [ppm]					
	SCRF®- 0		SCRF®- 2		SCRF®- 4		SCRF®- 0		SCRF®- 2		SCRF®- 4	
	In	Out	In	Out	In	Out	In	Out	In	Out	In	Out
1	345	352	403	387	411	401	213	200	203	205	141	116
3	158	160	161	198	198	249	121	116	131	88	124	75
6	795	808	743	967	793	1151	674	688	644	426	588	231
8	411	415	424	457	415	502	140	139	125	52	115	22

Table F.6: NO, NO_2 and NH_3 concentrations at inlet and outlet of the SCRF® at ANR 1.2 Repeat

Test Point	NO [ppm]						NO_2 [ppm]						NH_3 [ppm]					
	SCRF®-0		SCRF®-2		SCRF®-4		SCRF®-0		SCRF®-2		SCRF®-4		SCRF®- 0		SCRF®- 2		SCRF®- 4	
	In	Out	In	Out	In	Out	In	Out	In	Out	In	Out	In	Out	In	Out	In	Out
1	345	7	403	8	411	15	213	0	203	0	141	1	685	117	723	120	722	148
3	158	5	161	2	198	3	121	0	131	0	124	0	331	61	347	48	392	62
6	795	5	743	6	793	9	674	0	644	0	588	1	1685	208	1644	105	1596	124
8	411	35	424	40	415	75	140	0	125	0	115	0	657	85	646	33	642	121

Table F.7: NO_x conversion efficiency of the SCRF® at ANR-1.2 Repeat

Test Point	ANR			NO_x conversion efficiency [%]			Nitrogen Balance [%]		
	SCRF®-0	SCRF®-2	SCRF®-4	SCRF®-0	SCRF®-2	SCRF®-4	SCRF®-0	SCRF®-2	SCRF®-4
1	1.23	1.19	1.31	99	99	97	97	101	95
3	1.19	1.19	1.22	98	99	99	101	97	102
6	1.15	1.19	1.16	100	100	99	99	103	94
8	1.19	1.18	1.21	94	93	86	91	84	90

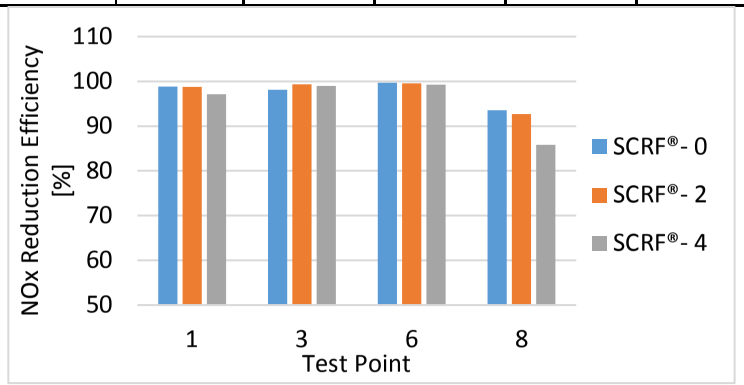

Figure F. 1 NO_x conversion efficiency of the SCRF® with and without PM at ANR – 1.2 Repeat

Appendix G. Pressure Drop Across the SCRF® - Configuration 2 (with and without PM loading)

The pressure drop across the SCRF® for each Test Point, with and without PM loading in the SCRF® is discussed in this section. Figures G.1, G.2, G.3 and G.4 show that the pressure drop remains constant for the tests without PM loading (0 g/L) in the SCRF®. This happens because a CPF was placed upstream of the SCRF®. Hence, there is little PM deposition or oxidation phenomenon occurring in the SCRF®.

Figures G.5 and G.6 show the pressure drop across the SCRF® with PM loading of 2 g/L in the SCRF®. $PM_{Retained}$ in the SCRF® at the end of the stages are indicated on the pressure drop plots. The Test Point 8 has high SCRF® inlet temperatures and therefore the SCRF® was loaded again in between NO_x reduction test denoted by repeat loadings as shown in Figures H.6 for 2 g/L loading. Similar repeat loadings were done for the same Test Points for PM loading of 4 g/L as shown in Figures G.9 and G.10.

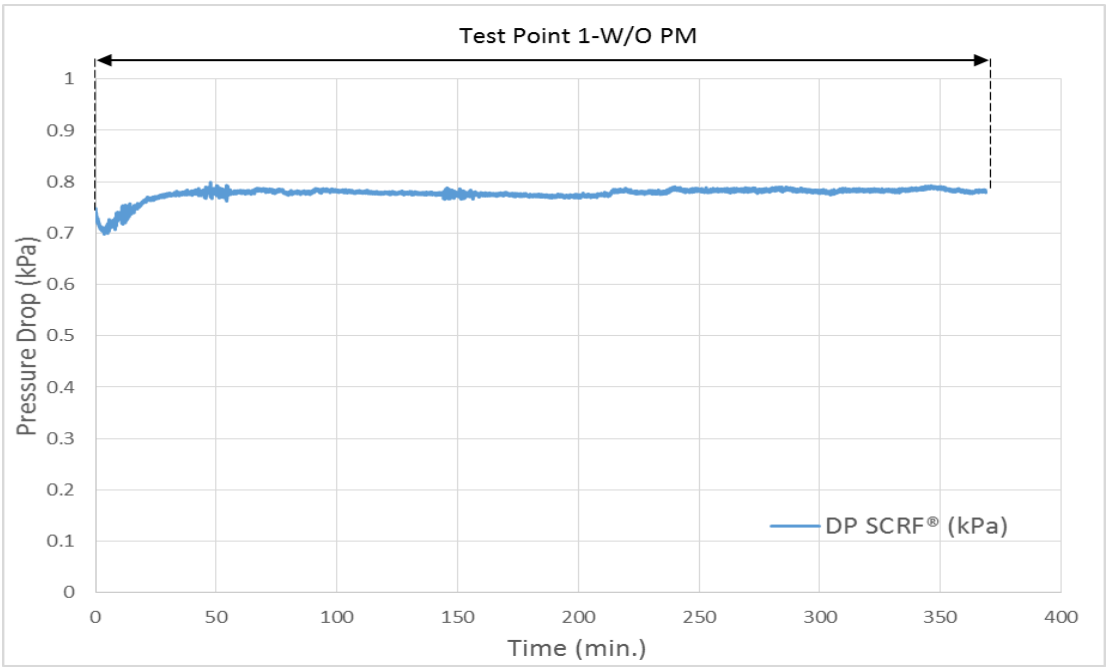

Figure G.1: Pressure drop across the SCRF® for the Test Point 1, PM loading 0 g/L

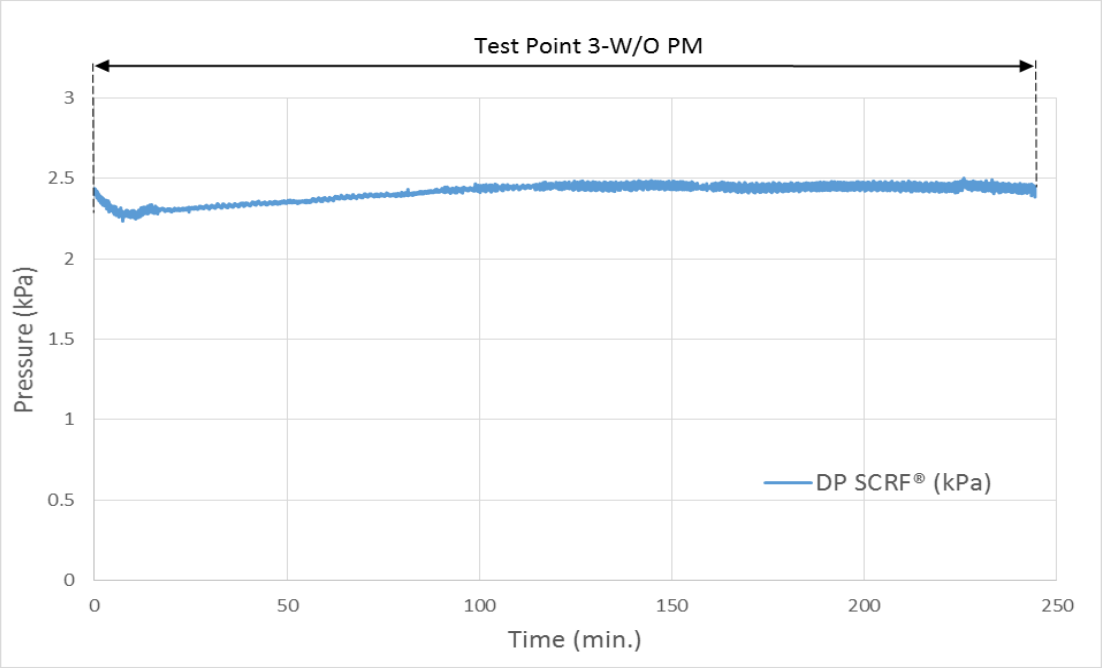

Figure G.2: Pressure drop across the SCRF® for the Test Point 3, PM loading 0 g/L

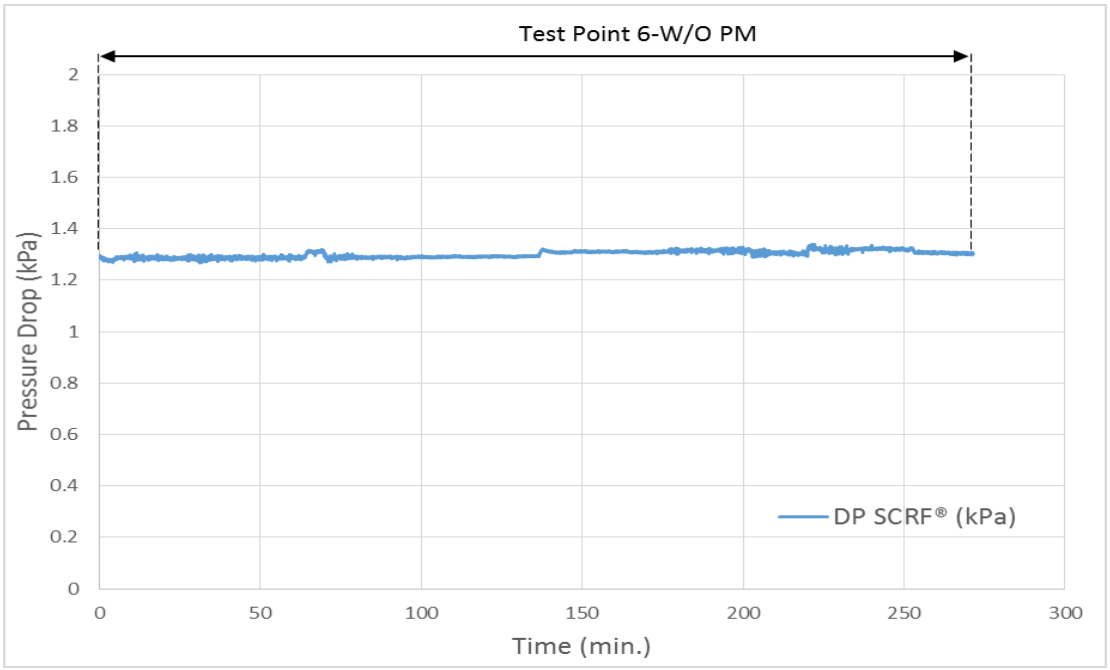

Figure G.3: Pressure drop across the SCRF® for the Test Point 6, PM loading 0 g/L

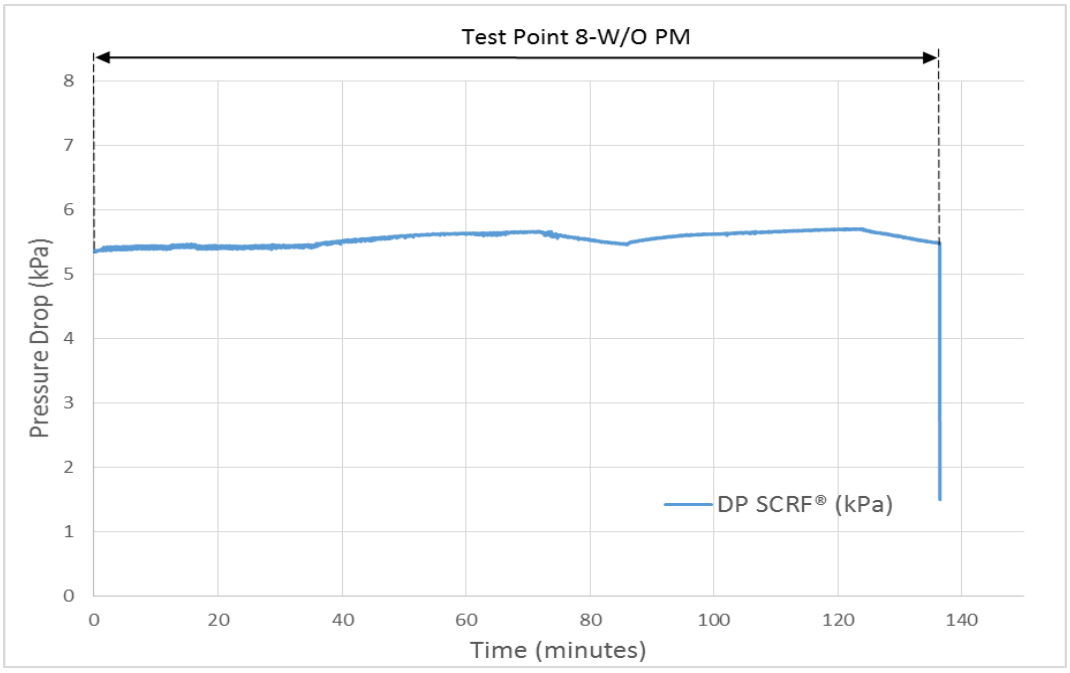

Figure G.4: Pressure drop across the SCRF® for the Test Point 8, PM loading 0 g/L

PM Loading at 4 g/L

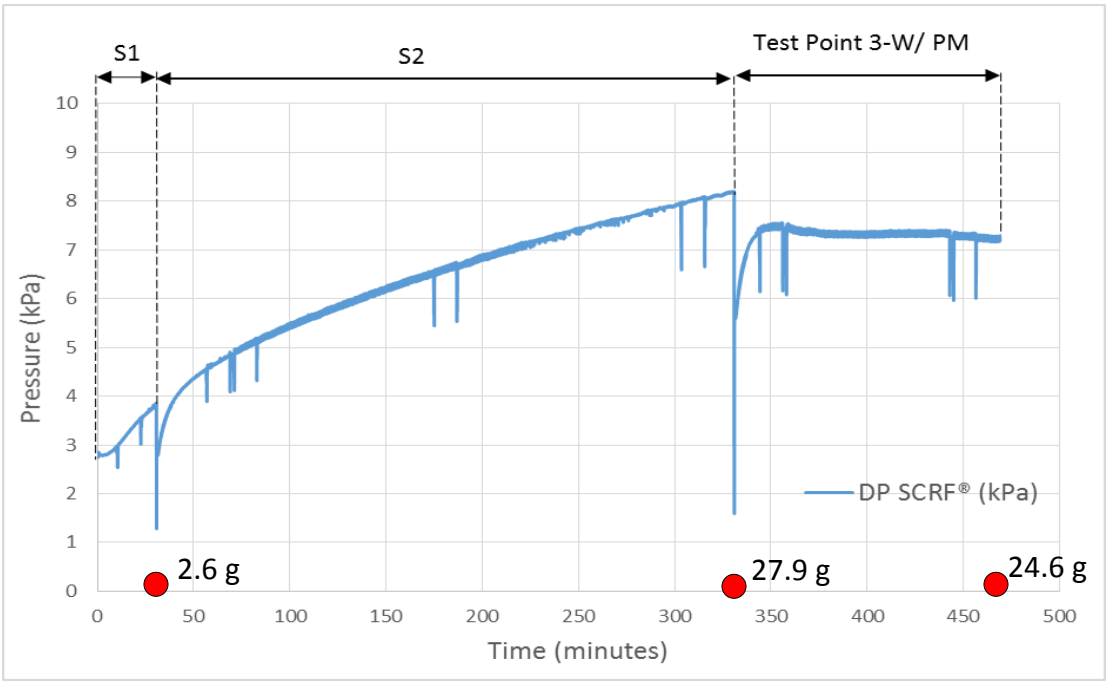

Figure G.5: Pressure drop across the SCRF® for the Test Point 3, with PM loading 2 g/L

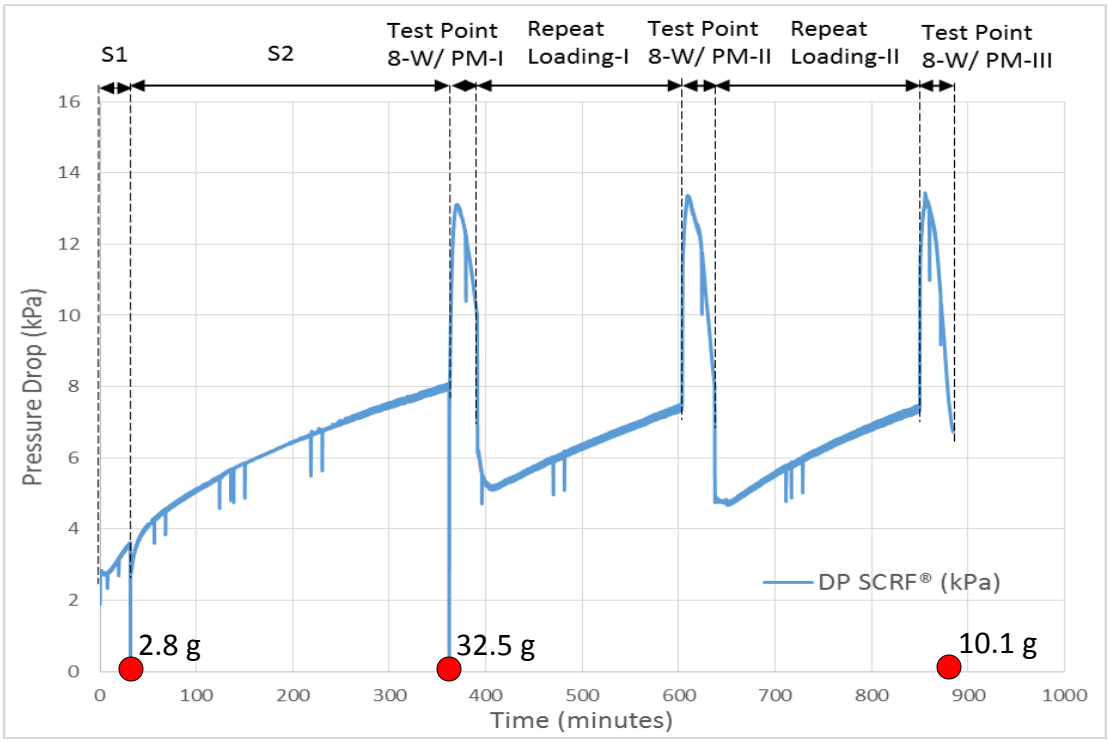

Figure G.6: Pressure drop across the SCRF® for the Test Point 8, with PM loading 2 g/L

PM Loading at 4 g/L

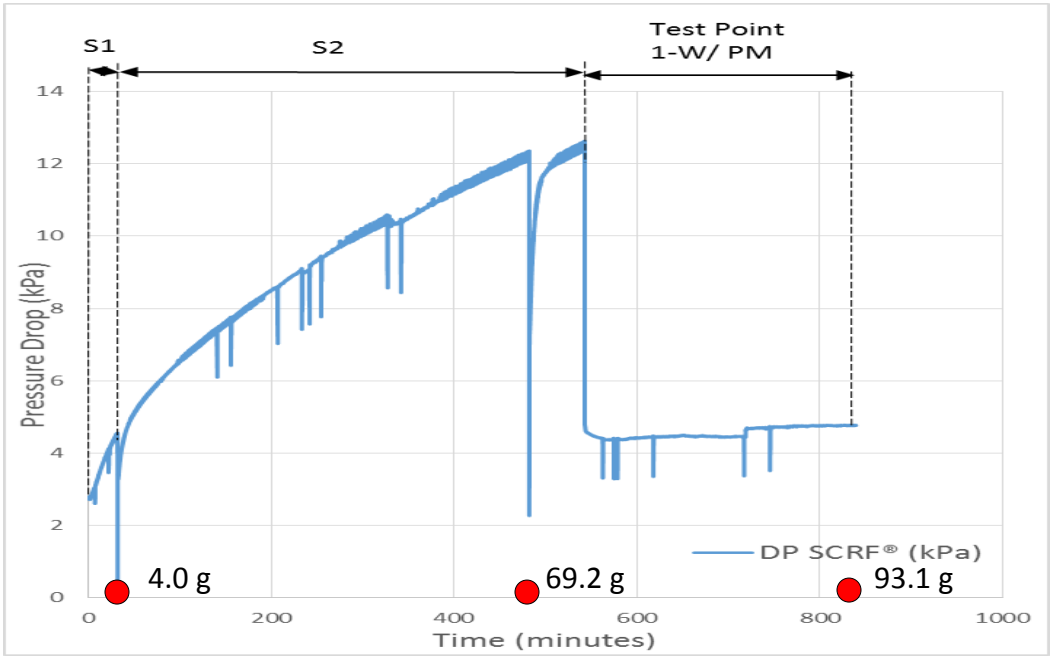

Figure G.7: Pressure drop across the SCRF® for the Test Point 1, with PM loading 4 g/L

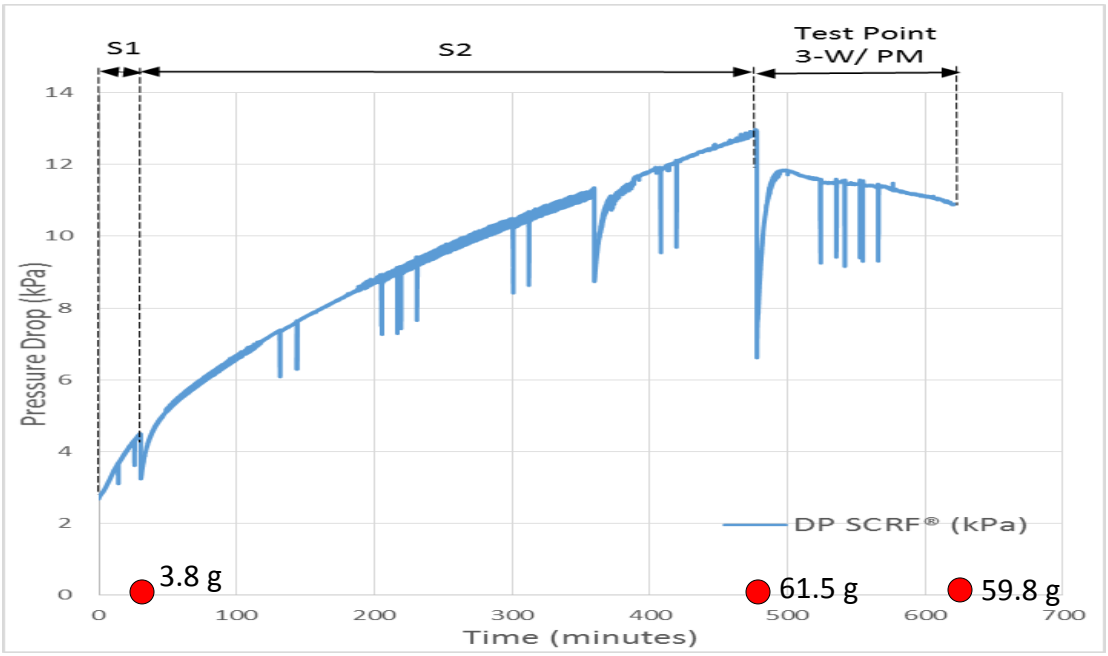

Figure G.8: Pressure drop across the SCRF® for the Test Point 3, with PM loading 4 g/L

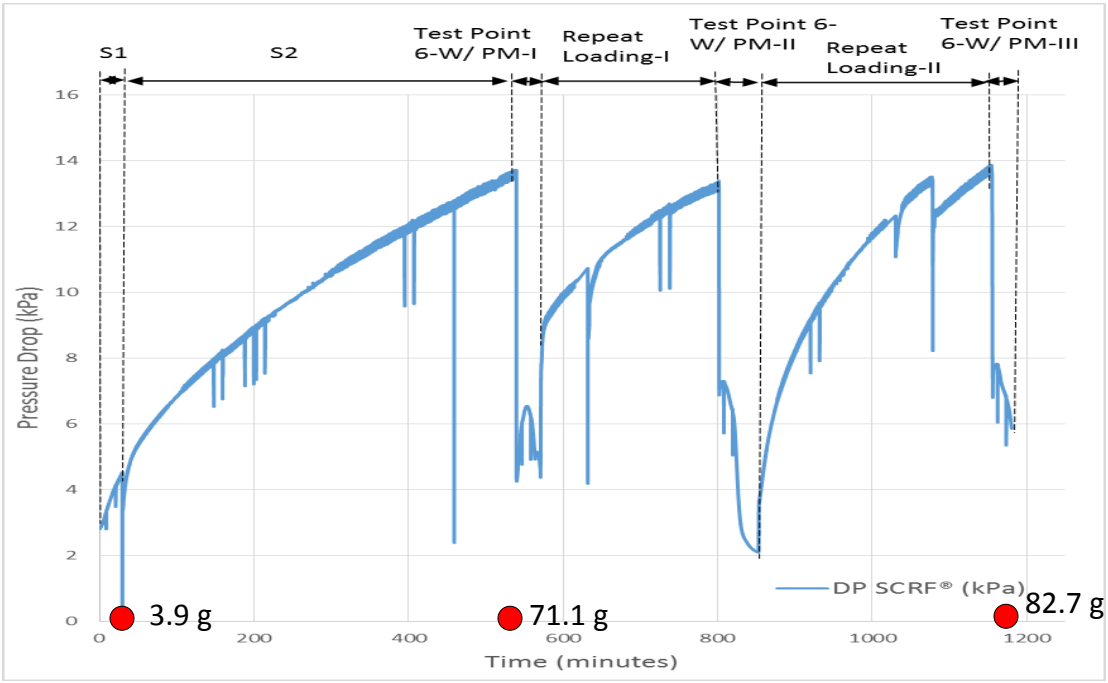

Figure G.9: Pressure drop across the SCRF® for the Test Point 6, with PM loading 4 g/L

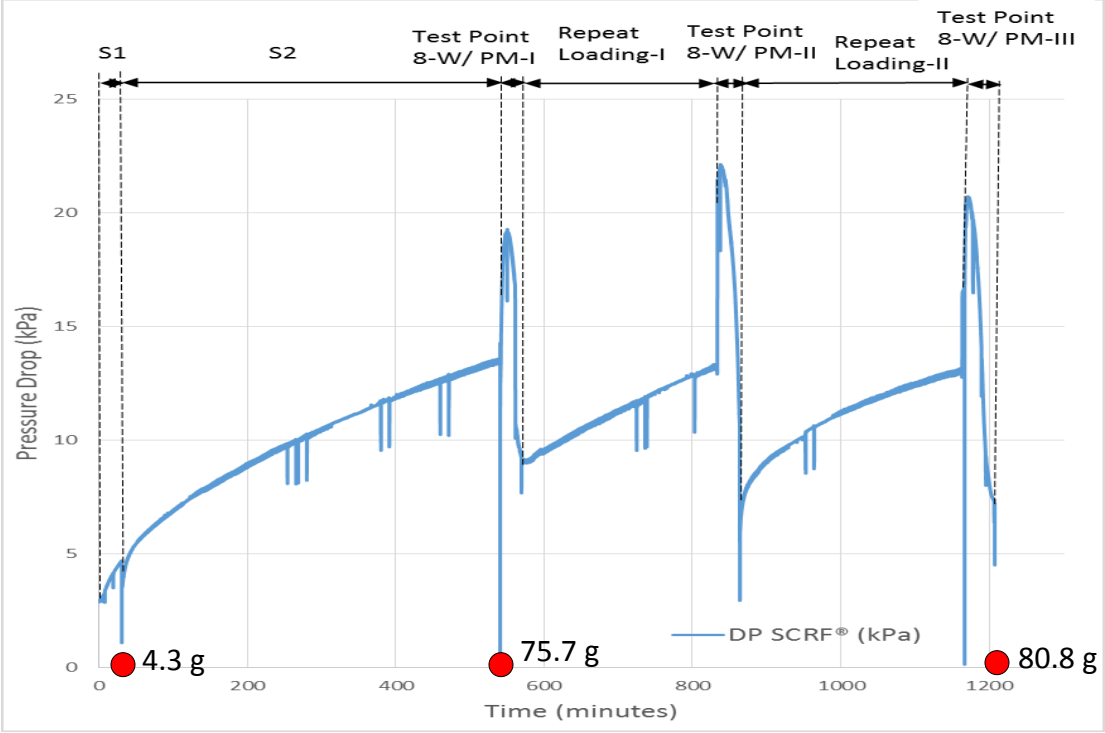

Figure G.10: Pressure drop across the SCRF® for the Test Point 8, with PM loading 4 g/L

Appendix H. Temperature Distribution in the SCRF® - Configuration 2 (with and without PM loading)

In this section, the gas temperature distribution in the radial and axial positions in the SCRF® during the NO_x reduction stage, with and without PM loading is discussed. The study of the gas temperature distribution obtained from experimental data is critical since the experimental data will be used to calibrate the SCR-F model being developed at MTU. Figure H.1 shows the thermocouple arrangement in the SCRF® at various radial and axial locations. Twenty thermocouples are labeled from S1 to S20. The thermocouples S1 to S10 were inserted into the SCRF® through the inlet channels of the SCRF® and the thermocouples S11 to S20 were inserted through the outlet channels of the SCRF®.

The gas temperatures in the SCRF® were monitored, recorded and studied using the K-type thermocouples for the loading and NO_x reduction stages, with or without PM loading in the SCRF®. The temperature distribution in the SCRF® during the loading stages performed in configuration 2 are discussed in reference [86].

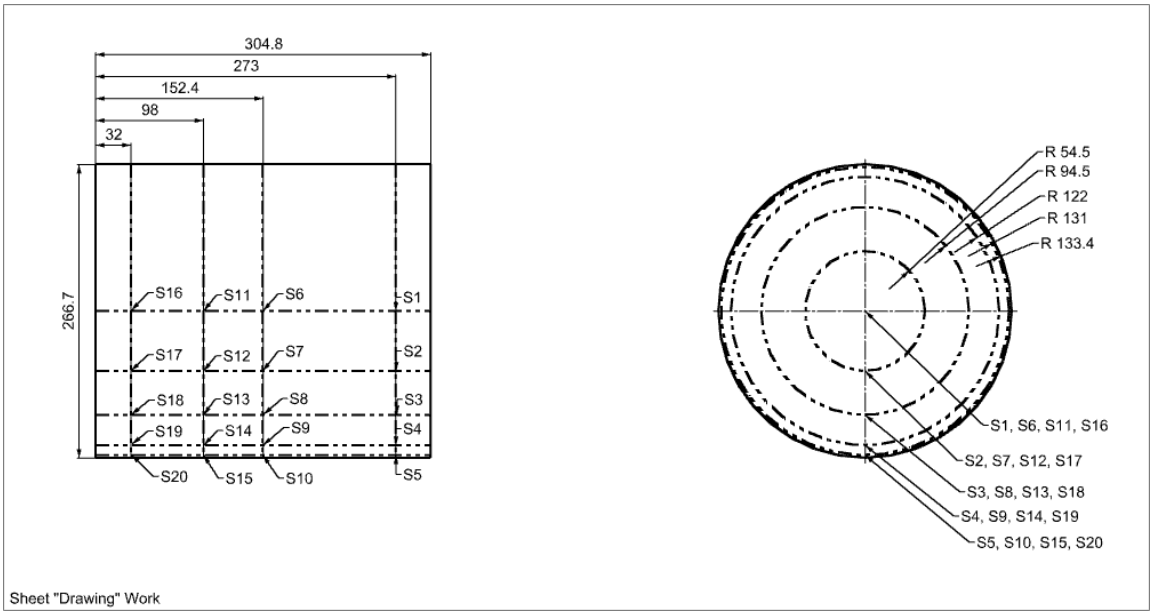

Figure H.1: Thermocouple arrangement in the SCRF® (all dimensions in mm)

Table H.1: Thermocouple temperatures during NO_x reduction stage for Test Point 1, with and without PM loading – Configuration 2

PM Loading [g/L]	Time [Hours]	SCRF□Thermocouple Temperature, [°C]																		
		S1	S2	S3	S4	S5	S6	S7	S8	S9	S10	S11	S12	S13	S14	S15	S16	S17	S18	S19	S20
0	3.53	215	214	213	210	203	222	221	220	213	204	222	221	220	212	200	222	222	221	213	198
2	10.56	214	213	213	211	205	221	220	220	213	206	220	220	220	213	199	221	221	220	214	195
4	14.07	208	208	208	205	196	213	214	211	205	194	215	215	213	205	193	216	215	215	206	193

Table H.2: Thermocouple temperatures during NO_x reduction stage for Test Point 3, with and without PM loading – Configuration 2

PM Loading [g/L]	Time [Hours]	SCRF□Thermocouple Temperature, [°C]																		
		S1	S2	S3	S4	S5	S6	S7	S8	S9	S10	S11	S12	S13	S14	S15	S16	S17	S18	S19	S20
0	3.27	306	305	305	301	295	310	308	308	302	292	309	308	308	302	288	308	308	308	303	286
2	9.35	314	314	313	310	304	319	317	315	310	303	318	318	315	310	293	317	318	317	312	290
4	11.44	316	310	314	311	304	320	319	318	313	298	319	325	318	313	295	320	318	318	314	296

Table H.3: Thermocouple temperatures during NO_x reduction stage for Test Point 6, with and without PM loading – Configuration 2

PM Loading [g/L]	Time [Hours]	SCRF□Thermocouple Temperature, [°C]																			
		S1	S2	S3	S4	S5	S6	S7	S8	S9	S10	S11	S12	S13	S14	S15	S16	S17	S18	S19	S20
0	5.42	338	336	336	331	320	355	354	354	338	330	355	354	353	341	326	355	355	354	344	320
2	13.13	344	344	345	339	328	360	360	360	350	337	361	361	360	348	325	362	361	361	350	323
4	15.92	354	356	354	351	338	359	360	360	355	341	364	365	364	357	333	367	369	368	356	333

Table H.4: Thermocouple temperatures during NO_x reduction stage for Test Point 8, with and without PM loading – Configuration 2

PM Loading [g/L]	Time [Hours]	SCRF□Thermocouple Temperature, [°C]																			
		S1	S2	S3	S4	S5	S6	S7	S8	S9	S10	S11	S12	S13	S14	S15	S16	S17	S18	S19	S20
0	2.22	444	442	442	437	430	451	448	448	439	430	450	449	449	440	426	449	449	449	443	422
2	12.25	441	444	441	437	429	447	446	445	440	430	445	446	446	441	418	447	447	448	442	422
4	16.02	447	448	447	444	439	454	453	453	447	430	454	454	449	448	426	454	455	454	447	426

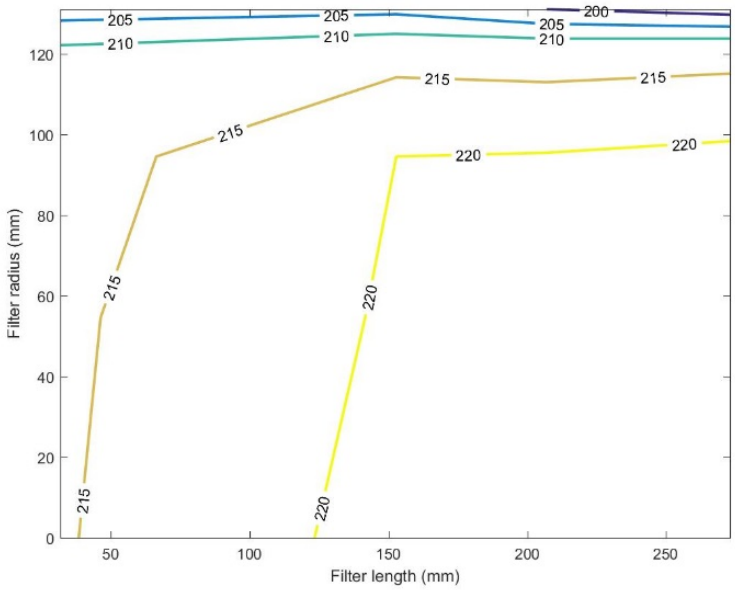

Figure H.2: Temperature distribution in the SCRF® during NO_x reduction stage for Test Point 1 without PM loading, at ANR 1.0

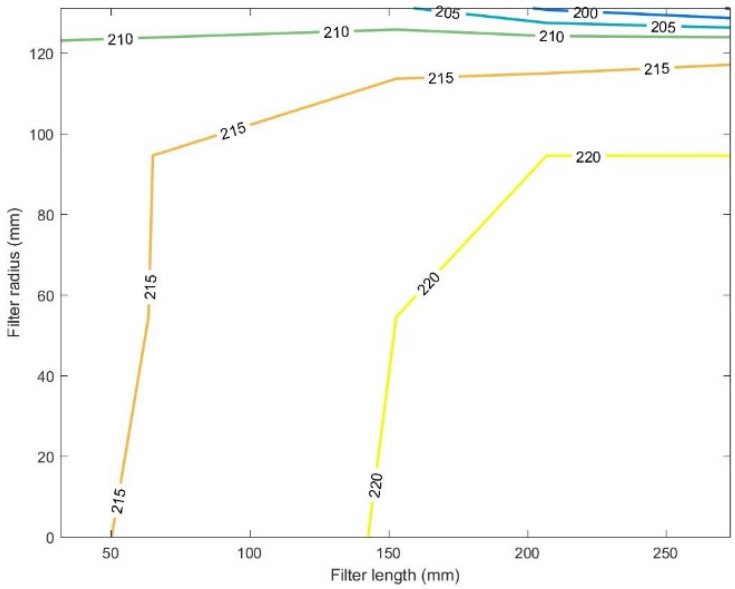

Figure H.3: Temperature distribution in the SCRF® during NO_x reduction stage for Test Point 1 with 2 g/L PM loading, at ANR 1.0

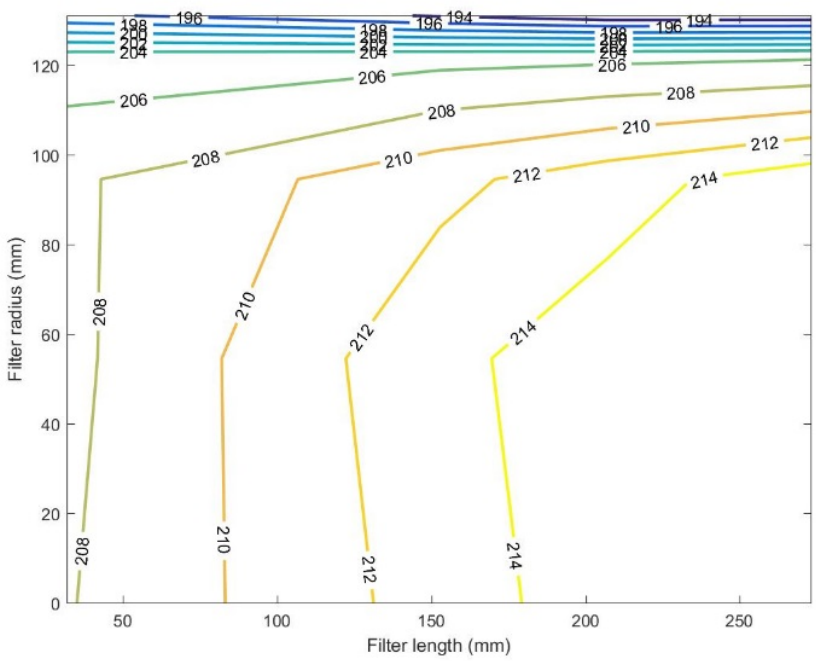

Figure H.4: Temperature distribution in the SCRF® during NO_x reduction stage for Test Point 1 with 4 g/L PM loading, at ANR 1.0

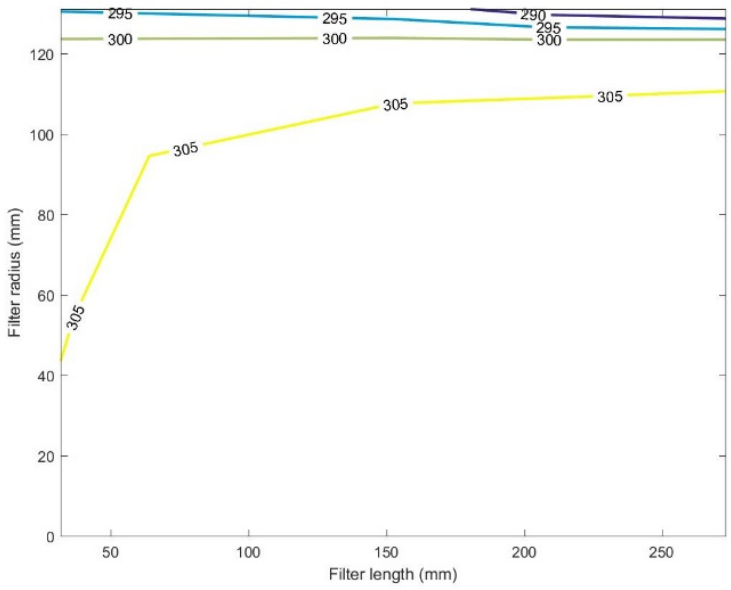

Figure H.5: Temperature distribution in the SCRF® during NO_x reduction stage for Test Point 3 without PM loading, at ANR 1.0

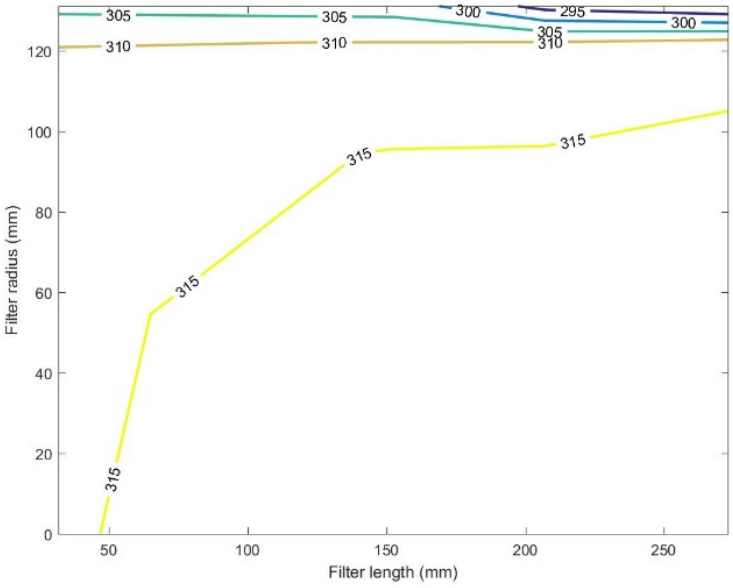

Figure H.6: Temperature distribution in the SCRF® during NO_x reduction stage for Test Point 3 with 2 g/L PM loading, at ANR 1.0

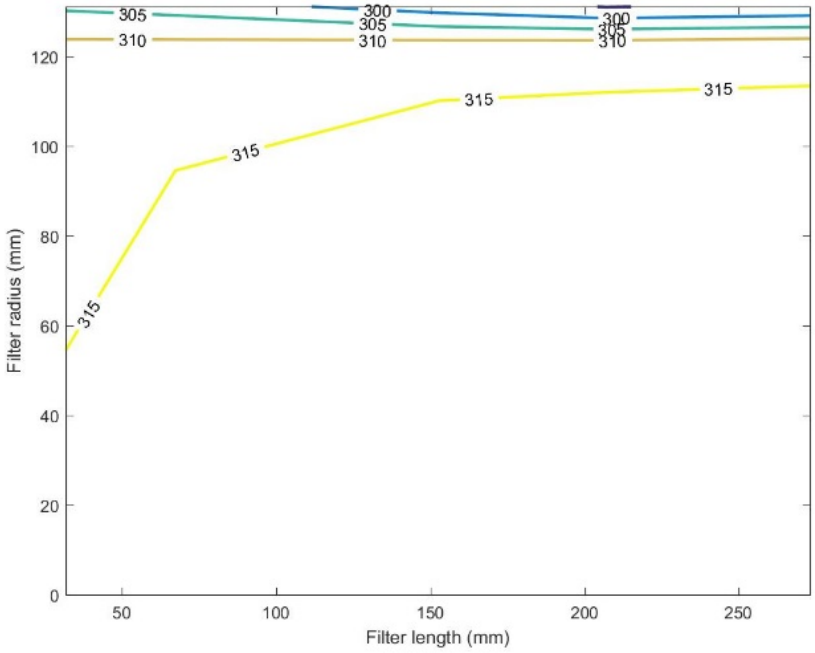

Figure H.7: Temperature distribution in the SCRF® during NO_x reduction stage for Test Point 3 with 4 g/L PM loading, at ANR 1.0

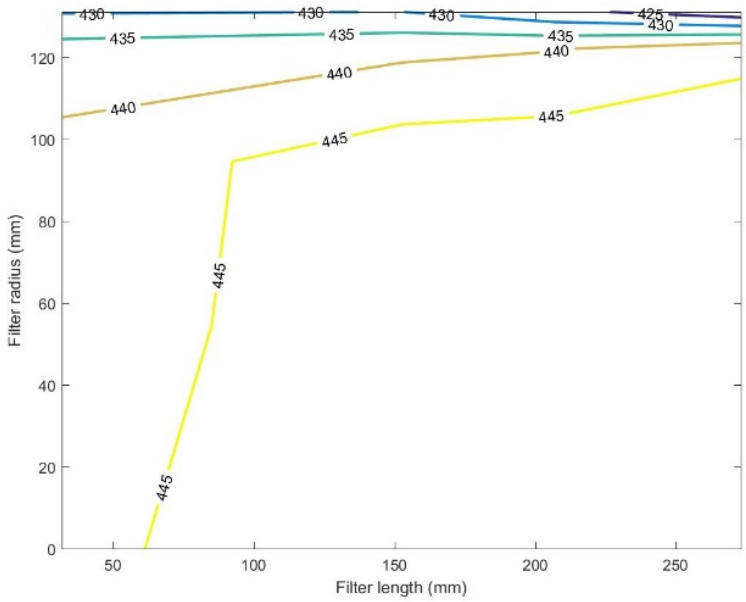

Figure H.8: Temperature distribution in the SCRF® during NO_x reduction stage for Test Point 8 without PM loading, at ANR 1.0

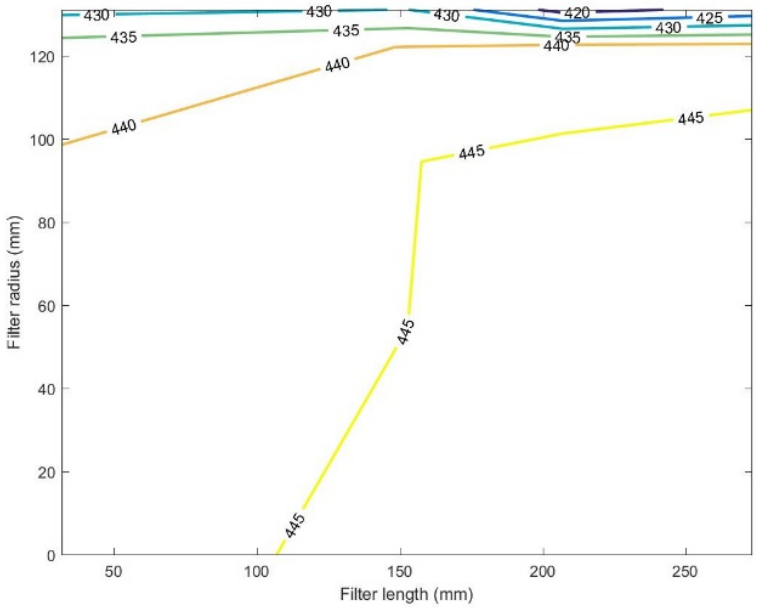

Figure H.9: Temperature distribution in the SCRF® during NO_x reduction stage for Test Point 8 with 2 g/L PM loading, at ANR 1.0

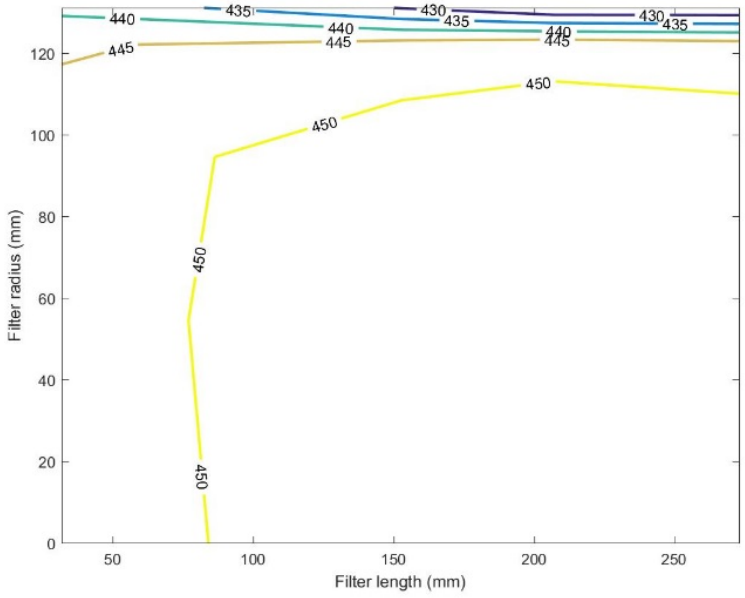

Figure H.10: Temperature distribution in the SCRF® during NO_x reduction stage for Test Point 8 with 4 g/L PM loading at ANR 1.0

The temperature factor calculated using Equation H.1 [13] for all Test Points in configuration 2, with and without PM loading in the SCRF® are shown in Figures H.11, H.12 and H.13.

$$Temperautre\ Factor, C = \frac{T_s - T_r}{T_s - T_m} \qquad \text{Eqn. H.1}$$

Where T_m is mean exhaust gas temperature, T_s is wall inner surface temperature, T_r temperature at a given radial location, y Axial location.

The diameter ratio is the ratio of SCRF® diameter at a given measurement location to the maximum SCRF® diameter [13]. From Figures H.11, H.12 and H.13 it is observed that the temperature factor is almost constant up to the SCRF® diameter ratio of 0.7 (indicating uniform temperature) and drops to 0 value (minimum temperature) at the SCRF® diameter ratio of 1.0 (outer radius of the filter). The maximum gradient in the temperature factor is observed at the SCRF® diameter ratio of 0.7 to 1.0, showing that

more than 90% of the radial temperature reduction is in the 30% of the filter section closest to the outer radius of the filter.

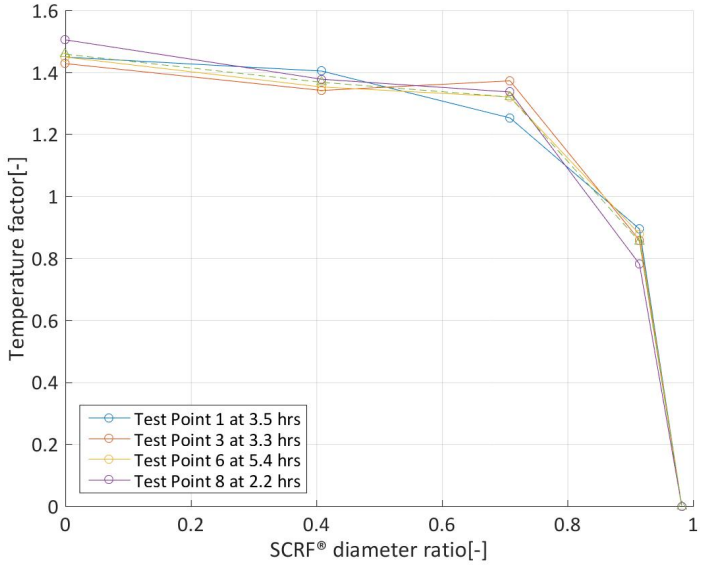

Figure H.11: Temperature factor profile at the SCRF® inlet during NO_x reduction stage without PM loading, at ANR 1.0

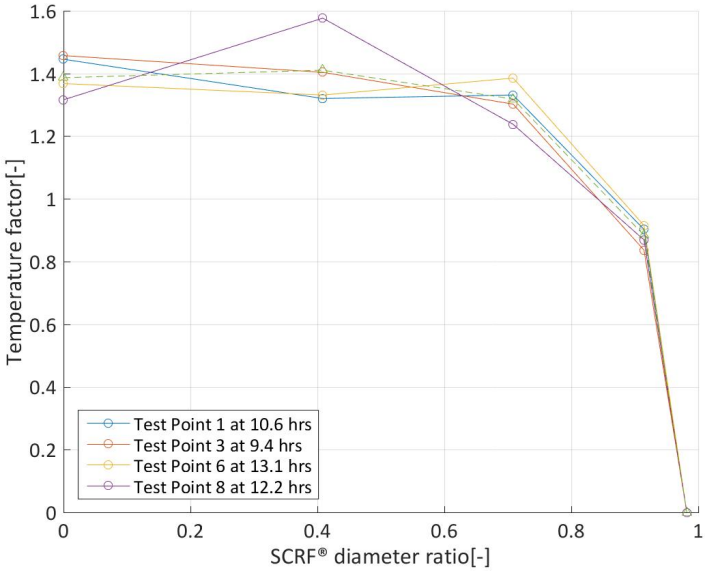

Figure H.12: Temperature factor profile at the SCRF® inlet during NO_x reduction stage with 2g/L PM loading, at ANR 1.0

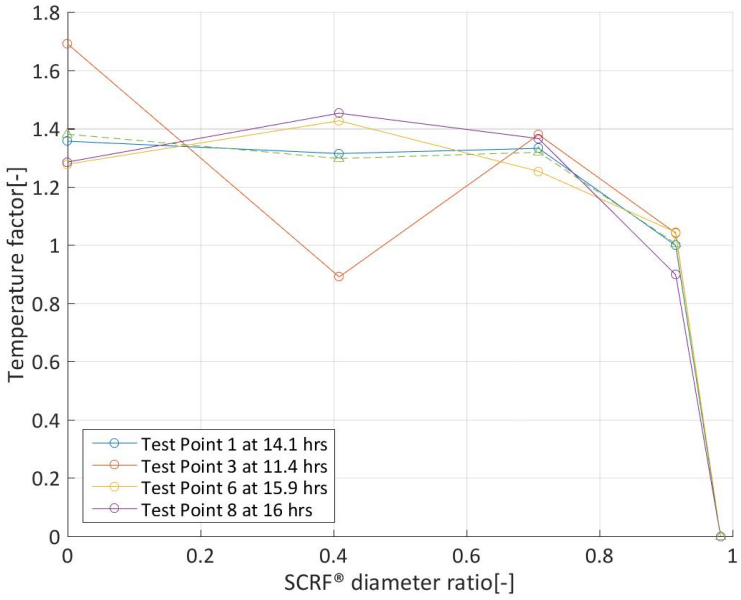

Figure H.13: Temperature factor profile at the SCRF® inlet during NO_x reduction stage with 4g/L PM loading, at ANR 1.0

Appendix I. Permissions to Use Copyrighted Material

The permission letter below is for Figure 2.1

Dear Mr. vaibhav kadam,

Thank you for placing your order through Copyright Clearance Center's RightsLink service. Elsevier has partnered with RightsLink to license its content. This notice is a confirmation that your order was successful.

Your order details and publisher terms and conditions are available by clicking the link below:
http://s100.copyright.com/CustomerAdmin/PLF.jsp?ref=638d9123-c178-4953-b7ca-e5c345f9c206

Order Details
Licensee: vaibhav kadam
License Date: Aug 17, 2016
License Number: 3931510428725
Publication: Applied Catalysis B: Environmental
Title: A novel Ce-Ta mixed oxide catalyst for the selective catalytic reduction of NOx with NH3

The permission letter below is for Figure 2.2.

Dear Mr. vaibhav kadam,

Thank you for placing your order through Copyright Clearance Center's RightsLink service. Elsevier has partnered with RightsLink to license its content. This notice is a confirmation that your order was successful.

Your order details and publisher terms and conditions are available by clicking the link below:
http://s100.copyright.com/CustomerAdmin/PLF.jsp?ref=ea897345-2b3e-4876-aada-40e51fcee96e

Order Details
Licensee: vaibhav kadam

License Date: Aug 17, 2016
License Number: 3931510836920
Publication: Journal of Catalysis
Title: Novel manganese oxide confined interweaved titania nanotubes for the low-temperature Selective Catalytic Reduction (SCR) of NOx by NH3

The permission letter below is for Figures 2.4 and 2.5.

Dear Vaibhav Kadam,

Thank you very much for your permission request.

Enclosed you will find the permission letter. Kindly abide the outlined conditions for the usage.

Springer reference

Emission Control Science and Technology
May 2015, Volume 1, Issue 2, pp. 134-151
First online: 08 May 2015
Interaction of NO x Reduction and Soot Oxidation in a DPF with Cu-Zeolite SCR Coating
Authors: E. Tronconi, I. Nova, F. Marchitti, G. Koltsakis, D. Karamitros, B. Maletic, N. Markert, D.
Chatterjee, M. Hehle

Materials to be reused: Figure 7 and Figure 14
DOI 10.1007/s40825-015-0014-y
Print ISSN 2199-3629
Online ISSN 2199-3637
Journal no. 40825

Your project
Requestor: Vaibhav Kadam
GRA. Michigan Tech
vkadam@mtu.edu
University: Michigan Tech
Purpose: Dissertation/Thesis

Sincerely,

Rights and Permissions
Springer Science+Business Media

Tiergartenstr. 17
69121 Heidelberg
Germany

Hello,

Attached please find a Microsoft Word document with a request to use a total of 2 figures in my Master's thesis (Master's student at Michigan Tech) from 1 publication in the Emission Control Science and Technology, May 2015, Volume 1, Issue 2.

If you have any questions, please do not hesitate to contact me at the information listed below.

Thank you

Vaibhav Kadam
GRA. Michigan Tech
vkadam@mtu.edu

The permission letter below is for Figures 1.1, 3.3, 3.4, 3.5 and 3.6

Hi Vaibhav,

Please feel free to use any material from my thesis as required. All the best for your thesis!

Regards,
Krishnan Raghavan

Krishnan,

I am planning to use Figures 1.1, 3.1 and 3.3 from your thesis (original or modified version) for my thesis. Please provide me your permission to use the copyrighted material.

Thank you,

Vaibhav Kadam
GRA, Michigan Tech
vkadam@mtu.edu

The permission letter below is for Figure 3.8.

Hi Vaibhav,

Yes, you have my permission. All the best for your thesis.

Warm Regards,
Erik Gustafson

Hi Erik,

I am planning to use Figure 1.1, 3.1 and 3.3 from your thesis (original or modified version) for my thesis. Please provide me your permission to use the copyrighted material.

Thank you,

Vaibhav Kadam

Figures 2.3 and 2.6. are reprinted with permission from SAE International.

Dear Vaibhav,

Thank you for your patience during processing of your request.

Please be advised, reproduction use of Figure 1, page 2 of SAE 2009-01-0274 and Figure 12, page 8 of SAE 2014-01-1523, is hereby granted, and subject to the following terms and conditions:

-Permission is granted for non-exclusive English language rights, and for the specific use as indicated in your email;

-Permission is required for new requests, or for further use of the material;

-The SAE material must be clearly identified and include the following statement "Reprinted with Permission from SAE International";

-We also request that you include a complete reference to the SAE document within the reference section for each figure replicated;

-This permission does not cover any third-party copyrighted work which may appear in the material requested;

-Licensor's use of this material, in whole or in part, is entirely its responsibility, and SAE International does not warrant or is not responsible for any use of the material.

Thank you.
Best Regards,

Nikole Aston
IP Compliance Specialist
SAE INTERNATIONAL
400 Commonwealth Drive
Warrendale, PA 15096 USA

Hello,

Attached please find a Microsoft Word document with a request to use a total of 2 figures from 2 different S.A.E. publications in my Master's thesis.

Figure 1 from article: He, Y., Brown, D., Lu, S., Paratore, M. et al., "Opportunities and Challenges for Blended 2-Way SCR/DPF Aftertreatment Technologies," SAE Technical Paper 2009-01-0274, 2009, doi:10.4271/2009-01-0274.

Figure 12 from article: Johansen, K., Bentzer, H., Kustov, A., Larsen, K. et al., "Integration of Vanadium and Zeolite Type SCR Functionality into DPF in Exhaust Aftertreatment Systems - Advantages and Challenges," SAE Technical Paper 2014-01-1523, 2014, doi:10.4271/2014-01-1523.

Please provide me permission to use the copyright material.

Thank you

Vaibhav Kadam
GRA, Michigan Tech
vkadam@mtu.edu